POLITECNICO DI TORINO

Collegio di Ingegneria Chimica e dei Materiali

Master of Science Course

In Material Engineering

Master of Science Thesis

Durability testing of 2304 Duplex stainless steel reinforced concrete structures in high chloride-containing environment

Supervisors

prof. Sabrina Grassini

prof. Alvaro Ridruejo

Candidate

Nicola Aversano

December 2019

To my beloved family.

POLITECNICO DI TORINO

COLLEGIO DI INGEGNERIA CHIMICA E DEI MATERIALI

DISAT

Master of Science Course in Materials Engineering

Abstract

Durability testing of 2304 Duplex stainless steel reinforced concrete structures in high chloride-containing environment

Nicola Aversano

Aim of this study is to test the corrosion behaviour of concrete structures reinforced by 2304 Duplex Stainless Steel rebars in high chloride-containing environment, in order to assess their resistance and durability. Although reinforced concrete (RC) is one of the most common material used in the construction field, in recent years many cases of failures because of corrosion occurred. Specifically, in marine environment, chloride-induced corrosion has revealed to be one of the most dangerous and frequent problem. Duplex AISI 2304 has been selected as reinforcement, because in the literature it is classified as one of the best materials for this application in terms of final properties and costs. The research work has been performed following the Spanish standard norm UNE 83992 "concrete durability", starting from the fabrication of the samples. More in details, during the test a modified accelerated chlorides attack has been performed on a set of twenty equal cubic mortar specimens, in in order to make the steels embedded in them de-passivate. The corrosion behaviour of the Duplex bars has been assessed by means of Linear Polarization Resistance technique (LPR), measuring the corrosion potential (E_{corr}) and the corrosion rate (I_{corr}). The tests have been stopped for the de-passivated samples, in order to break them up and to gather information about the service life, the steel final microstructure and its surface critical chloride content. Over the entire 2-months period of testing among the twenty tested sample, only one has been permanently de-passivated and subject to the final corrosion analysis.

Contents

Riassunto

Nel corso della storia, il genere umano ha sempre avuto grande interesse nella selezione di materiali per la costruzione di ponti e infrastrutture, che gli permettessero di poter solcare mari e corsi d'acqua e spostarsi per il mondo in modo più agevole. Oggigiorno queste infrastrutture sono per buona parte costruite in calcestruzzo armato, progettate per durare nel tempo e per resistere a ogni tipo di condizione ambientale o di fenomeno degradativo . Tra i fenomeni di deterioramento più ricorrenti per costruzioni in calcestruzzo armato viene annoverata la corrosione.

In generale, la corrosione rappresenta una delle principali cause di degrado dei materiali , in particolare di materiali metallici. Il processo di corrosione è frutto di reazioni chimiche attivate attraverso il contatto con l'ambiente circostante. Nello specifico, avviene un trasferimento di elettroni : gli atomi metallici perdono uno o più elettroni, trasformandosi in ioni metallici altamente reattivi. A seconda dell'ambiente in cui avviene il fenomeno, esistono prevalentemente tre principali tipi di corrosione: corrosione a secco, corrosione a umido (in sistemi acquosi) e corrosione in altri fluidi (in sistemi non acquosi) . La corrosione elettrochimica rappresenta il principale meccanismo coinvolto nel processo di corrosione dei metalli a contatto con soluzioni acquose. La forza motrice del processo è rappresentata dalla differenza di potenziale tra gli atomi del metallo all'interno della soluzione e gli elementi prodotti dalla corrosione. Nel suddetto sistema di corrosione, le reazioni anodiche di ossidazione consumano il metallo, che può disciogliersi sotto forma di ioni nell'elettrolita liberando elettroni. Questi elettroni vengono puntualmente consumati dalle reazioni catodiche di riduzione da parte di elementi come l'ossigeno o l'idrogeno presenti all'interno dell'acqua. La quantità relativa di O_2 o di H^+ all'interno della soluzione dirà quale tra le due reazioni di riduzione è favorita. La velocità del processo di corrosione può essere influenzata da diversi fattori, tra i quali la conducibilità elettrica dell'elettrolita, la presenza e quantità di elementi catodici in soluzione e sulla superficie del metallo, la possibilità di formazione di depositi sulla superficie metallica e la temperatura. Termodinamicamente, la corrosione avviene a causa del potenziale assunto dal metallo durante il processo, potenziale che viene definito potenziale di

corrosione E_{corr}. I tipi di corrosione elettrochimica sono vari e differenti. I più frequenti e rilevanti sono, senza dubbio, la corrosione per vaiolatura o pitting , la corrosione interstiziale (crevice), la corrosione galvanica, lo Stress Corrosion Cracking (SCC) o la Corrosion Fatigue (CF).

Il calcestruzzo armato è un materiale composito costituito di due elementi strutturali: il calcestruzzo che costituisce la matrice del composito e che fornisce duttilità, e le barre rinforzanti incorporate nella matrice che ,con una maggiore resistenza meccanica, provvedono ad aumentare la resistenza della struttura ai carichi applicati. I rinforzanti possono essere di vario tipo, ma nel campo delle costruzioni si usano prevalentemente quelli in acciaio. La grande alcalinità (pH>12.5) fornita dagli elementi presenti all'interno del calcestruzzo provvedono alla formazione di uno strato protettivo di Fe_2O_3 sulla superficie dell'acciaio. Tra calcestruzzo e rinforzante è necessaria la presenza di un legame resistente e compatibilità termica, in modo da garantire la durabilità nel tempo dell'intero sistema.. In sostanza, la durabilità (o vita utile) di una struttura indica la sua capacità di mantenere le sue proprietà pressoché inalterate per un dato intervallo di tempo, senza quindi avere dei cambiamenti o deterioramenti che potrebbero comprometterne la normale attività. Per quanto concerne le strutture in calcestruzzo armato, sono varie le cause che possono interessare sia il calcestruzzo che il rinforzo e provocarne il peggioramento nel corso del tempo.

Tra le principali cause si annovera proprio la corrosione, che si innesca sostanzialmente attraverso due fenomeni: la carbonatazione e l'attacco dei cloruri da parte di cloruri. La carbonatazione è sostanzialmente il frutto di reazioni chimiche tra gli elementi all'interno del calcestruzzo e la CO_2 atmosferica, in presenza di H_2O. Queste reazioni determinano l'abbassamento del pH della struttura e conseguente indebolimento dello strato di ossido sull'acciaio. La carbonatazione è un processo relativamente lento, ma in combinazione con altri fenomeni di deterioramento, può essere molto pericoloso. Tra gli altri fenomeni si inserisce la corrosione indotta da cloruri, il tipo di corrosione attualmente più pericolosa. La combinazione degli ioni cloruro, presenti all'interno di acqua di mare o sali disgelanti, con umidità e ossigeno può essere letale per le applicazioni strutturali. I cloruri hanno la capacità di penetrare lo strato di calcestruzzo per capillarità tramite cricche o porosità, di abbassarne il pH riducendo la solubilità di $Ca(OH)_2$, di aumentarne il contenuto di umidità e la conducibilità elettrica. Questi ioni sono in grado di raggiungere il rinforzo metallico e, se in concentrazioni elevate, provocare la rottura del film passivante. La concentrazione critica di cloruri necessaria ad attivare il processo di corrosione non è un valore costante, ma dipende da molteplici fattori, tra cui la

qualità del calcestruzzo e il pH, la quantità di umidità e ossigeno, ma prima ancora, il suo valore varia a seconda dal tipo di acciaio usato come rinforzo. Data la grande variabilità nei valori trovati, i ricercatori sono arrivati a stimare la relazione intercorrente tra la concentrazione critica di cloruri (%Cl^-) , calcolata in rapporto alla percentuale di cemento (%M), e il rischio di corrosione, per cui si avrebbe:

- Basso rischio di corrosione: %Cl^- < 0.2 %M
- Medio rischio di corrosione: %Cl^- = 0.4 %M
- Alto rischio di corrosione: %Cl^- > 1.0 %M

La penetrazione di cloruri all'interno di strutture in calcestruzzo armato a contatto con ambienti aggressivi è fondamentalmente mossa da un processo diffusivo e, come tale, viene caratterizzata dalla seconda legge di Fick modificata con la funzione errore. Questa permette di definire la concentrazione di cloruri a differenti profondità di penetrazione e tempi variabili e ,conoscendo la concentrazione critica per un dato materiale rinforzante, di ottenere informazioni sull'eventuale durabilità dell'intera struttura. In quest'ottica si mosse nel 1982 lo studio di Tuutti, che diede alla luce un modello per prevedere la vita utile di una struttura in calcestruzzo armato. Nel modello viene analizzata la variazione nel livello di corrosione rispetto al tempo di utilizzo della struttura; la vita utile è divisa in due fasi:

- Iniziazione: intervallo di tempo in cui gli ioni Cl^- e la CO_2 penetrano lo strato di calcestruzzo, arrivando alla superficie dell'acciaio e innescando la corrosione. Fase caratterizzata da un aumento relativamente lento del livello corrosivo.
- Propagazione: tempo che intercorre tra la rottura dello strato passivante sulla superficie metallica e il limite ultimo di deterioramento del calcestruzzo. Fase contraddistinta da un aumento rapido del livello di corrosione.

Negli ultimi decenni, si è diffuso in via sempre crescente l'utilizzo di acciai inossidabili in impianti strutturali, quali ponti e viadotti, per fronteggiare condizioni di alto rischio di corrosione. La scelta di un acciaio inossidabile (inox) per resistere ad ambienti aggressivi è piuttosto semplice. Dato il loro alto contenuto di cromo (>11%) gli acciai inox sono in grado di formare , a contatto con l'ossigeno, uno strato di pochi nm costituito prevalentemente da Cr_2O_3 e $Cr(OH)_3$. Il processo tradizionale di fabbricazione degli acciai inossidabili consta di varie fasi, tra le quali una prima fusione e successiva colata, formatura, trattamenti termici, disincrostazione, taglio, finitura, produzione e controllo qualità. Gli acciai inox sono comunemente suddivisi in cinque classi, a seconda della microstruttura e della differente

composizione interna (diagramma di Schaeffler-Delong). Variando il tipo e la quantità degli elementi in lega è possibile stabilizzare una struttura BCC o FCC ed ottenere un Accio Inox:

- Austenitico
- Ferritico
- Martensitico
- Duplex (austenitico-ferritico)
- Indurito per precipitazione (PH)

Gli acciai Inox sono caratterizzati da una resistenza elevatissima alla corrosione uniforme, ma possono soffrire di altri processi di corrosione, tra cui il pitting (o corrosione per vaiolatura). Ed è proprio un meccanismo di corrosione per pitting quello che i cloruri possono determinare sulla superficie di un acciaio inox all'interno di una struttura in calcestruzzo armato.

Nel campo civile e ,nello specifico, nel campo della costruzione di infrastrutture continuamente a contatto con ambienti aggressivi, gli acciai inossidabili più comunemente utilizzati sono del tipo austenitico. Il loro grande successo è principalmente dovuto all' affidabilità acquisita nel tempo, in fatto di resistenza meccanica e chimica. Tra i più utilizzati in campo strutturale si ritrovano l'acciaio austenitico AISI 304 e 304L e l'acciaio austenitico 316 e 316L. Negli ultimi decenni però , gli Inox austenitici hanno dovuto fare i conti con l'avvento di nuovi tipi di acciai inox ad alte prestazioni di differente microstruttura, tra cui gli acciai Dual-Phase (o duplex). Gli acciai Dual-Phase hanno una struttura bifasica austenitico-ferritica, struttura che conferisce loro una combinazione delle migliori proprietà delle due strutture: eccellente resistenza meccanica, ottima tenacità, alta resistenza a corrosioni in mezzi diversi, soprattutto a Stress Corrosion Cracking e Corrosion Fatigue. A questi fattori vanno aggiunti altri più legati alla sostenibilità di una costruzione, sostenibilità che risulta dalla combinazione di priorità sociali, ecologiche ed economiche. Tra questi il risparmio di materiale per la costruzione, il rispetto di persone e ambiente, il design con massimo risparmio energetico. L'acciaio duplex più utilizzato nel mondo ingegneristico è il AISI 2205, primo Duplex ad essere stato commercializzato e tuttora uno dei migliori in quanto a alte performance in ambienti ostili. Due famosi esempi di applicazione di questo acciaio sono l'Helix bridge di Singapore, ponte costruito interamente in acciaio Duplex 2205, e il Harbor Drive Bridge di San Diego, in California. Ma in alcune applicazioni, il Duplex 2205 rivela di avere delle proprietà meccaniche molto al di sopra di quelle richieste dall'applicazione stessa. Questo fattore, in combinazione con quello economico, ha portato i ricercatori e le varie aziende sparse per il mondo alla ricerca di nuovi

tipi di acciai Duplex che ,seppur con un livello di elementi leganti inferiore al grado 2205 , mantenessero la loro grande resistenza meccanica e a corrosione. Questo spiega la nascita degli acciai Duplex standard, tra i quali il AISI 2304. Il AISI 2304 si annovera tra gli acciai inossidabili di livello medio alto, al pari degli acciai austenitici AISI 304L e 316L ben più famosi e utilizzati. Ma analizzando le proprietà dei tre acciai equivalenti in ambienti fortemente corrosivi, sebbene il 2304 mostri un comportamento molto simile agli austenitici in caso di corrosione in differenti acidi (acido acetico, acido formico, acido acetico + formico e acido solforico), esso risulta nettamente migliore in tema di resistenza a pitting e al tipo di corrosione crevice in soluzioni ricche di cloruri e in caso di Stress Corrosion Cracking, grazie ad un contenuto superiore di Cromo e inferiore di Nickel (diagramma di Schaeffler-Delong). Il basso contenuto di Nickel è la ragione principale per cui il prezzo del Duplex 2304 non solo è inferiore, ma è soggetto a minori fluttuazioni rispetto agli equivalenti austenitici e agli altri acciai duplex e super-duplex. Ciò è dovuto al fatto che il Nickel è l'elemento in lega il cui prezzo varia maggiormente nel mercato sul mercato nel corso degli anni e che ha il maggior apporto sul costo finale di fabbricazione di un acciaio stesso.

Sulla base di queste considerazioni, questo lavoro di tesi ha come obiettivo principale quello di analizzare in che modo strutture in calcestruzzo armato con l'acciaio Duplex 2304 si comportino in ambienti di cloruri fortemente aggressivi, in modo da verificarne l'effettiva resistenza e considerare la possibilità di sostituire gli acciai inox tradizionali e poter ampliare in futuro il numero di applicazioni strutturali (quali ponti e infrastrutture) costruite con questo tipo di acciaio. Il lavoro svolto parte dal precedente studio di dottorato di Alicia Pachón Montaño presso l'istituto *Eduardo Torroja* di Madrid, in cui era stato comparato il comportamento a corrosione di cinque acciai inox differenti, tra cui due austenitici, due Duplex e un ferritico. Tra i cinque il Duplex AISI 2205 si era rivelato il migliore rispetto agli altri in termini di resistenza a corrosione da cloruri ma anche il meno economico. D'altra parte, il Duplex 2304 si era rivelato il più ottimale considerando complessivamente costi e proprietà finali.

L'acciaio Duplex 2304 è stato testato sotto forma di barre d'acciaio ottenute mediante lavorazione a freddo. Dalla microstruttura analizzata al microscopio ottico tramite osservazione di una sezione di un campione, è evidente la coesistenza di due fasi (austenitica e ferritica) contraddistinte da tonalità differenti. L'analisi ha mostrato inoltre la presenza di una struttura a grani fini, il quale conferisce una maggiore resistenza meccanica del materiale, dovuta alla grande densità di bordi di grano che ostacolano il movimento delle dislocazioni.

Il test di durabilità da ambiente di cloruri è stato eseguito seguendo la norma spagnola UNE 83992 "Durabilidad del hormigón" (durabilità del calcestruzzo), che ha come obiettivo principale quello di definire un metodo di test che porti alla misura degli effetti degli ioni cloruro Cl^- sulla composizione del calcestruzzo, in termini di:

- resistenza alla penetrazione degli ioni Cl^-
- contenuto critico di Cl^- che inneschino il processo di corrosione sul rinforzo metallico
- velocità di corrosione sulla superficie dell'acciaio

La metodologia del test ha previsto l'esposizione di venti campioni di calcestruzzo armato con l'acciaio Duplex 2304 ad un campo elettrico. Il campione in calcestruzzo armato è composto da un blocco cubico di calcestruzzo di volume $10x10x10cm^3$, nel quale è stata precedentemente incorporata perpendicolarmente una barra di acciaio Duplex 2304 di lunghezza di 10 cm e diametro pari a 1.2 cm. Il campo elettrico è stato generato per mezzo di una differenza di potenziale (ddp) pari a 10 V tra due elettrodi, applicata da parte di un sistema di energia a corrente continua Il primo elettrodo è rappresentato da una lamina di rame presente all'interno di una soluzione di NaCl 0.6M e $CuCL_2$ 0.4M versata in un contenitore cilindrico in PVC e a contatto con il calcestruzzo. La lamina di rame ha funto da catodo. Il secondo elettrodo (anodo), costituito da una rete metallica in acciaio inox, è stato posizionato al di sotto del blocco cementizio. Grazie all'applicazione della differenza di potenziale tra gli elettrodi è stato generato un campo elettrico, che ha accelerato gli ioni cloruro in soluzione verso la rete metallica alla base del campione, attraversando così la barra di acciaio inox. Quest'ultima era stata preventivamente ricoperta di resina epossidica bicomponente, in modo da garantirne la non conducibilità della corrente per tutta la sua estensione all'interno del calcestruzzo, ad eccezione di una finestra di are $2x1\ cm^2$, rappresentante la zona testata.

Il test integrale è stato sostanzialmente composto di 3 fasi successive:

I. Fabbricazione dei provini
II. Test accelerato e misurazioni online
III. Analisi finale della superficie di corrosione (per i provini de-passivati)

La fabbricazione dei provini ha avuto come primo step la preventiva preparazione delle barre di acciaio Duplex per mezzo di un coating di resina epossidica bicomponente *Sikagard 62*, preparazione che ha richiesto più giorni e passate, in modo da garantire la formazione di un coating uniforme. Successivamente è stato preparato il calcestruzzo, con composizione nota, e

la presenza al suo interno di 3 tipi di aggregati (di dimensione fine, media e grossolana), in combinazione con acqua e altri additivi. Una volta preparata la pasta di calcestruzzo, questa è stata colata in stampi di acciaio, sono stati aggiunti i provini in modo da far sì che la finestra sull'acciaio libera da resina epossidica fosse rivolta verso la faccia superiore del blocco cementizio. I provini sono stati lasciati in ambiente umido per 24 h per la solidificazione.

I campioni solidificati sono infine stati prelevati dagli stampi, numerati e lasciati per 28 giorni su griglie plastiche all'interno di contenitori, riempiti con acqua per uno spessore di 3 cm, in modo da creare condizioni di umidità relativa superiore al 95%. Successivamente, sulla faccia superiore di ciascun provino è stato applicato con del silicone un cilindro in PVC di altezza 10 cm, necessario a contenere la soluzione di NaCl e $CuCl_2$. Quest' ultima è stata così versata in ciascun cilindro in quantità tali da riempire il cilindro per un'altezza di circa 9 cm. Dopodiché, una lamina di rame (catodo) è stata inserita all'interno della soluzione, facendo in modo di lasciare all'esterno una delle due estremità, utile alla connessione del generatore di corrente continua. Infine, è stata applicato un film plastico numerato sui lati del blocco di calcestruzzo e sul cilindro contenente la soluzione di ciascun provino, in modo tale da evitarne l'evaporazione rapida durante il tempo. I provini sono poi stati spostati all'interno di un contenitore plastico con un livello di acqua di altezza 3 cm, su griglie plastiche. In questo caso ogni provino è stato posizionato su maglie metalliche in acciaio (anodo); tra il fondo del provino e la rete metallico sono state interposte delle basi in materiale spugnoso, utili ad assicurare le condizioni di elevata umidità relativa durante il test.

II. Il test effettivo è stato anticipato da un pre-test, effettuato per mostrare la ottima resistenza a polarizzazione da parte dell'acciaio Inox. Durante il pre-test, è stata calcolato il potenziale per ciascun provino prima e dopo l'applicazione di un voltaggio di 12 V per un minuto tramite l'utilizzo di un elettrodo di referenza standard in Ag/AgCl, rispetto al quale si può definire la variazione del potenziale all'interno del provino stesso. Dopo aver dimostrato che il potenziale di ciascun provino dopo l'applicazione della corrente tornasse al potenziale misurato inizialmente in un tempo inferiore a 10 minuti, si è passati al calcolo della corrente iniziale per ciascuno di essi e al test vero e proprio. Tutti i campioni sono stati connessi al generatore di corrente continua, la differenza di potenziale di 10V tra catodo e anodo è stata applicata, il giorno e l'ora di attivazione sono stati registrati. Il test è stato prevalentemente diviso in due fasi che si sono alternate durante i giorni: la fase di applicazione della corrente e la fase di misurazioni online. La prima è stata sostanzialmente svolta nelle ore notturne, la seconda nelle ore diurne. Durante il primo mese di test, la fonte di corrente continua è stata disattivata

quotidianamente e durante il weekend. Le misurazioni sono state effettuate quotidianamente. Nel secondo mese di test, l'elevata resistenza al passaggio di corrente da parte dell'acciaio ha portato a disattivare la fonte di energia solo a giorni alterni e a lasciare il sistema attivato durante i weekend, aumentando così le ore di applicazione della ddp tra gli elettrodi dei provini. In questo caso, le misurazioni sono state effettuate a giorni alterni.

Tutte le misurazioni sono eseguite ad un minimo di un'ora di distanza dalla disattivazione giornaliera della fonte di corrente continua, in maniera tale da permettere la stabilizzazione della corrente all'interno dei provini, prima delle effettive misurazioni online. Queste ultime sono state eseguite attraverso l'utilizzo di *Metrohm Autolab* , un dispositivo per test elettrochimici, e del Software *Nova 1.11*. La tecnica di misurazione elettrochimica è stata svolta mediante l'uso di una cella elettrochimica composta da 4 elementi fondamentali:

- Elettrodo di lavoro (WE): l'acciaio Duplex 2304
- Elettrodo di riferimento (RE): elettrodo standard Ag/AgCl
- Contro elettrodo (CE): maglia metallica in accaio inox
- Elettrolita : soluzione NaCl + $CuCl_2$

La metodologia di misurazione ha previsto la valutazione di due parametri fondamentali per capire il comportamento a corrosione di una struttura: il potenziale di corrosione E_{corr} a la velocità di corrosione I_{corr}. Alla base della suddetta metodologia vi è la tecnica di Resistenza a Polarizzazione Lineare (LPR). Questa tecnica muove dalla legge di Stern-Geary e consiste nell'applicare al provino variazioni di potenziale relativamente basse (tipicamente minori di 30 mV) al di sopra e al di sotto del suo potenziale di corrosione E_{corr}. Su questo ristretto intervallo di potenziale prossimo al potenziale di corrosione, la corrente misurata i_{corr} (o I_{corr}) viene caratterizzata da un andamento lineare, la cui pendenza è definita dalla resistenza del materiale alla polarizzazione R_p. Quest'ultima è definita inversamente proporzionale alla velocità istantanea di corrosione. Il test ha avuto una durata di quasi 2 mesi, per la precisione 58 giorni.

Secondo la norma seguita durante il test, un provino in acciaio all'interno di un blocco di calcestruzzo può definirsi de-passivato, cioè corroso se per un totale di 10 giorni consecutivi le misurazioni online dei parametri di corrosione evidenziano:

- Un potenziale di corrosione $E_{corr} > -300$ mV;
- Una velocità di corrosione $I_{corr} > 0.2$ uA/cm^2.

Studi precedenti fatti sugli acciai inox hanno dimostrato che, tra le due condizioni, la seconda aveva veridicità superiore rispetto alla prima, dal momento che sono stati osservati casi in cui solo E_{corr} si era mantenuta più alta del limite definito (-300 mV) per un tempo superiore a 10 giorni, senza osservare alcun tipo di corrosione. D'altra parte si era osservato che nel caso in cui fosse I_{corr} a restare permanentemente superiore al limite (0.2 uA/cm^2) per un tempo superiore a quello stabilito dalla norma, il materiale era risultato effettivamente corroso. Queste considerazioni hanno portato un maggiore interesse rispetto a quello che accadeva alla velocità di corrosione piuttosto che al potenziale durante il test. In sintesi, per i provini che durante il test hanno mostrato de-passivazione per mezzo di cloruri, la fonte di corrente continua è stata disattivata. I provini de-passivati sono stati ad ogni modo lasciati in ambiente umido con gli altri e soggetti ai test elettrochimici. Se nei successivi test nell'arco di 10 giorni dalla de-passivazione, questi provini hanno mostrato nuovamente valori di corrente al di sotto del limite prefisso dalla norma, essi sono stati nuovamente ricollegati al generatore di corrente e il test è proseguito. Nel caso in cui i provini abbiano mantenuto un valore di corrente e di potenziale comunque superiore al limite per un tempo superiore a 10 giorni, questi sono stati dichiarati permanentemente de-passivati e soggetti allo step successivo del test, ovvero alla rottura e all'analisi. Per questi provini, il blocco di calcestruzzo è stato rotto tramite carico a compressione, la barra di acciaio è stata estratta e il materiale all'interfaccia acciaio-calcestruzzo in prossimità della finestra libera della barra è stato prelevato per l'analisi composizionale. Analisi eseguita tramite strumento XRF. Lo studio qualitativo riguardante l'osservazione delle superfici di corrosione sulle barre di acciaio è stato svolto successivamente presso il *Dipartimento di Scienza Applicata e Tecnologia* (DISAT) del *Politecnico di Torino* . I provini , fabbricati e testati a Madrid, che avevano riscontrato un fenomeno corrosivo sono stati soggetti a iniziale troncatura nella zona corrosa, per l'ottenimento di un campione di dimensioni ridotte, che potesse essere studiato al microscopio ottico. Stesso procedimento è stato utilizzato per un equivalente provino di Duplex 2304 di riferimento. Successivamente, le sezioni di acciaio troncate sono state inglobate ,tramite utilizzo di resina epossidica bi-componente, e lucidate per la conseguente analisi microstrutturale. I campioni contenenti l'acciaio corroso sono stati osservati al microscopio ottico, senza alcuna necessità di attacchi chimici precedenti. Il campione di riferimento è invece stato sottoposto ad attacco chimico da parte di una soluzione di acqua regia, ottenuta in laboratorio dalla miscelazione di soluzioni concentrate di HNO_3 e HCl in rapporto 1:3.

Dai risultati del test elettrochimico è stato possibile classificare i 20 provini di calcestruzzo armato in tre tipi, a seconda della loro risposta complessiva al test:

a) Provini con passivazione permanente (PP), ovvero quei provini che non hanno manifestato un aumento dei valori di E_{corr} e I_{corr} al di sopra dei limiti definiti dalla norma durante il periodo di test.
b) Provini con passivazione non permanente (NPP) , ovvero quei provini che hanno manifestato un aumento dei valori E_{corr} e I_{corr} al di sopra dei limiti almeno una volta durante il test.
c) Provini de-passivati o attivati (A) , ovvero quei provini che hanno manifestato valori di E_{corr} e I_{corr} superiori ai limiti per un periodo maggiore rispetto a quello definito dalla norma (10 giorni consecutivi).

Del totale numero dei provini, 14 (70 %) sono risultati del tipo PP , 5 (25%) del tipo NPP e solo uno (5%) è risultato essere del tipo A. I provini classificati PP sono risultati estremamente resistenti alla corrente applicata, mantenendo valori di corrente e velocità di corrosione I_{corr} minimi e pressoché inalterati durante i due mesi di test, nonostante questi fossero stati soggetti ad un numero maggiore di ore di corrente , pari a 889 ore. I provini classificati NPP hanno avuto un comportamento piuttosto diversificato tra di loro e sono stati a loro volta suddivisi in tre fasce: quelli per cui la de-passivazione è avvenuta per cause non ragionevoli in un tempo breve e seguita da un lungo periodo di passivazione (provino 1 e 18), quelli per cui la de-passivazione è avvenuta nel periodo finale dei test in seguito ad un lungo periodo di passivazione (provino 12 e 13) e quelli per cui il comportamento all'attacco da cloruri ha evidenziato un periodo relativamente lungo di passivazione e de-passivazione (provino 17). Il provino 15 è stato classificato del tipo A, essendo stato caratterizzato da un t_{dep} pari a 420 ore e un conseguente periodo di de-passivazione pari a 14 giorni. Questo provino è stato l'unico sottoposto all'analisi completa di corrosione. Dallo studio composizionale mediante strumento *XRF* è risultato un contenuto all'interfaccia acciaio-calcestruzzo di Cl^- = 0.77% rispetto alla % in peso di calcestruzzo, contenuto relativamente alto tenendo in conto dei tempi in cui si è raggiunto tale livello e confrontando con il modello teorico di diffusione dei cloruri all'interno di strutture in calcestruzzo armato. Dall'analisi al microscopio ottico delle zona di interesse è risultata evidente la presenza di un processo corrosivo agli stadi iniziali, che può essere assimilato ad un fenomeno di esfoliazione, data la presenza di porzioni lamellari di acciaio distaccate lungo piani paralleli alla superficie. Un' osservazione più approfondita con strumenti a maggiore risoluzione e

ingrandimento sarebbe stata utile per comprenderne meglio l'entità della corrosione e il tipo di prodotti di corrosione.

In conclusione , dai risultati ottenuti è risultata evidente la elevata resistenza da corrosione indotta da cloruri dell'acciaio Duplex AISI 2304, all'interno di strutture in calcestruzzo armato. Date le aspettative iniziali, le condizioni e i tempi di prova , quasi il totale dei provini ha mantenuto intatto lo strato passivante, dimostrato proprietà ottimali. Per quanto concerne il provino corroso, i risultati ottenuti dalla analisi hanno evidenziato l'elevata probabilità di un errore occorso durante la fase di fabbricazione dei provini, che ha condotto alla presenza di difetti all'interno della struttura in calcestruzzo, difetti che hanno favorito e accelerato la penetrazione dei cloruri nel calcestruzzo stesso. Tra gli sviluppi futuri, un test simile ma più aggressivo potrebbe definire in maniera esatta le tempistiche e le condizioni necessarie alla corrosione da cloruri per un acciaio Duplex 2304.

Chapter 1

Introduction

In the last decades, a great number of infrastructures have been made of Reinforced concrete (RC) , by using a combination of steel and concrete. According to some estimates, every year more than two billion tons of RC is being used to build structures all over the world [1].

However, several risks of RC structures deterioration can affect their own service life in terms of sustainability, economy and, most of all, safety . The society usually supports the structures maintenance and repair, but their costs are enormous. Many cases of constructions collapses have been occurred during the passing of the years, because of corrosion. In the figure below three different cases of bridges collapses, due to corrosion or to other processes combined with corrosion.

Figure 1.1: *a) Silver bridge collapse (1967) [1] ; b) Taiwan bridge collapse (2019) [2]; c) Morandi bridge collapse (2018) [3]*

Among different mechanisms of corrosion affecting the structures worldwide, chloride-induced corrosion has been reported as the most serious and common issue for the durability of the RC structures themselves, in particular the ones exposed to marine/coastal conditions. In environment exposed to high concentrations of chlorides, the temperatures variations added to external humidity can lead to the development of hydration-dehydration and expansion-contraction cycles, resulting into reinforcement corrosion initiation and propagation until the loss of the entire RC structure load bearing capacity.

1.1 Corrosion

Corrosion is one of the main causes of deterioration of materials, due to chemical reactions activated through contact with the environment [5].

Generally, metals are the most frequent materials affected by corrosion but, in any cases, even non-metallic materials (as plastics and concrete) can be wasted by it.

Concerning with the process affecting metallic materials , it's well known that corrosion consist of electrons transfer reactions: uncharged metal (*M*) atoms lose their electrons (one or more) and turn into charged metal ions (M^+):

$$\mathrm{M} \leftrightarrows \mathrm{M}^+ + \text{electron} \tag{1}$$

According to the environment, corrosion can be divided into three main types:

- Wet corrosion: is the most common way. It's an electrochemical process occurring on metals surface exposed to wet/aqueous environment.
- Dry corrosion: process in which the metals/alloys are in contact with air or other gases, which could be aggressive.
- Corrosion in other fluids: metals/alloys in non-aqueous ambient (e.g. molten salts)

1.1.1 Electrochemical corrosion

Electrochemical dissolution represents the main mechanism involved in the complex corrosion process of metals. This is one of the most important causes of metal loss, microbiologically

induced corrosion, pitting and in some parts of stress corrosion cracking [5]. In aqueous systems, or in other ones where there is the presence of an electrolyte, corrosion results to be an electrochemical process. An idea of the different reactions occurring in this is shown in the figure below (*Figure 1.2*).

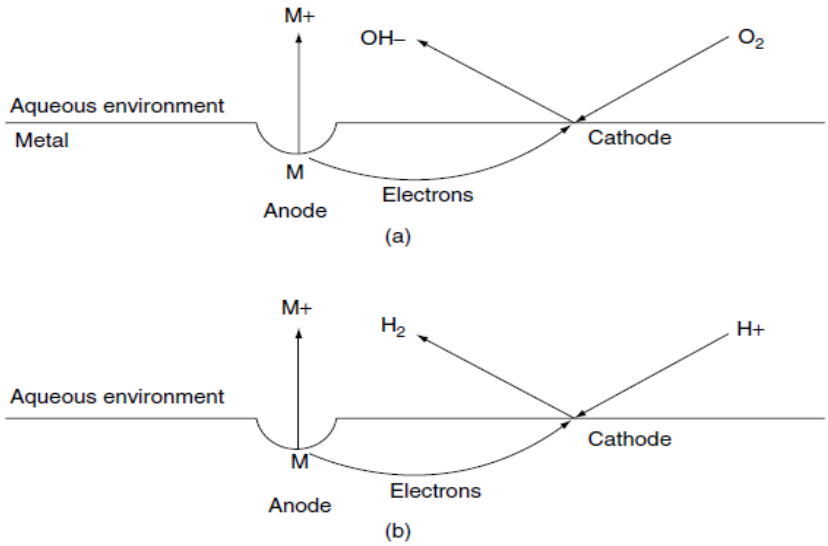

Figure 1.2: *Electrochemical reactions occurring onto the metal surface in aqueous environment; a) reaction with oxygen; b) reaction with the hydrogen [5].*

In this systems, the anodic reaction must be electrically balanced by the cathodic one, since electrical charge can't increase in any places. Here the necessity to keep a continuous electrical circuit through the metal and the environment

The different potential energies between the metal atoms present in the solid state and the elements produced during corrosion can be considered as the principal driving force of the process itself. For this reason, corrosion and extractive metallurgy can be seen as two opposite phenomena.

As known, a certain energy is required to obtain a metal from the ore (an oxidized form) ; the higher the energy, the more the metal is thermodynamically unstable and the higher is its trend to return to an oxidized form.

Therefore, metals which are found native as gold are able to resist to corrosion. Other elements existing in nature only in combined forms (as oxides or sulphides), if reduced to metals, they attempt to return to their initial combined form: it's the case of aluminium, iron and the most of the metals.

Four main elements to the corrosion chemistry of the solution are required:

1. An electrolyte (in the form of dissolved ions) has to exist, in order to make easier the passage of an ionic current in the solution.

2. Certain anions, especially chloride and sulphides, can penetrate the protective films present on some metals surface, giving rise to the corrosion process (in particular to a localized corrosion).

3. The pH of the solution is , on the one hand, a way to measure the availability of H^+ ,one of the most important cathodic agents. On the other hand, It can also determinate whether the metals will have an active or passive surface.

4. Dissolved oxygen (and even water) can make certain metals (as aluminium and stainless steels) resistant to corrosion, promoting the formation of a passivation coating. But, as oxygen is a very strong cathodic agent, it can also encourage corrosion in several metals (as iron and zinc).

Generally, as described in the system in *Figure 1.2*, corrosion will always occur for all those metals which are thermodynamically not stables with regards to their dissolved ions in the solution [5].

The corrosion rate is determined by many factors:

- The conductivity of the environment: a low conductivity can hinder the ionic current flow. That's why distilled water is considered less corrosive than a NaCl solution with the same pH and concentration of dissolved oxygens.

- The presence of cathodic elements, such as dissolved oxygen and H^+. These can promote metal corrosion in electrolyte solutions.

- The quantity of cathodic agents on the metal surface. It can regulate the overall corrosion rate, by diffusion processes.

- The construction of any deposits on the metal surface, obstructing corrosion. They may be adherent or not to the surface, the higher the adhesion, the greater their effect. Other

deposits can form, in addition to corrosion products. If the coverage is complete, the surface corrosion is mostly prevented, as the cathodic reactions cannot occur. Despite this, some cathodic elements (e.g. (Fe_3O_4)) and some iron sulphides can promote the cathodic reaction, resulting in a pitting corrosion.

- The temperature. Generally, an increase in temperature lead to an higher corrosion rate. This happens for chemical-kinetic processes and can be overridden by some physical effects, as the deposition of scales on the surface.

In *Figure 1.2* there are two main regions: the anodic and cathodic one.
The anode is the region in which the metal atoms are ionized, releasing n-electrons:

$$M \rightarrow M^{n+} + ne^{-} \tag{2}$$

This reaction proceeds significantly only if these liberated electrons are consumed by cathodic reactions, which can be commonly defined by:

$$O_2 + 2H_2O + 2e^{-} \rightarrow 4OH^{-} \tag{3}$$

where oxygen is consumed, as shown in *Figure 1.2a* , and

$$H^{+} + e^{-} \rightarrow H\ (\text{atoms}) \rightarrow H_2\ (\text{gas}) \tag{4}$$

in which hydrogen is released (*Figure 1.2b*).
The relative amounts of O_2 and H^+ available in the system, and their different kinetics of reduction on the material surface will say which of the two separate cathodic reactions is favourite for a particular combination of metal-environment.
Thermodynamically , the corrosion process occur because of the corrosion potential assumed by the metal while corroding. This potential is usually measured with the help of a standard reference electrode. The corrosion potential of different application materials are shown in *Table 1.1* [5].

Metal	Corrosion potential (V)
Aluminium alloys	-0.8/-1.0
Bronzes (Si, Sn)	-0.35/-0.25
Copper	-0.35/-0.2
Magnesium and alloys	-1.6
Nickel	-0.15
Steel	-0.55/-0.75
Stainless Steels (316,321)	-0.5
Stainless Steels (410,430)	-0.3/-0.2
Titanium	0/-0.1

Table 1.1: *Galvanic series in sea water [5].*

The table above is very useful to understand which type of corrosion would affect the materials, depending on the value of their corrosion potential. As shown in the list above , stainless steels appear twice. In relation to their potential, the mechanism of corrosion can change between different types of stainless steels.
The different mechanism of corrosion will be treated in the following paragraphs.

1.1.1.1 Pitting

Pitting is the name given to a localized form of corrosion, in which certain cavities, or better 'holes', are formed in the material. This process is nowadays considered more dangerous than uniform corrosion [6]; actually a single narrow pit in the material can lead to the failure of the entire structure. Pitting in the materials is strongly dependent on the amount of aggressive species in the working environment and on the oxidizing potential. Moreover, it's very difficult to detect and treat, as in many cases the pits are covered by several other corrosion products.

Each pit can be cup-shaped or hemispherical and assumes different sizes and shapes, the most important of which are:

- Trough Pits

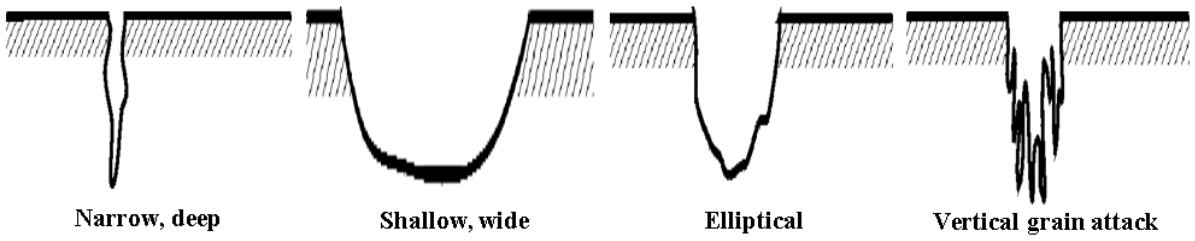

Figure 1.3: Types of trough pits [6].

- Sideway Pits

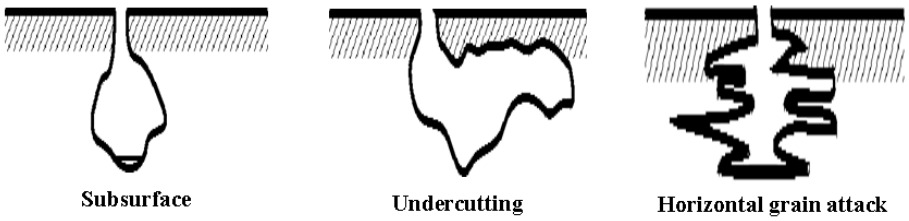

Figure 1.4: Types of sideway pits [6].

Pitting can be mainly provoked by:

1. Localized damage to the surface protective oxide film. The damage can be chemical or mechanical, caused by factors affecting the water chemistry such as high acidity, low concentration of dissolved oxygens and high chlorides concentration (e.g. in seawater).

2. Localized damage, or not uniform application, of an eventual protective layer.

3. Not uniform elements (as inclusions or defect in general) in the metal structure.

1.1.1.2 Crevice corrosion

Like pitting corrosion, this process mostly affects stainless steels. The first phase is marked by the generation of a crevice of suitable shape and dimensions. This crevice can be produced by manufacturing process , which can give rise to imperfections in the material, such as incompletely fused welds, O-rings, paint markings on surfaces ,and so on. Inside the crevice, the solution increases its acidity, while the metal surface becomes more and more anodic if compared to the bare metal all around. The initiation stage is truly depending on the crevice

geometry: a tighter crevice usually brings to shorter initiation time, as the main effect is to limit the oxygen inward diffusion to keep the passivity level high. The minimum crevice width leading to corrosion is the point corresponding to a watertight crevice [5].

1.1.1.3 Galvanic corrosion

Galvanic corrosion is the result of a metal contacting other metal in a corrosive medium [7]. A current, named galvanic current, starts to flow between two dissimilar conducting materials are in electrical contact in the same electrolyte environment, because of the potential difference between two metals: the more reactive metal is corroded, reducing the less reactive metal corrosion rate. An example of this phenomenon is shown in the figure below (in the case of aluminium and copper).

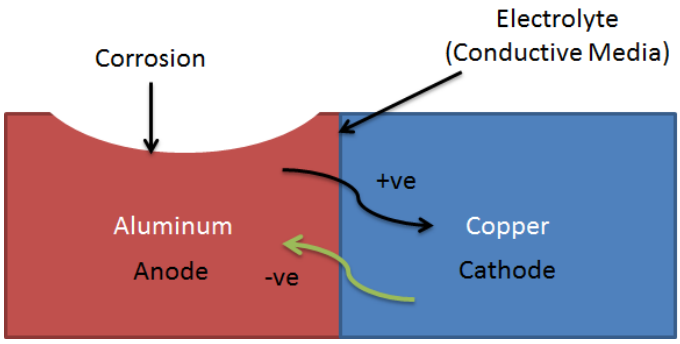

Figure 1.5: *Galvanic corrosion between Aluminum and Copper [8].*

The corroding metal is the one with the most negative corrosion potential between those of the galvanic series, where the corrosion potential is temperature strictly dependent. The corrosion can affect a small part at the interface between the two metals or spread throughout a more extended region, depending on the potential difference between them and of the environment conductivity; the intensity of the attack is instead due to factors as the their exposed area and the extension of the conductance path.

A possible solution to galvanic corrosion is represented by the use of electrical insulating materials , or in some cases, by the increase of electrical resistance between the materials, in order to reduce the corrosion current [7]. In other situations, it's better to paint or coat the cathodic metal , but not the anodic one, as this could lead to a faster corrosion in case of failures in the coating.

1.1.1.4 Stress corrosion cracking (SCC)

SSC is the conjunction of a tensile stress and corrosive environment. In many cases, these two conditions are accompanied by another metallurgical one , which is responsible for the initiation and propagation of cracks with high aspect ratio. The SSC failures are usually not predicable, as they can occur in any time, ranging from few months to several years of efficient service by the structures. In the figure below are described the different conditions, by which SSC occurs [9].

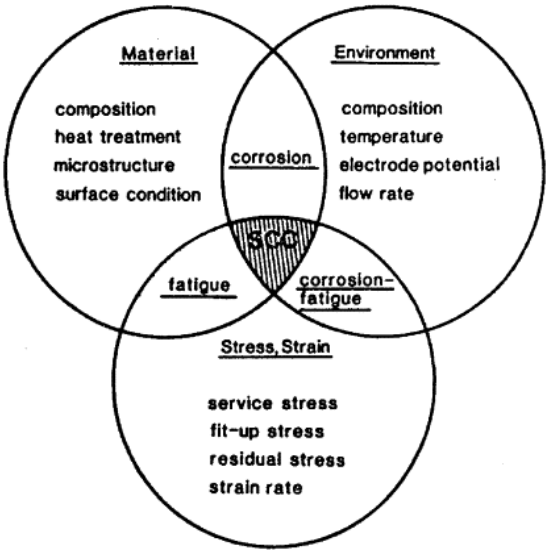

Figure 1.6: Simultaneous conditions for SCC to occur [10].

1.1.1.5 Corrosion fatigue (CF)

Corrosion fatigue is the result of the exposition of metals to cyclic stresses in a corrosive environment. This process is very similar to SCC with the difference that the stress is cyclic and that CF does not need a specific corrosive environment . In fact, in many cases moist air is enough to cause failures in the structures. The cycle of alternated stresses can only require a relative small tensile stress, as in the situation where CF occurs, this small stress in several cycles could be sufficient to break-up the entire system.

1.2 Reinforced concrete

Reinforced concrete (RC) is a composite material, made up of two main components (*Figure 1.7*):

a) a concrete matrix

b) reinforcement bars

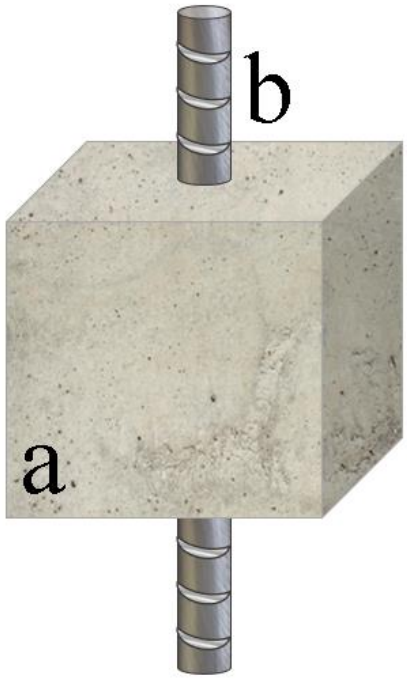

Figure 1.7: *Reinforce concrete section.*

in which the concrete matrix provides a low tensile strength and high ductility, while reinforcements give an higher tensile strength [11]. In the most of the cases the reinforcement is represented by steel reinforcing bars, or rebars, which are commonly embedded in the concrete before its solidification.

In a concrete structure, the reinforcing steel is able to adsorb the tensile, the shear and, in any cases, even the compressive stresses.

Nowadays , reinforced concrete includes a large number of reinforcing materials, from steels to polymers or an alternation of rebars and composite material. In order to improve the final behaviour of the structures under high working loads, reinforced concrete is usually permanently stressed (concrete kept in compression, reinforcement kept in tension), so as to

improve the behaviour of the final structure under working loads. In the United States, the most common methods of doing this are known as pre-tensioning and post-tensioning [11].

For a construction made to resist to any kind of stresses and environmental forces with the passing of the time, the reinforcements need to show ,at least, a great number of different properties as:

- High relative strength
- Excellent toleration of tensile strain
- Very good bond to the concrete, regardless of moisture, pH and other similar factors
- Thermal compatibility, in order to not cause unacceptable stresses in response to changes in temperatures.
- Durability in the concrete environment, regardless of corrosion or sustained stresses.

In some situations in which reinforced concrete has to face with wet and cold conditions (e.g. in bridges, roads and many other structures that could be exposed to de-icing salt) may resist thanks to the use of corrosion-resistant reinforcement stainless steel rebar. Therefore, an additional protection for several applications can be provided by a good combination of materials in the concrete structure and an optimal final design.

1.2.1 Durability

The durability of a structure represents the ability to keep its initial purposes unchanged for a certain period of time (supposed to be relatively long), or for all its expected service life [12]. However, a regular inspection and maintenance is necessary even for those structure designed and built to get high durability standard. Hence, concerning with the final life cycle cost of a structure, the future need of maintenance and the continuous controls for monitoring the materials situations have to be taken into account.

The reinforced concrete deterioration can be due to the deterioration of the concrete itself, to the corrosion of steel reinforcing bars or can be the sum of either the effects. Here there are some possible causes of deterioration and their suggested solutions for concrete and reinforcement:

1. Deterioration of concrete is almost always due to chemical attacks (e.g. sulphate attack). To overcome and avoid any problems due to the attack by chemical agents are necessary:

   - Sulphate resistant or proper types cement can be used
   - Minimum cement content can be utilized
   - A proper water-cement ratio has to be selected for the final concrete
   - Protective coatings can be added to the concrete surface

2. Corrosion of steel reinforcements, which can be controlled by:

   - Protective covers for reinforcement
   - Minimum content of cement
   - Appropriate water-cement ratio
   - Possible compaction and curing
   - Using epoxy-resin surface coatings

Phenomena like chemical attacks, freezing, fire, abrasion and alkali-aggregate reactions are only a part of the possible causes ,which lead to the worsening of structures conditions. But actually, the concrete deterioration is not the most common problem. The two main serious problems are carbonation and chloride attack, which normally don't affect the concrete but the reinforcing steel, mainly causing its de-passivation and the final corrosion. In fact in most cases, it's the steel corrosion the major cause of cracking and problems in the concrete and the reason why the entire structure can fail [12]. This study is principally concerned with the durability of reinforced concrete structures, related to the corrosion of the reinforcements.

1.2.2 Corrosion in reinforced concrete structures

Corrosion of steel rebars embedded in concrete is the main cause of most of the break-down occurred in concrete structures [13]. In the past , carbonation was the most serious problem, but in the recent years, chloride-induced corrosion has become more and more important for those structures permanently exposed to high chloride concentration environment.

Generally, different forms of corrosion can develop in concrete reinforcements, from general and widespread corrosion to very local attacks and pitting. The first type usually leads to cracking and spalling in the concrete and to the steel bars cross-section reduction (*Figure 1.8a*); the second type results in randomly localized pits along the steel rebars (*Figure 1.8b*).

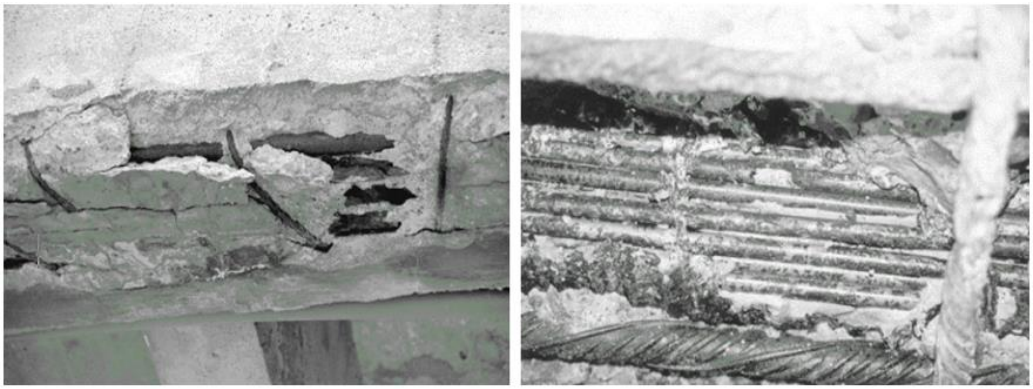

Figure 1.8: *Corrosion of RC bridges girders; a) Concrete spalling because of carbonation or chlorides; b) high corroded steel wire because of chloride-induced corrosion [13].*

Thanks to the great alkalinity in the concrete (pH > 12.5) , it's promoted the formation of a protective Fe_2O_3 layer (5-10 nm) (*Figure 1.9*) on the steel surface, reducing any corrosion risks. Despite this thin oxide film prevents metal from dissolution, it can only make the corrosion process slower but cannot stop it at all:

- with the passive layer steel corrosion has a rate of typically 0.1 µm per year ;
- without the passive layer, the steel mostly corrodes almost 1000 times faster [13].

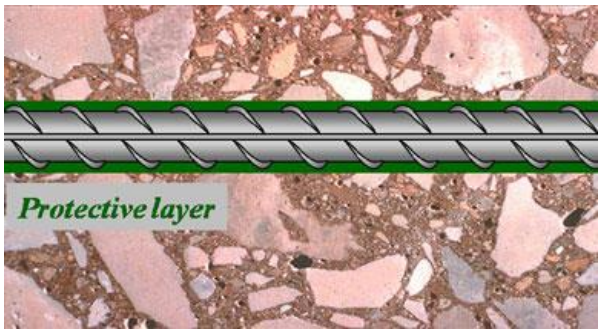

Figure 1.9: *Oxyde thin film on the steel surface inside concrete [14].*

Indeed, there are two main processes by which the protective layer can be destroyed:

- Carbonatation of concrete
- Chloride attack

1.2.2.1 Carbonatation of concrete

The carbonatation is the effect of chemical reactions between the alkaline components in the cement paste and the atmospheric CO_2 [15] .

$$2NaOH + H_2O + CO_2 \rightarrow Na_2CO_3 + 2H_2O \quad (5)$$

$$2KOH + H_2O + CO_2 \rightarrow K_2CO_3 + 2H_2O \quad (6)$$

$$Ca(OH)_2 + H_2O + CO_2 \rightarrow CaCO_3 + 2H_2O \quad (7)$$

The reactions can only occur in presence of water (in many cases in the form of moisture) , it leads to a reduction in the concrete initial pH (from 12-13 to values between 6 and 9), so that the cement paste can no longer provide a passive protection for the steel rebar.

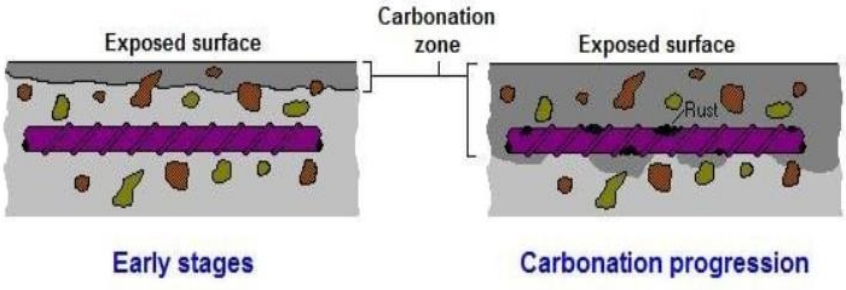

Figure 1.10: *Carbonation main stages [15].*

In order to make the carbonation occur, the best condition is to have an sufficient moisture content for activating the different reactions, but not high enough to act as a barrier to the carbonatation itself [15].

After a complete carbonatation process, the final pH value will be the result of different acting factors:

- Alkali content in the cement
- Cement degree of hydration
- Moisture content
- CO_2 partial pressure
- Temperature

The extent of carbonation is enormously increased in concrete with a low cement content (higher water/cement ratio), low strength , high concentration of pores. Carbonation of concrete can also reduce the chloride ions content needed to activate corrosion. In the newest concretes with a very high pH (12-13), a chlorides amount of 7000-8000 ppm is required to start corrosion in the steel, but if the pH is lowered to 10-11 by carbonation, the final chlorides threshold reveals to be lower (about 100 ppm). At the end, carbonation is a relative slow process (e.g. for high-quality concrete, its rate has been assessed to be maximum 0.04 inches per year). Corrosion induced by corrosion usually affect those building facades with a very poor concrete cover over the steel , permanently exposed to water (i.e. rainfalls) and shaded by sunlight [15].

1.2.2.2 Chloride attack

Chloride ions are the primary causes of corrosion in steel reinforcement [13]. The combination of these ions, greatly present in de-icing salts and seawater environments, with moisture and oxygen can be lethal for different structures and applications. According to the literature, there is no other contaminant as dangerous as chloride ions, in terms of corrosion.

Chlorides penetrate the concrete by capillary suction, reaching the reinforcement through sound or cracks. Generally, the process finally results in different chloride profiles in the reinforced concrete; chloride has four principals negative effect in the structure:

1. It is the main responsible of the protective layer break-down on the rebar.
2. It provokes the reduction of pH in the pore water, since it lowers the $Ca(OH)_2$ solubility.
3. It increases the moisture content in the structure.
4. It increase the electrical conductivity in the concrete.

But not all the chlorides are dangerous.

There are chlorides which are not freed to move in the concrete, as they can bound to the cement matrix, and this capacity depends on the mineral additions and the type of matrix as well. Despite this, these chloride can be released at any moment, starting to be a danger for the structure (e.g. in case of carbonatation and consequent reduction in pH). During the years, several analysis have been made, in order to find the exact chloride of content which can start the corrosion in concrete, leading to an important research work (Hunkeler et al.,2000) [13]. Thanks to the values obtained, it has been possible to assess the concrete structures condition and to repair any kind of damage in time. Now a draft European standard (*CEN 2003*) involved in the determination of the chloride amount in hardened concrete exists.

Critical Chlorides content for corrosion

As it's well know , in environments where the chloride concentration is high , the probability of pitting or chloride-induced corrosion is high as well.

The chloride threshold value represents the chloride ions content on the steel bars over which the corrosion process can be initiated. The threshold cannot be assessed as a single constant value , since it mostly depends on many factors, among which the concrete quality, moisture content, the oxygen availability and the pH in the structure. However, in recent years several researches have been carried out, in order to obtain the major number of information about this specific corrosive process, and in 1969 Richartz [13] found a chloride critical value of 0.4% in respect to the mass of cement present in the system. In the wake of this research, many others have moved in that direction, coming to estimate the relations between the chloride concentration (by mass of cement M%) and the risk of corrosion in this way [13]:

- Low corrosion risk : < 0.2 M %
- Medium corrosion risk: 0.4 M%
- High corrosion risk: >1.0 M%

Chloride concentration and corrosion initiation can be evaluated by several separated measuring methods, such as half-cell potential technique, EIS (*Electrochemical Impedance Spectroscopy*), macro-cell current monitoring technique or LPR (*Linear Polarization Technique*).

Chlorides Profile evaluation

Service life prediction of RC structures in high chloride content environments can be achieved, by analysing the different chloride profiles as a function of the time passed and the depth of penetration in the structures themselves [13]. Until 1990, every service life prediction model was erroneously based on the Fick's second diffusion law. But, after a very high number of newest analysis, scientists decided to correct the model, by incorporating an error function in the equation, resulting as:

$$C_x = C_s \cdot \left[1 - erf\left(\frac{x}{2\sqrt{D_{eff} \cdot t}}\right)\right] \tag{8}$$

Where:

C_x= chlorides content at depth x (% of concrete weight)
C_s = surface or near surface chlorides content (% of concrete weight)
erf = error function
D_{eff} = effective chloride diffusion coefficient (m^2/s)
x = depth (cm)
t = time passed (s)

Chlorides ingress in the matter is not properly a diffusion process. Moreover, It must be said that the chlorides diffusion coefficient is not a constant value in the reality, but it can vary, depending on different factors as the moisture content, time and depth [13]. Although this equation is not the perfect mirror of the complex phenomenon related to chloride penetration, it's very useful in the design of RC structures. A typical curve representing the chloride profile inside the material at a given time is shown in *Figure 1.11*.

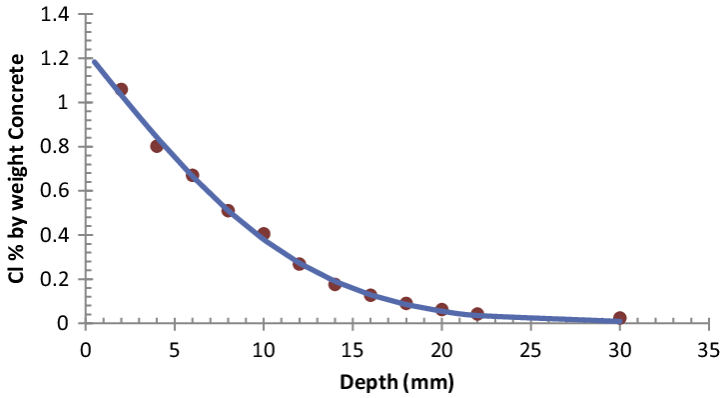

Figure 1.11: *Example of Chlorides concentration profiles in RC at a given time [16].*

1.2.3 Service life prediction for RC structures

The structure service life is the period of time in which the structure itself keeps acceptable conditions as concern its functionality, resistance, safety and appearance. Since it's not easy to continuously monitor the conditions of structures , several models have been formulated to estimate residual service life in the structures, one of the most relevant is the Tuutti's model [17]. In the figure below the model is described, by associated each corrosion process stage to the possible phenomena occurring in the RC structure.

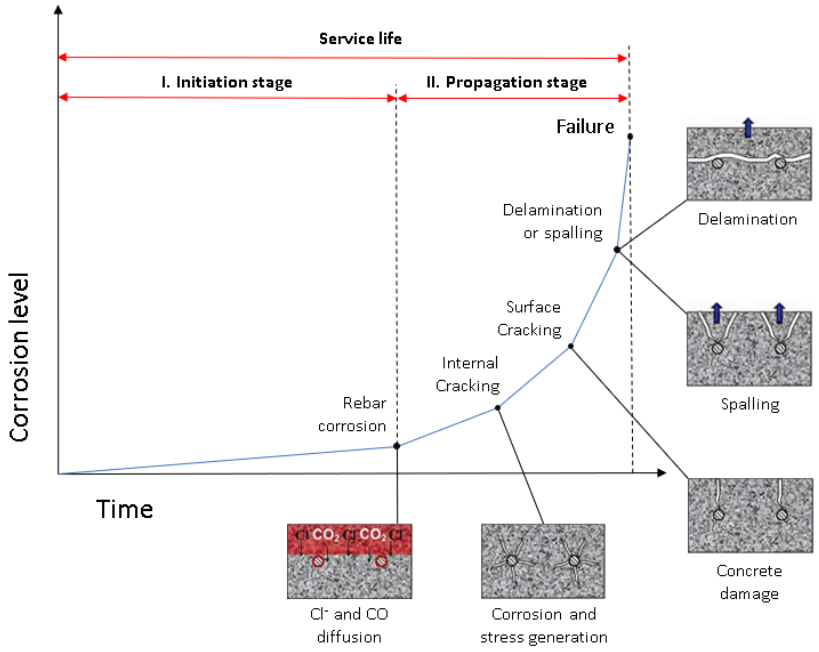

Figure 1.12: *Service life model by Tutti (1982).*

Tuutti's model divides RC structures service life in two stages:

I. Initiation : time required for CO_2 or Cl^- to penetrate the concrete, reaching the steel rebar level and initiating the corrosion process. At the time zero, the steel keeps passivated thanks to the concrete alkalinity. During the period of initiation, steel rebars could be affected by depassivation because of several factors such as the concrete deterioration, the penetration by aggressive elements.

   The initiation period can vary according to:

   - Cracks formation
   - Aggressive elements content

- Critical chlorides concentration
- Concrete cover condition
- Working external conditions
- Aggressive element penetration rate

  The latter strongly depends on concrete type and the water-concrete ratio, which depends on the concrete porosity: the higher the porosity, the higher the rate of penetration by aggressive elements.

II. Propagation: time elapsing between the starting of corrosion and the final limit of concrete deterioration, which correspond to the end of the structure service life. This stage starts when the steel gets a permanent depassivation and it's characterized by a large increase in the corrosion rate. The total propagation period depends on the same factors of the initiation one; furthermore temperature, relative humidity and oxygen content can accelerate reinforcement corrosion.

Tuutti's model provides information about the structures service life, by linking the reduction in the steel rebar section with the deterioration index in the structure. C.Andrade et al.[18] were the first to quantify the Tuutti's model, by assessing a relation between the corrosion rate found with the Linear Polarization technique (LPR) and the section reduction. But their studies were developed prevalently on carbon steels. Since nowadays stainless steel are more and more used as reinforcements in the concrete structures, this model need to be extended to a wider range of experimental cases.

1.3 Stainless steel

Stainless steel (SS), or inox steel, is currently one of the most applied materials. Its composition is characterized by at least the 11% of chromium content by mass and a carbon concentration not over the 1.2%. The great amount of chromium provide this material a very high resistance to corrosion: the higher the chromium content, the stronger the steel. Furthermore, additions of molybdenum can make the material more efficient in reducing acids and more resistant in case of pitting in high chloride concentration solutions. By varying chromium and nickel contents it can be made different types of stainless steel , in order to suit the environment conditions.

Stainless steel can be fabricated in different forms: sheets, bars, tubes, plates, wire. Its resistance to corrosion, combined with the common steel mechanical properties , makes Stainless Steel an ideal material for several applications, ranging from construction field to surgical instruments, from industrial equipment to chemicals and food products and many others.

1.3.1 Brief history

The French metallurgist Pierre Berthier was the first man to recognize the corrosion behaviour of iron -chromium alloys in 1821, since he assessed their great resistance to acids and their possible use in cutlery. But during that time, metallurgists were only able to produce very brittle materials cause it was impossible for them to combinate in the best way low carbon and high chromium content in a single material. Only in England in 1872, John Clark and John T. Woods patented an alloy resistant to water, today known as stainless steel. Several other steps forward were made in the following decades: the German Hans Goldschmidt developed a process for the production of carbon-free chromium around 1890. In 1908, a chrome-nickel steel sailing yacht named Germania was built by Friedrich Krupp Germaniawerft. Philip Monnartz was one of the first to realize a report, dealing with the strict relationship between materials corrosion resistance and their chromium content in 1911. One year later, Krupp engineers patented for the first time an austenitic stainless steel known as Nirosta.

Contemporaneously, on the other side of the world in United States, Frederick Becket and Christian Dantsizen industrialized the first ferritic stainless steel. The first patented martensitic alloy came to life in Sheffield ,England, in 1912, when Harry Brearley discovered and produced it, trying to seek an alloy for gun barrels. Only in 1919 the martensitic alloy reached the US, where Elwood Haynes obtain the patent after a real struggle begun in 1912. At the end, Haynes and Brearley formed with other investors the American Stainless Steel Corporation, headquartered in Pittsburgh, US.

At the beginning, stainless steel alloys were sold under different brand names, among which *Nirosta steel* and *Allegheny metal*. Before the Great depression affecting the world in 1929, over 25000 tons of stainless steel were sold in the United States. By the ‘50s the technological advances, such as AOD process and continuous casting, made possible the production of greater

amounts of materials at more affordable costs. The final progress has been due to the introduction of computer controlling processes in most recent years [19].

1.3.2 Traditional Manufacturing process

The entire manufacturing process [20] of stainless steel involves a series of singular steps:

1. Melting and Casting
2. Forming
3. Heat treatment
4. Descaling
5. Cutting
6. Finishing
7. Manufacturing at the fabricator or end user
8. Quality control

Melting and casting

The whole process starts with the melting of the raw materials in an electric furnace, requiring a time between 8 and 12 hours.

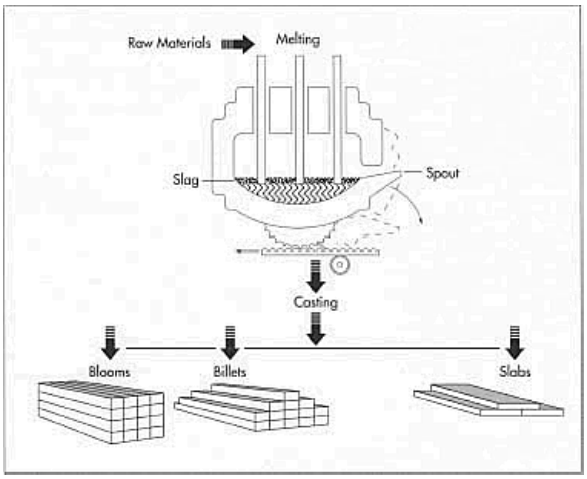

Figure 1.13: *Melting and casting scheme [20].*

After the melting, semi-finished forms are casted by the melted material, including many different shapes and dimensions [20]:

- billets (square or round)
- blooms (rectangular)
- wires
- slabs
- tube rounds
- robs

Forming

The semi-finished products withdraws a series of forming operations, starting with hot rolling. During this step, heated steel is passed through very huge rolls, in order to turn the blooms and billets into bars and wires while slabs into plates, sheets and strips [20]. Here is a table containing the main possible sizes for each shape:

Available form	**Available sizes** (cm)
Bars	$\simeq 0.63$
Wires	< 1.27
Plates	> 0.47 (thick) , > 25.4 (wide)
Sheets	< 0.47 (thick) , < 61 (wide)
Strips	< 0.47 (thick) , > 61 (wide)

Table 1.2: *Available forming shapes and sizes for SS [20].*

Heat treatment

This stage is not always present, but most of the formed product is subjected to an annealing step [20]. The latter is an heat treatment used to soften the material and relieve any kind of internal stresses, by alternating cycles of heating and cooling under controlled conditions. This step could be critical and it's important to have a deep control of every treatment parameters, such as temperature, time and cooling rate. For example, in one of the most applied treatment, known as *age hardening*, a very small change in one of the previous parameters can produce non-reversible effects on final material properties: lower aging temperatures can lead to an higher strength and lower fracture toughness, while higher aging temperatures can give rise to a tougher material with lower strength. Unlike the cooling one, the heating rate doesn't

have significant effects on the properties The toughness could be increased by a rapid cooling (Post-aged quenching) and a successive water quenching in a 1.6 °C ice water bath for at least two hours. Different types of steel can undergo different kinds of heat treatments.

Descaling

The scale produced on the steel by the annealing step can be removed by many processes [20]. Pickling is one of the most used one, descaling the steel by using a nitric-hydrofluoric acid bath. Electro-cleaning is another descaling step, by which the scale is eliminated by the application to the surface of an electrical current, built-up by a cathode and phosphoric acid. Depending on the type of formed steel, the separate steps of annealing and descaling can occur at different stages (*Figure 1.14*):

- Bars and wires usually undergo more than one forming step (combining hot rolling with forging or extrusion), between the initial hot rolling step and the annealing and descaling.

- Sheets and strips go through an annealing and descaling stage right after hot rolling step; then, they are subjected to a cold rolling (in low temperature rolls) , in order to further reduce their thicknesses, and annealed and descaled one more time. Finally, a new cold rolling step render the material ready to be processed.

- Plates commonly go through a shorter process, made up of finishing and final packaging, after the initial hot rolling.

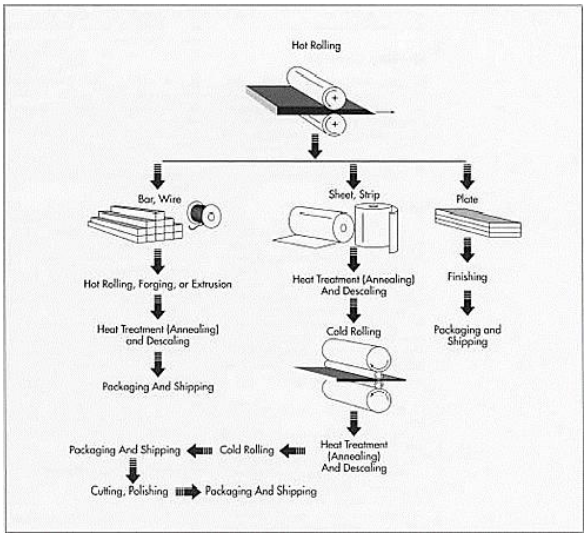

Figure 1.14: *Hot rolling stage and following different steps for SS [20].*

Cutting

This step is useful to obtain the final exact shape or size and can be done in different ways [20]:

- Mechanical cutting consists of an high variety of techniques, including:

    - circle shearing,
      which uses circular knives located horizontally and vertically;
    - straight shearing,
      which uses guillotine knives;
    - sawing,
      which uses high speed steel blades
    - nibbling,
      through which blanks out overlapping holes to cut formed products, in order to obtain irregular shapes
    - blanking,
      which obtains final shapes using metal punches and dies.

- Flame cutting, a fast and clean method, using a combination of oxygen and propane with iron powder to produce a flame-fired torch.

- Plasma jet cutting, using an electric arc combined with an ionized gas column passing through a very small hole. The metal is usually melted by the gas high temperatures.

Finishing

Surface finishing is the very differentiated step consisting of a great variety of methods, each one is suited for obtaining a particular surface finish . For instance, a combination of hot rolling, annealing and descaling produces a dull finish; a first hot rolling followed by cold rolling can produce a very bright finish; by combining cold rolling and annealing in controlled atmosphere furnaces and by grinding with abrasives, it's possible to produce highly reflective surfaces; mirror finishes are produced by polishing and large buffing. Many other finishing methods exist, including tumbling , sandblasting and wet etching which uses acid solutions [20].

Generally, this stage is necessary when the steel application requires a certain surface appearance. Furthermore, the finishing allows a better and easier surface cleaning, especially

important in the sanitary field. Commonly a smooth surface is suited for applications resistant to resistance, while a rough one is better for lubrification applications.

Manufacturing at the fabricator or end user

The stainless steel is not ready to be used after the packaging and shipping to the fabricator, but needs some other passages to achieve a further shaping, among which roll forming, forging, press forming, extrusion and press drawing. The process often require a further annealing, to be follow by machining and cleaning [20].

In most of the cases, then steel have to be joined. Welding represents the most common way to do it and can be divided into two basic methods :

- Fusion welding,
  in which heat is supplied by an electric arc generated between a specific electrode and the welded metal.

- Resistance welding,
  in which heat is supplied by the resistant to the electric current flow in the different parts to weld. In this case, bonding results from combination of pressure and heat.

Welding stage usually need a final cleaning in proximity of the joined area.

Quality control

Besides the on-line control monitoring during the different manufacturing stages, Stainless steel is usually subjected to the final quality control, in order to assure certain correct properties given by the *American Society for Testing and Materials* (ASTM). These are generally related to mechanical properties as fracture toughness or resistant to corrosion [20].

For instance, metallography can be used to help monitor quality, especially in corrosion test.

1.3.3 Types of Stainless Steels

The different SS microstructures are strictly affected by their distinct composition [21]. Since these systems are very complex to analyse, there have been introduced some simplified

relations, the most famous of which is represented by the Schaeffler-Delong Diagram (*Figure 1.15*)

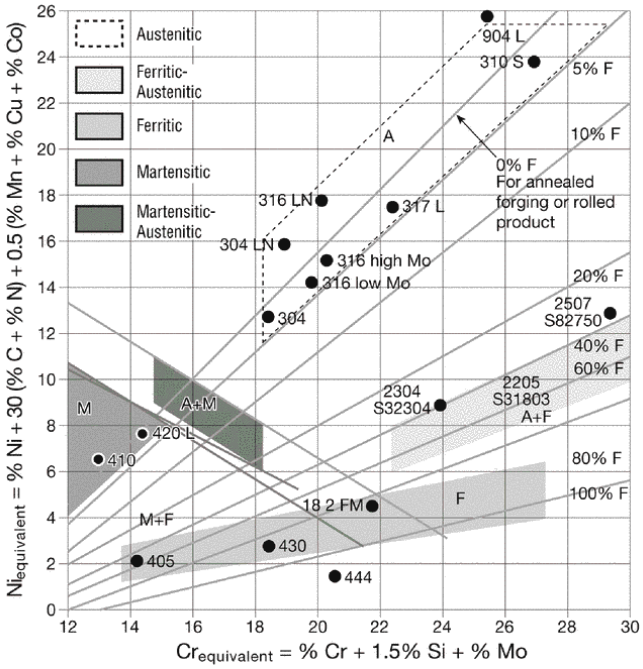

Figure 1.15: *Schaeffler-Delong Diagram for SS [22].*

By a real approximation, it can be possible to forecast the final material phases, by accurately choosing the alloys elements , as they can be stabilizers of a BBC structures (included in Chromium equivalent calculation) or stabilize a FCC structures (included in the Nickel equivalent calculation) :

$$\%\ Cr_{equivalent} = \%\ Cr + 1.5 \cdot Si + \%\ Mo \tag{9}$$

$$\%\ Ni_{equivalent} = \%\ Ni + 30\ (\%\ C + \%\ N) + 0{,}5\ (\%\ Mn + \%\ Cu + \%\ Co) \tag{10}$$

Stainless steels are commonly divided into 5 distinct classes, according to different alloying elements and to their respective contents, which influence their microstructure :

1. Austenitic stainless steels
2. Ferritic stainless steels
3. Martensitic stainless steels
4. Duplex (ferritic-austenitic) stainless steels
5. Precipitation-Hardening (PH) stainless steels

PREN Index

Pitting Resistance Equivalent Number (PREN) is a theoretical index measuring the stainless steel resistance to pitting corrosion: the higher the index, the more resistant the material. PREN value is not constant but mostly depends on the steel composition and , with lower influence, by the working conditions.

There are several ways to calculate PREN index for a given steel , but the most common is the following:

$$PREN = 1\%Cr + 3.3\%Mo + 16\%N \tag{11}$$

In some variants, the amount of tungsten is added:

$$PREN = 1\%Cr + 3.3(\%Mo + 0.5\%W) + 16\%N \tag{12}$$

According to the type of application and the environment aggressivity, the selection of the steel with the most suited PREN value is made. Among steels with similar PREN value, the selection is usually made taking into account other materials properties such as physical ones, availability and costs. In the table below are listed the PREN index for the most common stainless steels.

Type	Grade (AISI)	PREN
Austenitic SS	AISI 304	18.1
	AISI 316	24.1
	AISI 317	28.4
Ferritic SS	AISI 409	11.5
	AISI 430	16.5
	AISI 436	21.6
Duplex SS	AISI 2304	25.6
	AISI 2205	35.0
	AISI 2507	42.5

Table 1.3: *PREN index for most common SS [23].*

1.3.3.1 Austenitic stainless steels

Austenitic SS are iron-chromium-nickel alloys .The most common ones show an FCC structure, thanks to which they can be applied in cryogenic and high Temperature systems .They are characterized by high Chromium and Nickel content, providing excellent corrosion resistance and good mechanical properties. The hardening step is not usually achieved through heat treatment, but through cold-working. No austenitic SS is magnetic [22].

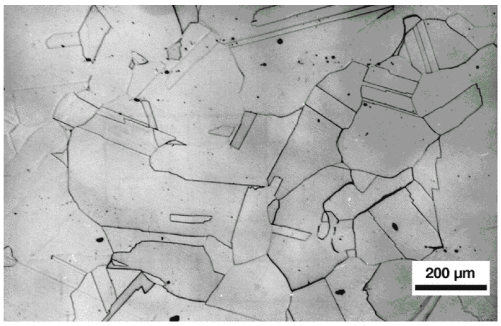

Figure 1.16: *1.4439 Austenitic SS microstructure [22].*

They are commonly divided into three main grades:

- Standard Grades **:** maximum of 0.8% in carbon, no minimum carbon content required.
- Low Carbon Grades (or L Grades) **:** maximum of 0.3% in carbon, in order to avoid any carbide precipitations and to provide better behaviour in corrosion conditions. The most applied ones are 304L and 316L.
- High Carbon Grades (or H Grades) **:** minimum of 0.4% and maximum of 0.1% in carbon. The higher content of carbon provides higher strength at in a wider thermal range, thus they are mostly applied in extreme temperatures environments. The most common ones are:
  - Type 304: probably the most used one. High content of chromium and nickel give it a very excellent combination of fabricability, strength and corrosion resistance. Applied in many fields, even in those who requires special properties for food and beverage industries.

- Type 316: the combination of 18% in chromium, 14% in nickel and addition of molybdenum make it very resistant to corrosion. In particular, molybdenum can drastically reduce pitting attack. Resistant to very high T (up to 1600 F). Generally used in chemical and food processing ,paper industry, but also in the marine field, thanks to its corrosion resistance.

- Type 317: higher content of molybdenum(more than 3%) if compared to 316. It's applied in highly corrosive conditions and in particular devices for the air pollution controls.

- Type 321: addition of titanium (minimum five times the carbon concentration), in order to reduce or better eliminate chromium carbide precipitates, which could be formed through welding. Applied in the aerospace industry.

- Type 347: very high resistance to strongly oxidizing conditions. It's used in construction applications.

1.3.3.2 Martensitic Stainless Steel

Martensitic SS are iron-chromium alloys with carbon content higher than 0.1% .They are formed in carbon steels, by the quenching (rapid cooling) of the austenitic iron form, followed by an eventual tempering. The rate of the cooling is so high that carbon atoms have no time to form cementite (Fe_3C), leading to the formation of a BCC structure instead of the FCC most common one. Martensitic SS are made to be very hard and corrosion resistant; they have an high content of chromium and no nickel.

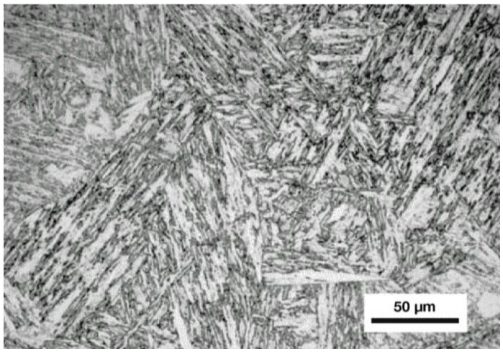

Figure 1.17: *AISI 410 Martensitic SS microstructure [22].*

They are used in all those application where the combination of strength, hardness and wear resistant is a priority [22].

The most common ones are:

- Type 410 : the most basic one, very poor alloy content, used for its low cost. It can be applied where the corrosion conditions are not so severe (air, water and food acids), and in parts needing a quite good combination of strength and resistance to corrosion (e.g. fasteners).

- Type 416 : additions of sulphur and phosphorus improve machinability. Commonly applied in screw machine parts

- Type 420 : increased content of carbon improves mechanical strength . Typically used in many applications, including surgical instruments

- Type 431 : increased chromium content improves corrosion resistance. Typically utilized in high strength components, as pumps and valves

- Type 440 : increased chromium and carbon content improve toughness and resistance to corrosion. As the 420 type, even this is mostly applied for surgical instruments.

All the grades are magnetic.

1.3.3.3 Ferritic Stainless Steel

Ferritic SS are iron-chromium alloys with a ferritic BBC structure in a great range of temperatures (up to the melting point). They usually present an higher chromium and lower carbon percentage if compared to martensitic SS, showing a better corrosion resistance but don't harden by heat treatment. They are mainly used for sinks and some automotive applications (e.g. exhaust systems) [22].

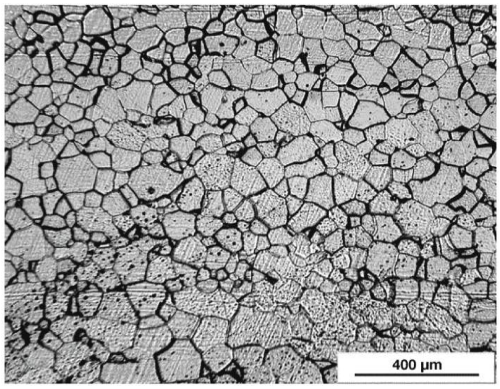

Figure 1.18: *AISI 409A Ferritic SS microstructure [22].*

Some of them are:

- Type 409 : very cheap SS with low content of chromium. Used in interior or exterior parts in not severe corrosive environment. A typical application is the muffler stock.

- Type 430: basic grade with acceptable corrosion resistance , especially in contact with sulfur gases, nitric acids, and several food acids.

- Type 436 : with addition of columbium for higher heat and corrosion resistance. Mostly applied in deep-drawn parts.

- Type 442: the increased chromium content provides a better scaling resistance. It can be used in heater parts and furnaces.

- Type 446 : further higher chromium percentage added to improve even more scaling and corrosion resistance at high T. Good behaviour in sulfuric environment.

1.3.3.4 Duplex Stainless Steels

Duplex SS are a combination of austenitic and ferritic material. Their final microstructure is the result of a balance of iron, chromium, nickel and molybdenum contents, resulting in almost equal volume fractions of austenitic and ferritic phase [22].

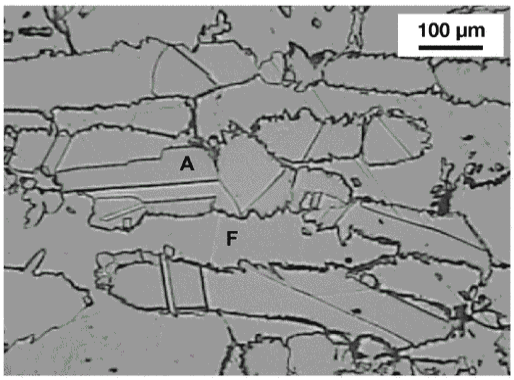

***Figure 1.19**: 1.4501 Duplex SS microstructure; A:austenitic zone, F:ferritic zone [22].*

These are high performance steels, as they combine in the same material the best properties characterizing the austenitic and ferritic steels: excellent strength, very good toughness, high resistance to corrosion in various media, good resistance to SSC and CF.

They must be welded carefully, in order to avoid the possible precipitation of embrittlement intermetallic phases (σ or χ).

Here the most applied ones:

- Type 2205 : the most widely used. Suited for facing with high corrosion and high pressure conditions, very resistant to erosion fatigue. It shows an higher thermal conductivity and lower thermal expansion with respect to austenitic steels. The only limitation is that it can't be used at T higher than 315°C for extended period, in order to not convert into a brittle material.

- Type 2304 : high corrosion resistance and double yield strength if compare to the more used austenitic steels (304 and 316), good resistance to SSC and excellent mechanical strength. Suited for use in thermal range between 50°C and 300°C. Optimal weldability and machinability. Mostly used in the same applications in which the austenitic 304 and 316 are used.

- Type 2507: super duplex SS. Exceptional strength and resistance to corrosion, it can withstand chloride stress, high thermal conductivity and corrosion cracking. It's highly resistant to general, crevice and pitting corrosion. Applied in petrochemical, chemical process and seawater equipment.

1.3.3.5 Precipitation-Hardening (PH) Stainless Steels

Ph stainless steels are alloys containing iron, chromium, nickel, molybdenum and other alloying elements which promote the low carbon martensite precipitation hardening , resulting in the formation of intermetallic compounds (e.g. aluminium, titanium, etc). By heat treatment, they can be hardened and strengthened, in order to achieve very excellent mechanical properties [22].

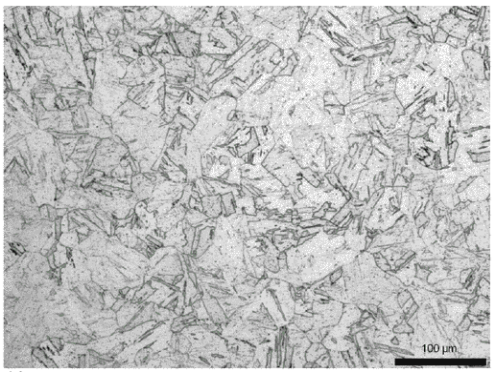

Figure 1.20: *AISI 630 PH SS microstructure [22].*

PH stainless steels are divided into three groups: austenitic, semi-austenitic and martensitic. The most common ones are:

- Type 17-4 : chromium-copper precipitation hardening stainless steel. High resistance to stress and good corrosion performances in different heat conditions, it can be treated in a great range of temperature, depending on its final purpose. It should not be used at very low T and T higher than 300°C.

- Type 15-5 : chromium-nickel-copper precipitation hardening martensitic stainless steel; greater toughness in respect to 17-4. Used in applications, generally requiring better properties if compared to common martensitic steels.

1.3.4 Stainless steel corrosion

Thanks to their high number of alloying elements, SS are more resistant to corrosion compared to the carbon steels; furthermore, they do not suffer uniform corrosion. Their high resistance

is mainly due to the presence of Chromium, which reacts with the oxygen to form a (Cr_2O_3 and $Cr(OH)_3$) protective film on the surface, a self-healing film in presence of O_2. Despite SS are not usually affected by general corrosion, stainless steel can be subjected to other kind of corrosion, among which the most dangerous is pitting corrosion described in the paragraph. In fact, pitting can seriously damage the SS protective layer , involving different corrosive reactions [5].

Figure 1.21 describes the evolution of pitting in an ideal stainless steels (as the austenitic 304 or 316).

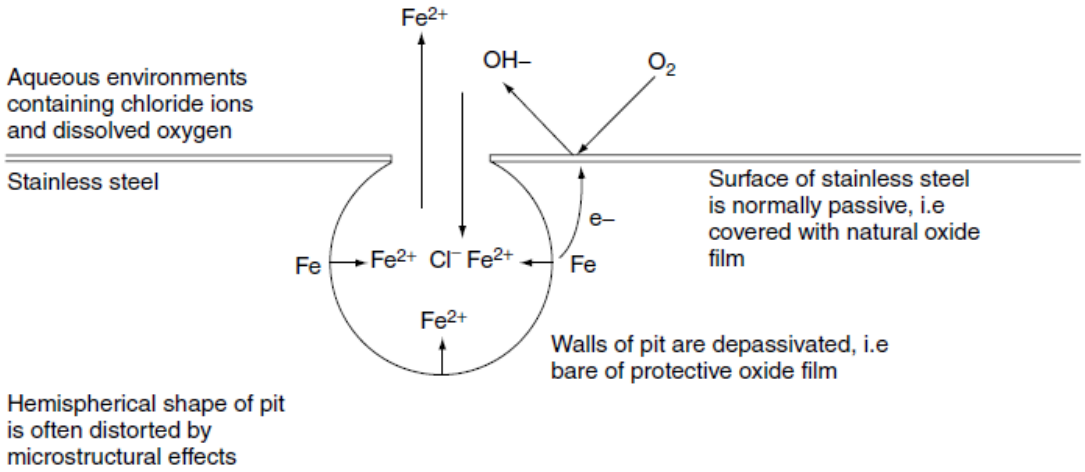

Figure 1.21: *Pitting mechanism for SS in chloride-containing environment [5].*

I. The first phase of pitting corrosion process is the initiation.

This phase can be pushed by oxidizing conditions. Starting on the metal surface in conjunction with an heterogeneity (e.g. a sulphide inclusion or any oxide film defects), pitting can take few seconds or weeks to develop, getting large enough to be called 'pit'. In the case described in the figure above, the chloride ions are the responsible of the localized attack, by raising the metal potential and conducting to the break-down of the protective layer.

II. Then, there is the propagation phase.

Oxygen can't diffuse into the pit region because of the geometry of the pit itself. This lead to the falling of the pH in the pit region provoked by the creation of a potential difference between this region and the rest. This difference can promote self-acidification in the pit, resulting in an increase of pit penetration rate with time.

III. Finally, the termination phase occurs.

The enormous amount of different insoluble corrosion products can stifle the pit at its mouth. It can finally restart to grow only if the big part of these products are removed or extracted through mechanical or chemical technique.

At the end, chlorides are the primary cause in the initiation of corrosion, but they are not so influent in the following steps, where other rate-controlling factors (as oxygens availability, electrical resistivity, pH, relative humidity and temperature) are more significant [5].

Chapter 2

Work starting points and objectives

2.1 Starting points

All around the world infrastructures are mainly built using RC structures, assuring safety and long-service performances. For those constructions permanently facing with humidity and different ambient conditions, Stainless Steel RC has always represented a good solution. Across several decades, many bridges and infrastructures have been projected and designed using common Stainless Steel, as they were well-know and provide good protection. Two of the most used SS in infrastructures are the austenitic SS AISI 304 (and 304L) and AISI 316 (and 316L). But nowadays they have to face with other more efficient alternatives: the Duplex stainless steels.

Duplex stainless steels (DSS) were originally developed by '30s of the XX century, even if at the beginning there were several problems in providing them good performances, as the metallurgical processes of the time were not perfectly suited for obtaining a balanced austenite-ferrite material. But in the period between 1960 and 1970, duplex steels finally found the right conditions to spread, thanks to the introduction of argon and vacuum oxygen decarburization processes (AOD and VOD), giving rise to very high performances steels, especially in terms of resistance to uniform and local corrosion, as well as to chloride stress corrosion cracking. Off-shore industries began to prefer duplex steel to austenitic ones, cause they not only were generally better in aggressive environment, but first of all because they were cheaper [24].

DSS 2205 was the first duplex to develop commercially by the German Krupp producer and still remains the most used duplex nowadays. As all the other duplex steels, the 2205 is mostly applied in the construction of :

2 oil transportation pipes
3 heat exchangers
4 Cooling pipes
5 Structural components

In recent years, thanks to their strength higher than carbon steels, DSS have been chosen to build civil structures in different part of the world as they commonly reduce structural sections sizes and weight. Here below two most famous instances. In 2010 , the engineering *Arup* society designed the Helix Bridge (*Figure 2.1a*), an high-strength 2205 DSS bridge in Singapore, in order to reduce the total structure weight, compared to a carbon steel choice. During the following year (2011) , *T.Y.Lin* designed the San Diego Harbor Drive Bridge (*Figure 2.1b*), one of the largest self-ancorched pedestrian bridge in the world with its 170 meters [25].

Figure 2.1: *a) Helix Bridge, Marina bay, Singapore [26]; b) Harbor Drive Bridge, San Diego [27].*

Both were fabricated by using DSS 2205.

But in some applications, 2205 DSS revels to have mechanical characteristics higher than needed. For this reason, more and more manufacturing industries have developed lean Duplex stainless steels with a lower content of alloying elements. Among these, Duplex 2304 has revealed to be the most interesting one.

Several studies have been carried out about the possible application of 2304 DSS in structures facing with corrosive environment, with special focus on the possible advantages of using this grade of SS instead of others more commonly applied.

The most relevant starting point is the work by Alicia Pachón Montaño et al.[28] of the Institute of Construction Science *Eduardo Torroja* (ETSII) in Madrid. In the work five different grades of stainless steel , among which two commonly applied austenitic stainless steel (AISI 304L, AISI 316L) and two Duplex stainless steel (AISI 2205, AISI 2304) had been compared in aggressive conditions. It had been simulated a modified chloride attack to each grade, in order to obtain data about the service life and chloride threshold. At the end, DSS revealed to be more

resistant than the austenitic ones: 2205 DSS proved to be the best in marine environment for their high performances, but 2304 DSS proved to be generally the best choice for the combination of performances and costs. In addition to this , according to the literature [29]:

- In the case of general corrosion, the 2304 steel behaves in a similar way as the 316L, as shown in *Figure 2.2*.

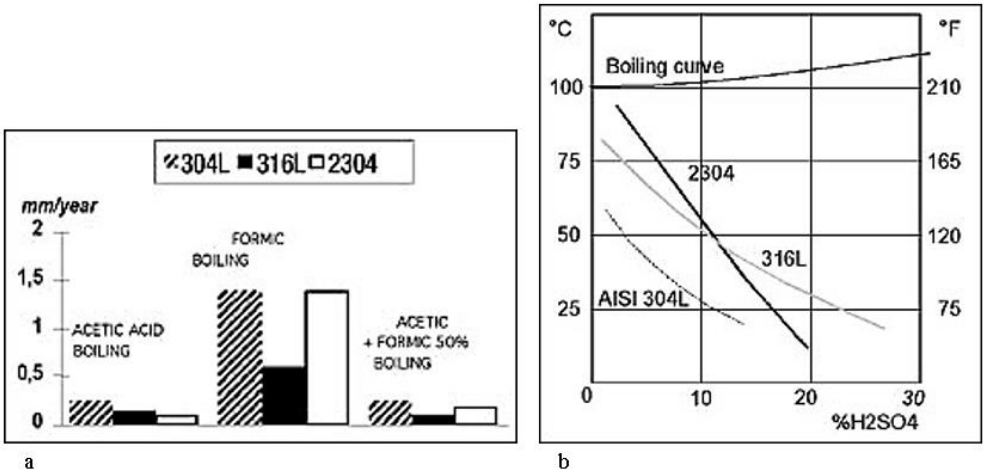

Figure 2.2: *a) Corrosion resistance in different acids; b) Corrosion resistance to sulfuric acid [29].*

- In the localized corrosion, Duplex 2304 reveals to be much better than the austenitic steels (316L and 304L), in terms of pitting and crevice corrosion resistance (*Figure 2.3*). The better resistance is due to the different amounts of Chromium (23%) and Nitrogen (1%) in the Duplex steel.

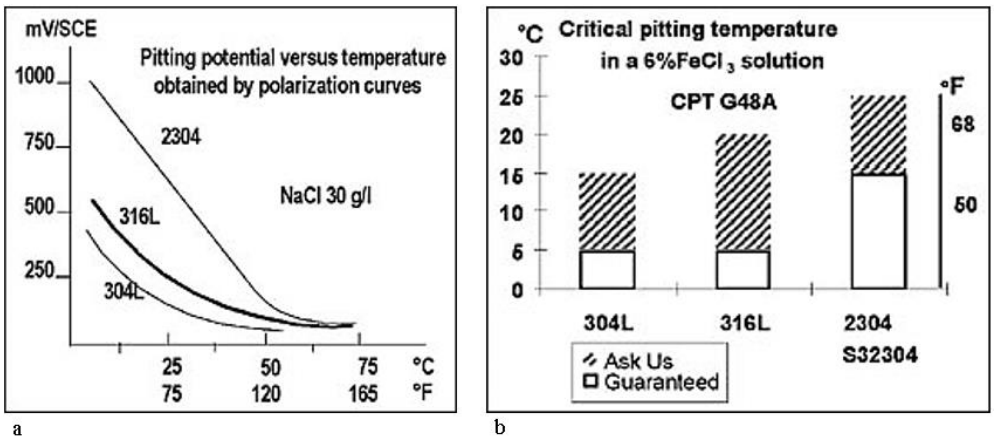

Figure 2.3: *a)Pitting Polarization curves in NaCl solution; b) Critical pitting T in 6% $FeCl_3$ solution [29].*

- For stress corrosion cracking in chloride containing solutions, tests (pH=7, t >1000 h, applied stress > yield strength) show that DSS 2304 outperforms austenitic 304L and 316L, thanks to high chromium and low nickel contents (*Figure 2.4*).

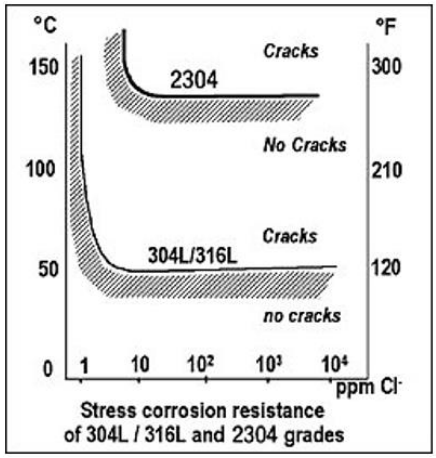

Figure 2.4: *SCC resistance in a chloride-containing solution [29].*

Overall Duplex stainless steel are best suited for the development of sustainable constructions [30], thanks to a perfect balancing between economic, social and experimental factors (*Figure 2.5*).

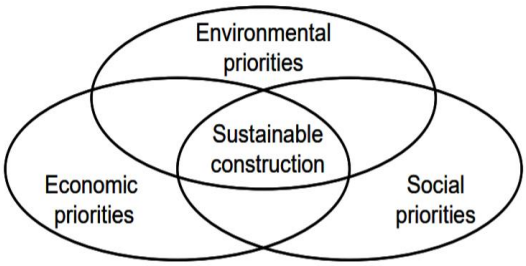

Figure 2.5: *Sustainable construction main factors [30].*

The factors can be listed this way:

- Minimum energy for construction and use
- Minimum waste design
- Pollution avoidance
- Biodiversity preservation
- Respect for people and environment

– Water resources conservation

In addition to this, the use of DSS enables to achieve important goals , in term of construction final weight. Their high strength to weight ratio allows the working constraints to meet a lighter structure, which is not only better in reducing the amount of materials spent but also has a better appearance in respect to the alternatives. Finally, costs have to be considered, as economics drives every construction project nowadays. Since SS 304L and 316L are the workhorses in that field, all the newest stainless steel types are compared to these alloy as they are benchmarks. Economically, lean duplex SS (e.g. 2304 grade) are characterized by a little lower price per pound in respect to the SS 304L and 316L and to the other duplex and super-duplex SS. This is due mainly to a lower content of Nickel in the final composition. Nickel is the leading factor for the price of stainless steels. Furthermore, Nickel price is severely affected by the market variations, this means that the price of the SS containing high levels of Nickel is strongly variable during a certain time, while for those SS (as 2304 DSS) which contains a relative low content of Nickel ,the final price does not fluctuate so much for increasing of Nickel costs. *Table 2.1* describes the alloy surcharges for long SS products updated to December 2019.

Steel Type	**Steel Grade**	**Price/tonne (EUR)**
Austenitic SS	AISI 304	1602
	AISI 304L	1793
	AISI 316	2363
	AISI 316L	2363
Ferritic SS	AISI 409	451
	AISI 430	535
	AISI 436	749
Duplex SS	AISI 2304	1351
	AISI 2205	1852
	AISI 2507	2207

Table 2.1: *Europe monthly alloy surcharges for long products.December 2019 [31]*

2.2 Objectives

This work has been carried out to study how concrete structures reinforced by rebars of 2304 Duplex Stainless Steel behave in a very aggressive condition with high concentration of chloride ions, in order to make DSS spread among the several applications for structures in marine environment. This study was born by the need to find an alternative steel which better suits with marine structures, replacing the currently used ones.

In this field, the research group headed by the eng. Javier Sánchez Montero of the Spanish Institute of Construction Science *Eduardo Torroja* (ETSII), located in Madrid, have been investigating for years on the selection of the best steel to use.

In the laboratory for steel corrosion testing at ETSII, an electrochemical corrosion testing for 2304 Duplex Stainless Steel reinforced concrete specimens has been performed, in order to evaluate their behaviour in simulated marine environments, to estimate their durability and the chloride critical concentration at the steel-concrete interface, responsible for the initiation of corrosion.

CHAPTER 3

Materials Characterization and Methodologies

3.1 Materials

3.1.1 Duplex Stainless Steel AISI 2304

The tested material is a Duplex Stainless Steel 2304.

It is characterized by high strength and toughness, optimal resistance to SSC, good thermal conductivity, relative low thermal expansion, and high machinability. It is not recommended to use this type of steel in places where it would be exposed to very high temperatures (> 1058°C) for large periods of time.

Its resistance to general corrosion is quite similar to that of AISI 304L and 316L but the yield strength is almost double. The dual-phase microstructure with high chromium and low nickel contents permit Duplex 2304 to show improved properties in stress corrosion conditions, if compared to the austenitic common grades [29].

Standards

- ASTM/ASME: UNS S32304
- EURONORM: 1.4362 - X2CrNiN23-4
- DIN**:** 1.4362

Chemical composition

C	Si	Mn	P	S	Cr	Ni	Mo	Cu	N	PREN
≤0.030	≤1.0	≤2.0	≤0.035	≤0.015	22.5	4.5	0.3	0.3	0.1	26

Table 3.1: *2304 DSS chemical composition [29].*

Mechanical properties

Tensile strength min	Yeld Strength min	Elongation (% in 50mm) min	Hardness (Brinell) max	Hardness (Rockwell) max
600 MPa	400 MPa	25	293	31[j]

Table 3.2: *2304 DSS main mechanical properties [29].*

Physical properties

At room temperature.

Density	Young Modulus *E*	Shear Modulus *G*	Coefficient of thermal expansion	Thermal Conductivity	Electrical Resistivity	Specific Heat
7800 Kg/cm^3	200 GPa	75 GPa	13 a·10 M^{-b}·K^{-1}	17 W/(m·K)	80 μ_cm	450 J/(Kg·K)

Table 3.3: *2304 DSS main physical properties [29].*

Processing

- Welded steel by TIG (manual and automatic) , MIG, SMAW, SAW, PLASMA, FCAW;
- Machined steel.

Applications

Duplex 2304 is mostly used in the same applications in which Alloys 304 and 316L are used, including:

- Chloride containing environment
- Transportations
- Chemical, Petrochemical and Water Treatment industries
- Architectures, buildings, constructions
- Pressure vessels
- Heat exchanger tubes

- Caustic solutions, organic acids
- Food industry

The tested 2304 DSS sample has been previously machined in the form of bars (*Figure 3.1*) through cold working, with the sizes shown in the table below.

Figure 3.1: *2304 DSS Stainless steel rebar.*

Length, L	**Diameter, D**	**Lateral surface, A_{lat}**
10 cm	1.2 cm	1.25664 cm

Table 3.4: *2304 DSS tested rebar main dimensions.*

Microstructure

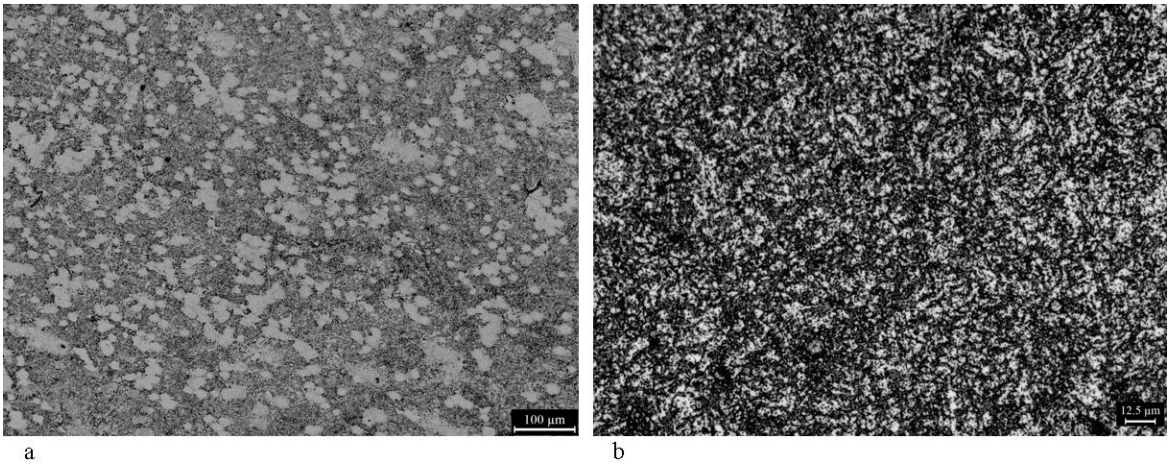

Figure 3.2: *2304 DSS microstructure observed by optical microscope with lower (100 µm) (a) and higher (12.5 µm) (b) resolution.*

From *Figure 3.2a* it is clear the presence of two different phases with two distinct structures. Specifically austenitic part (light grey) is γ-phase with the FCC structure, while the ferritic one (dark grey) is α-phase with a BCC structure. In *Figure 3.2b*, it can be observed a very fine microstructure, resulting from the cold working process. This is responsible of the DSS high mechanical resistance, as small grains mean higher density of boundary grains, which better hinder the dislocations movement.

3.1.2 Concrete

The concrete used in the test presented the following composition (*Table 3.5*).

Components		**Kg/m^3**	**Batch**
Aggregates	AF-0/4	766,00	17,62
	AG-4/12	823,60	18,94
	AG-12/20	325,60	7,49
Cement	CEM I 42,5 R	350,00	8,05
MasterRheobuild1222 addictive	0,89%	3,12	71,65
a/c	0,45	157,50	3,62

Table 3.5: *Tested concrete composition.*

The concrete samples were in the form of full cubic block (*Figure 3.3*) with the sizes of 10x10x10 cm^3.

Figure 3.3: *Concrete block type [32].*

3.1.3 Epoxy resin

The epoxy resin *Sikagard 62* has been obtained by mixing two types of epoxy resins: A type and B type (*Figure 3.4*). The mixture is composed by the A and B type in a ratio of 3:1.

Figure 3.4: *Epoxy resins as result of a mixture of Type A and Type B.*

3.2 Methodologies

3.2.1 Testing Methodology

The test methodology has been related to the Spanish UNE 83992 "concrete durability ". It concerns with exposing twenty concrete test-tube , in which is perpendicularly positioned an AISI 2304 bar, to an electric field. The steel rebar is coated all the length long with epoxy resin, in order to prevent the polarization process during the testing . The electric field is generated by the voltage between two electrodes by a DC power supply, as the model shown in *Figure 3.5*:

a) The first electrode is a copper cathode, placed in a polymeric cylinder fixed to the upper side of the concrete specimen , containing a dissolution of Sodium chloride NaCl (0,6 M) and Copper chloride $CuCl_2$ (0,4 M).

b) The second one is a stainless steel mesh anode , attached to the lower part of the concrete specimen.

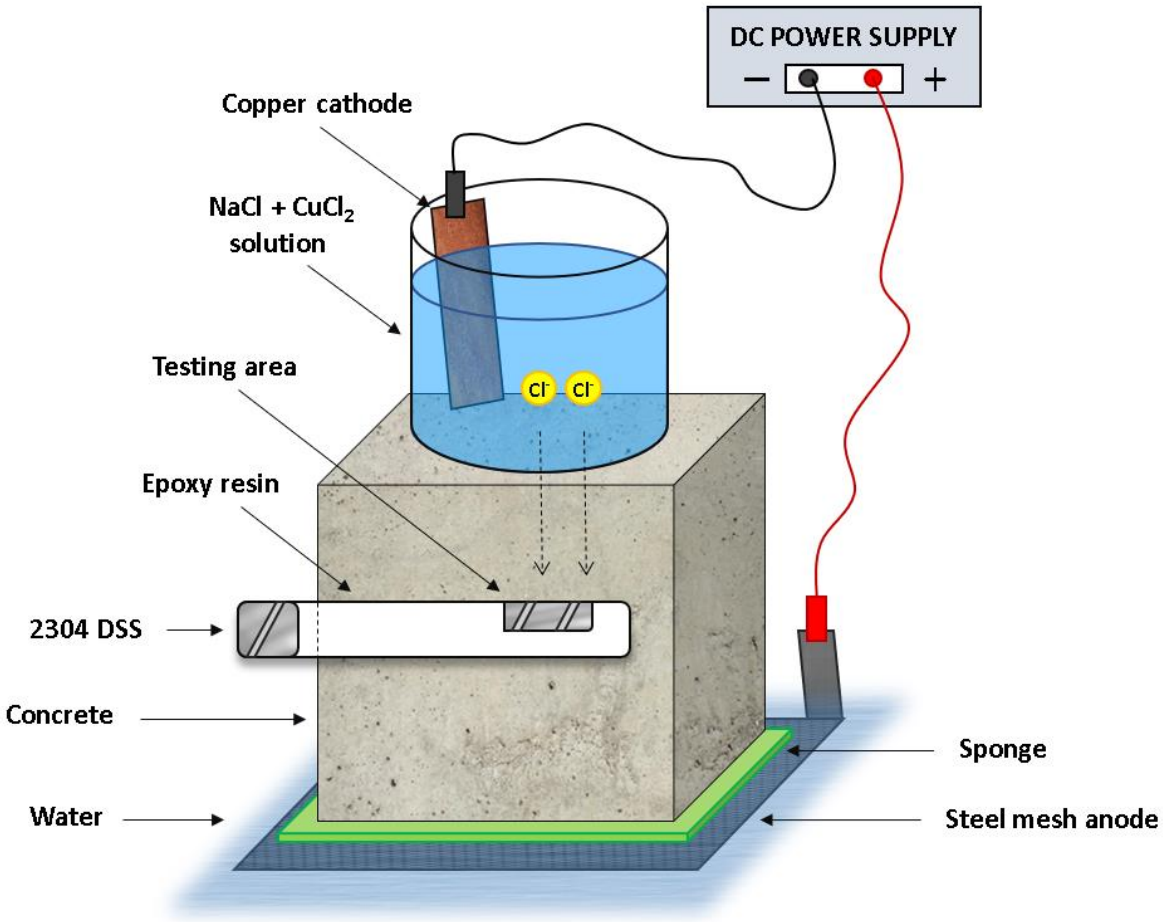

Figure 3.5: *Testing methodology main characteristics.*

Thanks to the electric field applied, Chloride ions are accelerated in the specimen from the cylinder containing the dissolution to the steel mesh, by passing through the steel bar. Every day the samples are disconnected from the DC power supply and analysed through the non-destructive *Linear Polarization Resistance* (LPR) technique, in order to measure diary values of corrosion potential E_{corr} and corrosion rate I_{corr} obtaining data about the diary evolution of corrosion. The time between the activation of the electric field and the steel depassivation is recorded. This time is important for calculating the diffusion coefficient in unsteady state (D_{ns}). Steel depassivation by the ions coming into contact with the rebar is detected by a change in the corrosion potential or a rise in the bar corrosion rate (I_{corr}). The critical chloride concentration is calculated by stopping the test and break up the specimen, in order to analyse the composition of the material close to the corroded free window bar.

3.2.2 Electrochemical techniques

The great part of the corrosion processes acting at T_a corresponds to electrochemical corrosion processes, where the electrochemical mechanism is due to two partial reactions, the anodic oxidation and the cathodic reduction. Generally, the equilibrium is mostly displaced to the right side of the corrosion processes.

When there is no external influence the matter is corroded at its free corrosion potential E_{corr} and a strict equivalence between anodic and cathodic processes is reached:

$$I_t = I_a + I_c = 0 \tag{13}$$

$$I_a = I_c = I_{corr} \tag{14}$$

Where I_c and I_a are the intensity of the cathodic and anodic semi-reactions respectively. Corrosion exists thanks to the formation and movement of electrical charged particles and to the cathodic and anodic partial processes, which are characterized by an intensity depending on the phenomenon's rate. This makes possible to assess the corrosion rate, simply measuring the electrical magnitudes [33].

The number of different techniques developed to study electrochemical corroded system is quite large. In a big part of those techniques there are some necessary elements to take into account:

- Working Electrode (WE): the metal, object of the study.
- Reference Electrode (RE): not polarizable electrode, respect to which the WE potential's variations are evaluated.
- Counter Electrode (CE): electrode thanks to which the WE is polarized. It is made to not produce any kind of distortions in the system.
- Electrolite: substance containing free ions in its composition, thanks to which it behave as an electrical conductor.

3.2.2.1 Linear Polarizazion restistance

There are several ways to estimate the corrosion rate. In order to activate the corrosion process, where a great number of reactions between charged particles take place, it's necessary to overcome an energy gap. This can be demonstrated thanks to the use of the electrochemical kinetics, according to which the electrochemical equations are adjusted to new ones [33]:

$$i_a = i_0 \, e^{\frac{\alpha n F}{RT}\eta} \tag{15a}$$

$$i_c = -i_0 \, e^{\frac{\beta n F}{RT}\eta} \tag{15b}$$

Where i_0 is the exchange current density, T the absolute temperature, R the gas constant, F the Faraday constant, n the number of electrons, α and β $(1-\alpha)$ are related to the potential drop through the matter around the electrode, η is the activation overpotential.
The electrical equilibrium in the free potential of corrosion, which is expressed in the equation above, doesn't permit a direct evaluation of i_{corr}. However, when this equilibrium is broken , it can be clearly seen an external current, which results from the algebraic sum of the various partial processes:

$$i_t = i_a + i_c = i_0 \left[e^{\frac{\alpha n F}{RT}\eta} - e^{\frac{\beta n F}{RT}\eta} \right] \tag{16}$$

This is called Butler-Volmer equation.

By using the slope of Tafel and the linear polarization technique, this equation allows to calculalate the i_{corr} (or I_{corr}), or corrosion rate [33].

Tafel extrapolation

For a better understanding of the *Linear Polarization Resistance* method, it's important to describe the Tafel extrapolation method [34].

By dealing with the kinetics and thermodynamics of the reactions which take place on an electrode's surface, this technique is able to predict the corrosion rate and potential.

As described in the previous paragraph , the relationship between the potential E and the current density i, is given by the Butler–Volmer equation for all those reactions in which the rate is reduced by the activation overvoltage. The latter can be so expressed:

$$\eta = E_{applied} - E_{corr} \tag{17}$$

For anodic and cathodic considered as separated reactions, if the anodic polarization from the reversible potential is quite large (η_a>50 mV) , the net current density is given by:

$$i_{net} = i_0 exp\left[\frac{\alpha n F \eta_a}{RT}\right] \tag{18}$$

Which rearranged, can lead to the Tafel equation:

$$\eta_a = \frac{B_a \log i_a}{i_0} \tag{19a}$$

$$\eta_c = \frac{B_c \log i_c}{i_0} \tag{19b}$$

B_a and B_c representing the Tafel slopes and are given by:

$$B_a = 2{,}303\ \frac{RT}{\alpha n F} \tag{20a}$$

$$B_c = 2{,}303\ \frac{RT}{\beta n F} \tag{20b}$$

In the condition in which α is equal to 0.5 ,the anodic and cathodic slopes will be the same.

Tafel gave an experimental relationship between the activation over-pontential and the current density:

$$\eta = a \pm b\ logi \tag{21}$$

With b representing the Tafel slope of either the anodic or cathodic reactions. By comparing the equations of η_a and η_b with the latter one, it can be calculated the value of both constants a and b.

A Tafel plot is a graph describing the relationship between the current density in logarithmic form and the overpotential. Through the extrapolation approach, this graph is useful for finding the Tafel slope, and consequently, to evaluate the corrosion potential and the corrosion current density. As shown in *Figure 3.6*, extrapolating the linear part of the curve to E_{corr} permits to find the corrosion current density [33].

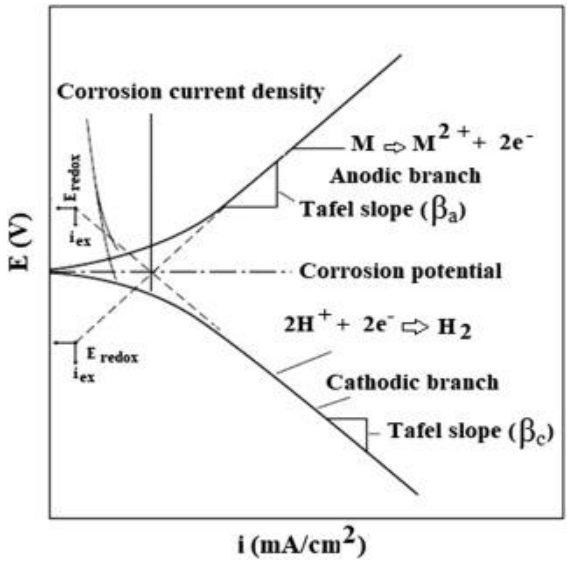

Figure 3.6: *Tafel extrapolation of metal in acidic mediums [34]*

If corrosion is presumed uniform, it can be used Faraday's law to turn the corrosion density into the rate of penetration. This technique allows to measure not only low corrosion rates but also to have a no-stop monitoring of the investigated system.

Linear polarization resistance technique (LPR)

The technique was introduced by M. Stern and A. L. Geary [35] in 1957 and finally improved by C. Andrade et al. [18], for the specific case of carbon steel in reinforced structures. The resistance to linear polarization is also called LPR, or easier known as R_p.

The method is non-destructive method ,based on the fact of considering the polarization curves in a small range of E_{corr} as straight lines, the slope of which is related to the corrosion rate.

As the limit for x⟶0 , $e^x = 1+x$ and $e^{-x} = 1-x$, the Butler-Volmer eq. (16) changes into:

$$i_t = i_{corr}\left(\frac{\alpha nF}{RT}\eta + \frac{\beta nF}{RT}\eta\right) \tag{22}$$

Putting the values of Tafel slopes in the equation above:

$$i_t = i_{corr} \cdot \eta \cdot 2.303\left(\frac{1}{\beta_a} + \frac{1}{\beta_{c1}}\right) \tag{23}$$

For η→0 :

$$i_{corr} = \frac{1}{2.303 \cdot \left(\frac{1}{\beta_a} + \frac{1}{\beta_c}\right)} \cdot \frac{di_t}{d\eta} = -\frac{\beta_a \cdot \beta_c}{2.303 \cdot (\beta_a + \beta_c)} \cdot \frac{di_t}{d\eta} \tag{24}$$

As $\frac{di_t}{dn} = \frac{\Delta i}{\Delta E}$, i_{corr} can be calculated. For a given system, Tafel slopes can be taken as constant and the Stearn-Geary equation can be approximated this way:

$$i_{corr} = B \frac{\Delta i}{\Delta E} = \frac{B}{R_p} \tag{25}$$

In the practice, a small polarization or ΔE is applied, of ±10 or ±20mV, then the corresponding Δi is measured, taking into account that the product $\Delta E \cdot \Delta i$ is characterized by the same units as the resistance.

The constant $B = \frac{\beta_a \beta_c}{2.303 \cdot (\beta_a + \beta_c)}$ has a value varying in a small range as well as the Tafel slopes which, in the most of the cases, range from 60 and 120 mV [35].

Even if the β_a and β_c parameters are not known, the B average value can be approximately estimated. This method is very easy and beneficial, since it is required a so small polarization that, in almost all the studied cases, the specimen keeps unchanged. This allows to measure the i_{corr} evolution in a particular specimen with the passing of the time.

LPR methods is more general than Tafel extrapolation technique. In the case in which β_a and β_c are infinitely large, from the equation above is deduced that:

$$i_{corr} = \frac{\beta_a}{2.303\, R_p} \tag{26a}$$

or

$$i_{corr} = \frac{\beta_c}{2.303\, R_p} \tag{26b}$$

This procedure can be applied even when the Tafel extrapolation can't be. The Linear Polarization Resistance technique can supply important information in many studies as:

1. Assessment of corrosion rate changes with the time.
2. Comparison between different alloys of the corrosion rate in the same environment.
3. Studies about the ways in which environmental variables can affect the corrosion rate.

4. Possibility of finding inhibitors for controlling corrosion processes.
5. Evaluation of the service coatings condition, evaluation which can't be made by other methods (likes the visual ones).

3.2.3 Electrochemical Instrumentation and Software

3.2.3.1 Autolab

As instrument for the corrosion measurements, a *Metrohm Autolab PGSTAT30* is used (*Figure 3.7*).

Figure 3.7: *Metrohm Autolab PGSTAT30 used for the testing.*

The Autolab is a modular high current potentiostat-galvanostat able to perform virtual electrochemical measurements. Here (*Table 3.6*) some important features:

Technical Specifications	
Maximum current	± 1 A
Compliance voltage	± 30 V
Potentiostat bandwitch	1 MHz
Computer interface	USB
Control software	Nova
Manufacturer	Eco Chemie

Table 3.6: *Metrohm Autolab PGSTAT30 main features [36].*

It's mostly used for *Electrochemical Impedance Spectrometry* technique (EIS) and *Linear Polarization Resistance* technique (LPR), in association with Nova 1.11 Software [36].

3.2.3.2 Nova 1.11 for linear polarization

All the testing are done thanks to the use of *NOVA 1.11*. It is an electrochemistry software from *Metrohm Autolab*, which can be used to manage and control every instrument compatible with *Autolab*.

The initial setup of the various instruments and software parameters is necessary. After that the measurement can be done, dividing into two main phases:

I. The linear polarization procedure firstly measures the *Open Circuit Potential* (OCP) for the samples with OCP determination command, where the OCP is the potential of the working electrode in respect to the reference one when the current applied is zero. During the measurement Time and WE potential are sampled (*Figure 3.8*). This step last for 120 seconds , unless the variation of potential is smaller than 1 µV/s.

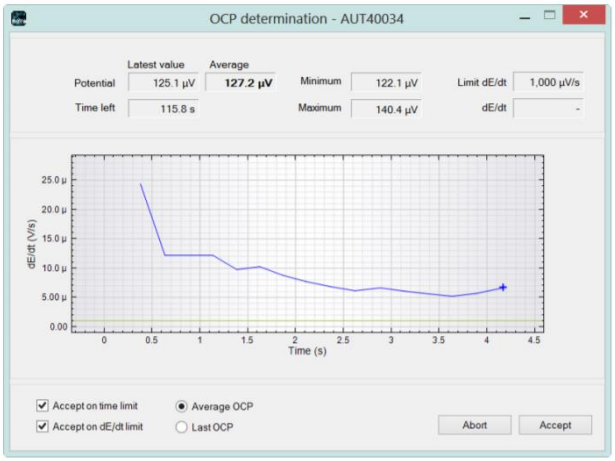

Figure 3.8: *OCP determination with time and dE/dT limited [38].*

II. The instantaneous voltage (*E*) versus the instantaneous measured current (*I*) is measured, in order to obtain the linear polarization curve, which is shown for a typical sample in *Figure 3.9*. The inverse of slope calculated for the liner portion of the curve, in the area of the graph where the current change from negative to positive, results to be

equal to polarization resistance R_p , which is inversely proportional to the corrosion rate [36].

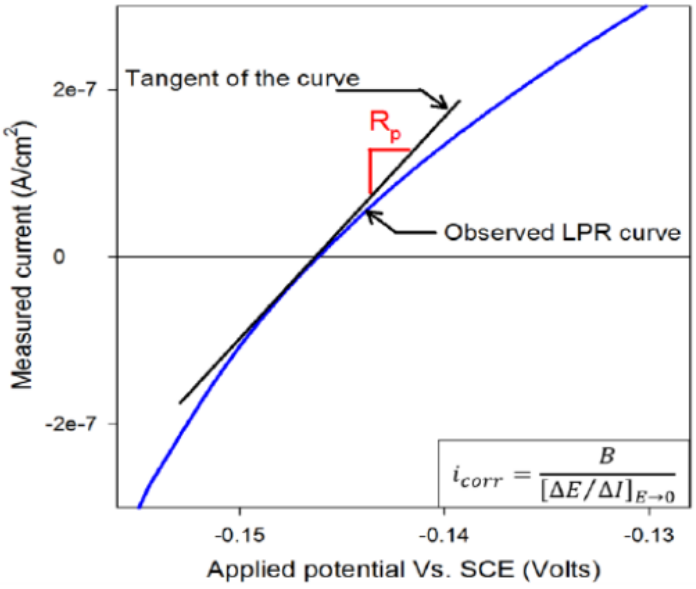

Figure 3.9: *Typical LPR curve for a given sample [37].*

In order to evaluate the corrosion initiation, regular measurements of R_p during the time are transcripted and by these, periodical values of the current inside the sample I_{corr} and the potential E_{corr} are obtained through the Stern-Geary eq. (25).

Finally, thanks to a statistical method using *Excel* software, the periodical values are plotted in function of the exposed time, in order to estimate the starting of the corrosion.

3.2.4 Microstructure analysis instrumentation

3.2.4.1 Polishing machine

A *Presi Mecatech 234* polisher (*Figure 3.10)* has been used to polish the DSS surface, in order to make possible the final analysis of the microstructure. It's an automatic polishing machine. The main thecnical specifications in the *Table 3.7*.

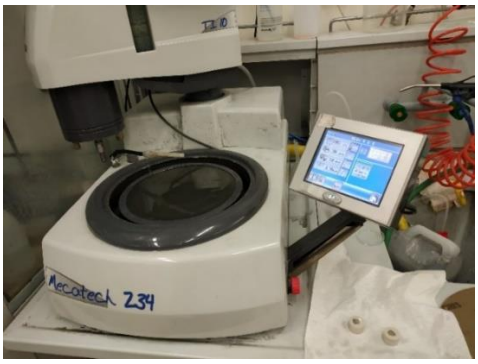

Figure 3.10: *Presi Mecatech 234 polisher available at DISAT.*

Technical specifications	
Ø Polishing plate	200 to 250 mm
Rotation speed	20 to 700 rpm
Rotation direction	clockwise/anticlockwise
Motor power	250 W
Voltage	230 V

Table 3.7: *Presi Mecatech 234 polisher Main technical data.*

3.2.4.2 Optical Microscope

A *Leica DMI 5000 M* (*Figure 3.11*) has been used to analyse the DSS microstructure and the corrosion DSS surface.

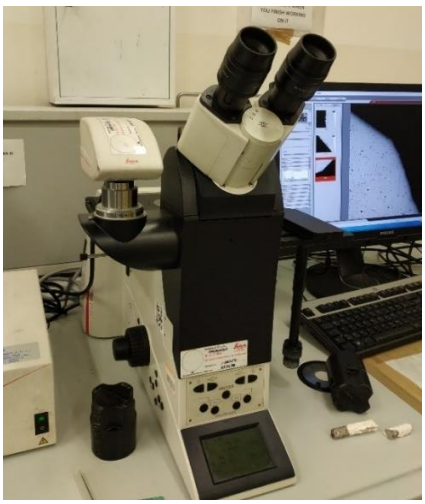

Figure 3.11: *Leica DMI 5000M Optical Microscope available at DISAT.*

Chapter 4

Experimental Test

The whole test consisted of three main stages:

I. Fabrication of samples
II. Effective Test
III. Corrosion surface analysis

The fabrication of the samples and the effective testing have been carried out at the Institute of construction science *Eduardo Torroja*, in Madrid, as well as the first part of the corrosion analysis, related with the composition analysis. The second part has been done at the *Department of Applied Science and Technology* (DISAT) of *Politecnico di Torino*, related with the microstructure analysis.

4.1 Testing characteristics

4.1.1 Standard norm

The followed norm is the Spanish UNE 83992 *"concrete durability"*. This norm is made up of two different parts:

1) Natural method for determining the time occurred for the corrosion.
2) Accelerated integral method

This norm is used to determine a testing method, in order to measure the effects of concrete mix composition on :

- Resistance to the chloride ions penetration
- Critical concentration of chloride ions needed to provoke corrosion in the steel
- Steel corrosion process rate

4.1.2 Units

- dimensions in centimeters (cm) ;
- time (t) in seconds (s);
- temperature (T) in Celsius degrees(°C);
- current (I) in Ampere (A);
- voltage (ΔV) in Volt (V);
- chloride concentration (C_x) in weight percentage of concrete (concrete weight %);
- time for de-passivation (t_{dep}) in hours (h);
- Corrosion rate (I_{corr}) in μA/cm^2;
- Corrosion potential (E_{corr}) in mV.

4.1.3 Service conditions

The service temperature is kept at (22±3)°C and the relative humidity is more than 45%. During the test, the concrete lateral surfaces are protected with a thermoplastic film, in order to avoid the evaporation.

4.2 Fabrication of samples

Overview

The test tubes have been made up of a 10x10x10 cm^3 concrete block (cube geometry), in which a SS threshold have been incorporated.

The Duplex threshold bars measured 10 cm and have been obtained by cutting a duplex threshold. Firstly they have been cleaned up, then they have been covered with epoxy resin for the entire length, except for one extremity of 3 cm length, for an easier electrical measurement, and a one-side window of 2x1 cm^2 , which represented the testing area. These precise areas have been marked with a pencil. The sample main characteristics are shown in the *Table 4.1*.

Free window dimensions	
Length, l	2 cm
Width, w	1 cm
Lateral Surface, A_{lat}	1.26 cm^2

Table 4.1: *DSS sample free window dimensions.*

The epoxy resin coating was fundamental, since it allowed the sample to not be penetrated by the electric field , by behaving as a real insulating material (*Figure 4.1*).

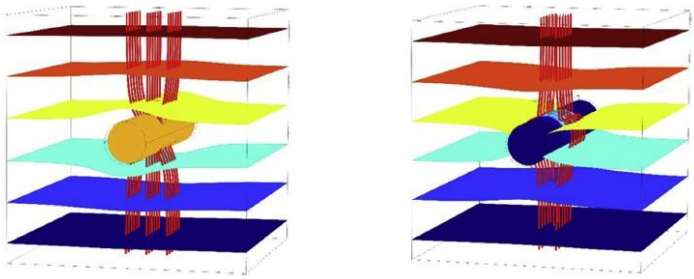

Figure 4.1: *Current flow and Electrical potential field in not-coated rebar (left) and in epoxy-resin coated rebar (right).*

Thanks to a brush, the epoxy resin have been spread in the marked areas of the specimen. This process has been repeated four times, in order to create a uniform insulating cover on the steel (*Figure 4.2*).

Figure 4.2: *Epoxy-resin coated 2304 DSS tested rebars.*

Between two following coverings, it was important to wait for the solidification (almost one day of waiting). Moreover, it was necessary the using of a lime for reducing the unevenness,

since the gravity force causes the falling of the mixture droplets from one side of the specimen. Once finished the duplex steel bars preparation, the entire specimen could be fabricated. First of all, the preparation of concrete was necessary (*Figure 4.3*). According to the Table, the final composition has been achieved using three types of aggregates of different sizes (*Figure 4.3a*), which have been taken, cleaned up by impurities, pressured and finally put in an electric furnace for 24h, in order to be dried. The day after, they have been withdrawn and mixed with water and the other elements in a mortar (*Figure 4.3b*).

Figure 4.3: *a) Three different types of aggregates used for the concrete; b) Final concrete mixture.*

The concrete produced has been then spilled in steel moulds (*Figure 4.4*), here it has been compacted to obtain a more uniform materials without any kind of voids or bubbles inside.

Figure 4.4: *Steel moulds used for the samples preparation.*

The Duplex bars have been marked with a pencil (*Figure 4.5a*); specifically, lines on each bars (8-8,5 cm starting from the embedded bar end) have been marked, in order to insert them in the

concrete for the desired length. In addition to this, each bar has been completely marked on the free window side in the external part, this for understanding which side was the one with the free window penetrated by the current.

Then the duplex bars have been incorporated in the concrete (*Figure 4.5b*), taking care to put it perfectly vertical and leaving one extremity out of the system. The concrete have been compacted again to avoid the presence of air bubbles along the concrete-steel interface.

***Figure 4.5**: a) Coated and marked tested rebar; b) Tested rebars embedded in wet concrete inside the moulds.*

Finally, all the test-tubes have been left in a humid chamber for 24 h for the solidification (*Figure 4.6*).

***Figure 4.6:** Tested samples left in humid chamber for solidification.*

The day after, every mould have been disassembled, cleaned up and reassembled. The specimens have been collected , identified with a number and left for 28 days in 3 tappet tubs

(*Figure 4.7*). Here they have been put on a 2 cm-tick plastic grid with almost 3 cm of water, in order to create the condition for having a relative humidity >95%.

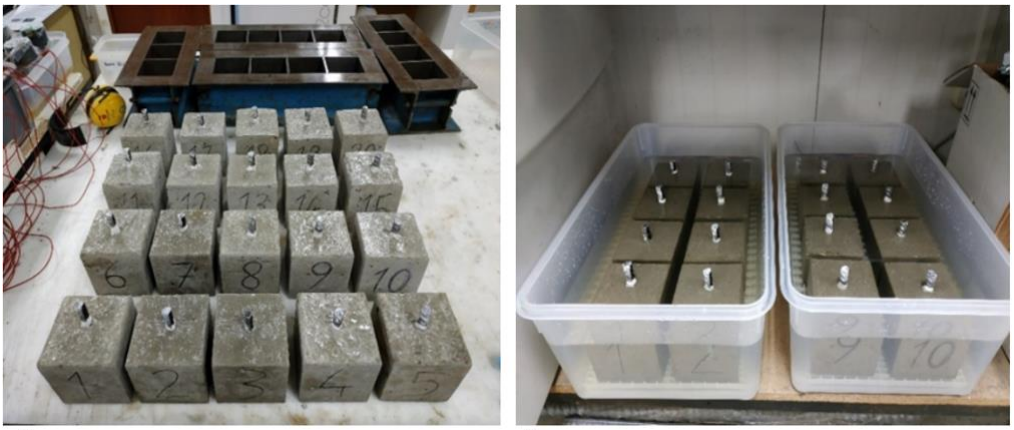

Figure 4.7: *a) RC samples from 1 to 20;*
b) RC samples put in plastic grids with water to create humid conditions.

After this period, the test-tubes have been withdrawn to be dried on in 1 or 2 hours. Then, a PVC 10 cm-high cylinder has been fixed on the upper side of each specimen, thanks to the use of a silicone cordon. To assure that the cylinder was well fixed to the concrete block and there was no water leak, the plastic tube has been filled up with distilled water for a short time (*Figure 4.8*).

Figure 4.8: *Tested samples with extra PVC cylinder containing water.*

Proved that there was no water leak, the cylinder has been emptied of the water and refilled with the chloride dissolution for almost its entire height. Then the copper foil has been inserted in the dissolution, taking care to leave one extremity out of the system, in order to attach the voltage source (*Figure 4.9a*). Finally, each specimen has been covered sideways

with a plastic film (identified with a number between 1 and 20) as well as the top of PVC cylinder , so that the chloride content did not reduce so much for evaporation during the testing. Then, all the samples have been placed in the same large bath on the 2 cm plastic grid, with a 3 cm-high water level (*Figure 4.9b*) . Each sample has been positioned on a Stainless steel mesh; between the metal meshes and the samples it has been interposed a sponge, kept wet all the testing long to assure the humid testing condition (relative humidity >95%).

a b

Figure 4.9: *a) Final tested sample configuration with chloride solution and copper foil; b) Tested samples with plastic cover for avoiding solution evaporation.*

4.3 Test

Before starting the real test, all the samples have been subject to a pre-test, consisting of the calculation of their potential before and after 1 minute of voltage applied (12 V).

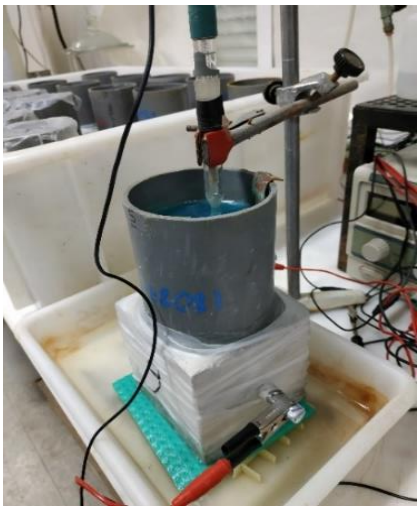

Figure 4.10: *Re-passivation pre-testing with silver electrode.*

This has been done to better understand how the duplex SS is able to resist to the polarization process. This process has been performed thanks to the help of a silver electrode, connected to a voltmeter and submerged in the sample solution (*Figure 4.10*). In the table below, the initial current passing in the samples and the values of their potential measured before and after the application of the voltage are shown. In particular , after the charging , the values have been measured each 20 seconds, for a total time of 10 min; this time represented a good time for making the voltage values stabilize.

Sample	**Distance steel-concrete surface e (mm)**	**Initial current I_0 (mA)**	**Initial potential measured P_0 (mV)**	**Final potential measured P_f (mV)**
1	46.2	12.54	-144.6	-119.2
2	42.6	11.57	-105.2	-95.0
3	46.9	11.04	-119.2	-117.3
4	46.3	12.67	-109.5	-105.7
5	46.8	12.10	-95.0	-85.2
6	48.8	12.56	-80.1	-73.5
7	48.8	12.66	-96.4	-110.1
8	39.4	12.91	-99.0	-100.1
9	46.4	11.07	-93.1	-91.0
10	39.8	11.21	-82.0	-81.9
11	49.1	11.25	-80.1	-81.4
12	46.1	12.19	-91.2	-87.5
13	44.7	11.78	-65.5	-64.5
14	44.5	11.52	-94.6	-98.6
15	42.6	12.02	-93.2	-99.1
16	44.7	12.9	-96.5	-88.9
17	46.0	13.1	-90.5	-90.1
18	44.2	13.63	-306.1	-295.0
19	44.1	13.54	-98.2	-102.7
20	40.9	12.24	-141.1	-140.6

Table 4.2: *Re-passivation data.*

After these measurement, the samples have been connected to the voltage source (10 V), so that the real testing could start (*Figure 4.11*).

Figure 4.11: *Testing activation.*

The DC power supply has been switch on, recording the activation test time. Just after the activation, the effective current passing in each sample has been monitored, so as to be sure that the testing was proceeding in the right way.

4.3.1 Measurements

As reported in the paragraph 3.2.2 , all the testing have been done by the use of Autolab device for electrochemical testing and the software NOVA 1.11 for the online measurements.

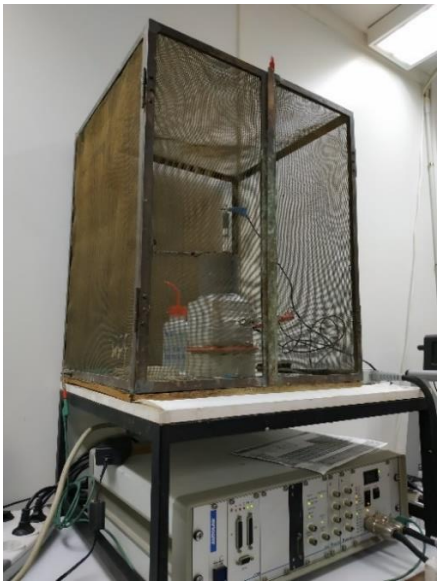

Figure 4.12: *Autolab device and electrochemical cell.*

The electrochemical technique have been performed on a electrochemical cell (*Figure 4.12*) with many different kinds of electrodes (*Figure 4.13*) :

- Working Electrode (WE) : Tested Duplex SS 2304

- Reference Electrode (RE) : Ag/AgCl (SSE: Standard Silver Electrode); it is the electrode with respect to which the working electrode's voltage variation is measured.

- Counter Electrode (CE) : thanks to which the WE's polarization is done.

- Electrolite: NaCl+$CuCl_2$ dissolution

Figure 4.13: *Electrochemical measurement configuration: RE (Reference electrode), WE (Working electrode), CE (Counter electrode).*

Thanks to *Nova* and *Autolab*, *Linear Polarization Resistance* (LPR) method has been used to characterize the material medium pair by scanning the current–potential (*I–E*) domain. The linear polarization resistance method consisted of applying to the metal very small voltage variations (typically less than 30 mV) above and below its corrosion potential. Over this narrow range in the vicinity of the corrosion potential the current response obtained was linear. The polarization resistance (*Rp*), defined as the slope of this current–potential curve, was therefore

constant. According to the Stern-Geary eq. (25), *Rp* is inversely proportional to the instantaneous corrosion rate, at least under certain constant conditions.

4.3.2 Effective Procedure

In the first period, the DC power supply has been regularly switch off daily in the morning. In order to make the current to stabilize in the samples , measurements were taken after at least one hour. Then, the corrosion rate (I_{corr}) and corrosion potential (E_{corr}) were measured. After almost one month of testing, the measurement were done every other day in the morning.

According to that standard norm UNE 83992, E_{corr} values less than or equal to 300 mV and I_{corr} greater than or equal to 0.2 µA/cm^2 were indicative of depassivation. Actually for stainless steels , I_{corr}>0.2 µA/cm^2 was the only necessary condition for depassivation, since previous tests by Pachón Montaño et al. [28] had proved no corrosion for SS rebar in case of E_{corr}>300 mV and I_{corr}<0.2 µA/cm^2. The time to that value has been regarded as the depassivation time (t_{dep}).

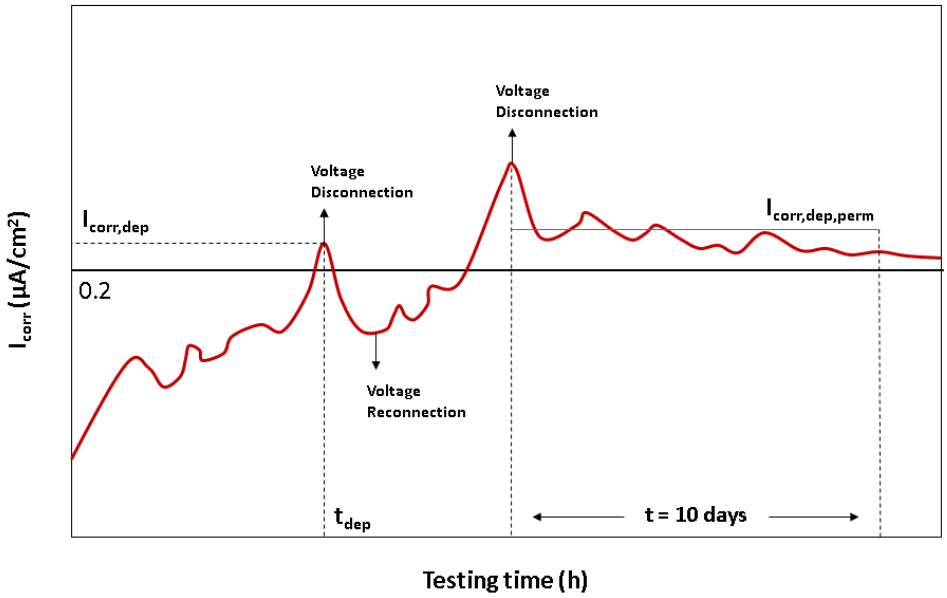

Figure 4.14: *Testing times and Passivation main parameters.*

- When I_{corr} remained above or near 0.2 mA/cm^2 for at least 10 consecutive days with the current off, the test has been interrupted and the specimen are broken down. Then, the mean corrosion rate $I_{corr,med}$ and the permanent corrosion rate $I_{corr,dep,perm}$ have been calculated, where first was the average of corrosion rate measured over the entire testing

time, while the second was the mean corrosion rate measured during the period of 10 days with no current applied (*Figure 4.14*) . Otherwise, the current were reconnected and the test continued.

4.4 Corrosion surface analysis

4.4.1 Chloride concentration at the steel-concrete interface

For the samples that kept corrosion for more than 10 days, the procedure continued with the emptying of the chloride dissolution, the disconnection of the plastic cylinder and the final breaking down of the concrete by a compressive machine (*Figure 4.15*).

- For the depassivated samples , their acid-soluble chloride concentration Cl^- has been subsequently determined with a method described by the eq. (8) and expressed in % of concrete weight.

- The corroded rebar has been observed and micro-graphed before and after pickling.

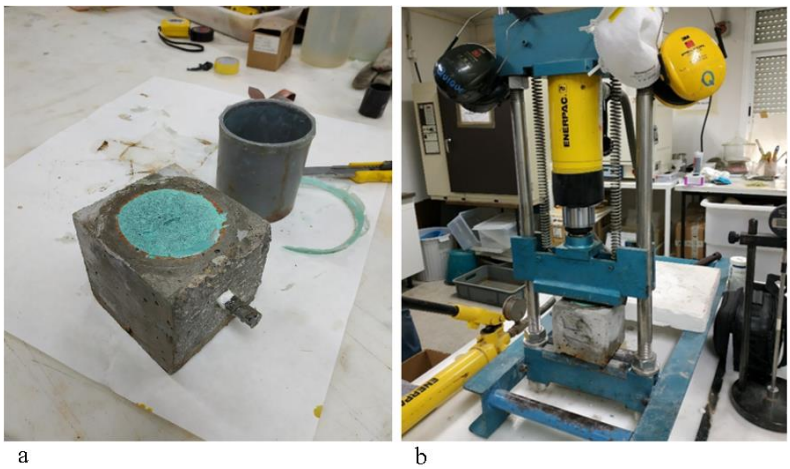

a b

Figure 4.15: *a) Plastic cylinder Disconnection; b) Sample breaking down by compressive stress.*

After the breaking of the samples, the Duplex rebars have been withdrawn and part of the concrete which was in contact with the steel has been collected , in order to measure the chloride

concentration in the steel-concrete interface. Particularly, thanks to a power drill, the material to study has been taken from specific points, that were located in the area which was closest to the steel free window (*Figure 4.16*), taking care to not collect the bigger parts.

a b

Figure 4.16: *a) De-passivated sample (DSS rebar and concrete); b) use of power drill to withdraw corroded material for the analysis*

Then, the collected aggregates have been reduced in a mortar, to make the final material as uniform as possible, and put in a container (Figure 51a).

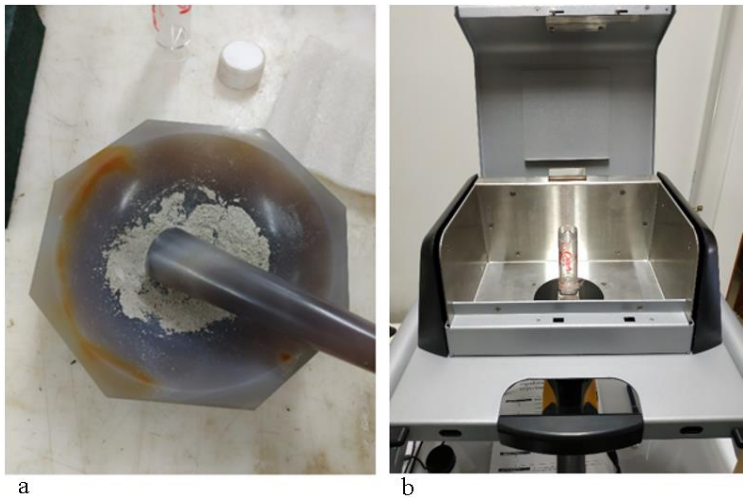

a b

Figure 4.17: *a) Collected material reduced in mortar; b) XRF machine for composition analysis.*

Once the finest material has been collected, the composition and the chloride concentration at the concrete-metal interphase could be analysed thanks to a XRF device, connected to a computer (*Figure 4.17b*).

4.4.2 Corroded steel surface analysis

The Corrosion surface analysis has been carried out at *Politecnico di Torino*. The procedure has been composed of different steps:

I. The corroded DSS rebar and one not-corroded 2304 rebar have been withdrawn and subject to the initial cutting of the corroded cross-section though cutting machine *Remet TR 100S* (*Figure 4.18*)

Figure 4.18: *DSS 2304 rebar cutting step.*

I. By metallographic incorporation, the corroded and not-corroded steel section have been sampled in a solidified bi-component epoxy resin, necessary for the following Polishing step. The samples have been polished by the use of *Presi Mecatech 234* combined with various SiC sandpapers of different grit sizes (from 180 to 4000). Finally, a diamond paste has been introduced on a cotton cloth to obtain a perfect mirror-like surface.

Figure 4.19: *incorporated DSS 2304 corroded and not-corroded rebars after polishing..*

II. The surface analysis step has been performed using a Optical Microscope with a different magnification grade for the corroded and not-corroded sample.

a) The corroded 2034 DSS sample has been micro-graphed with resolutions in the order of 200 µm, just after the polishing step without any previous chemical attack, in order to look at the surface areas interested by corrosion.

b) The not-corroded 2304 DSS sample has been previously chemically attacked by a solution of aqua regia, obtained by the mixing of 69 % HNO_3 solution and 37% HCl solution in a ratio 1:3, through which it has been possible to observe the Dual-phase microstructure with resolutions in the order of 50 µm and 12.5 µm.

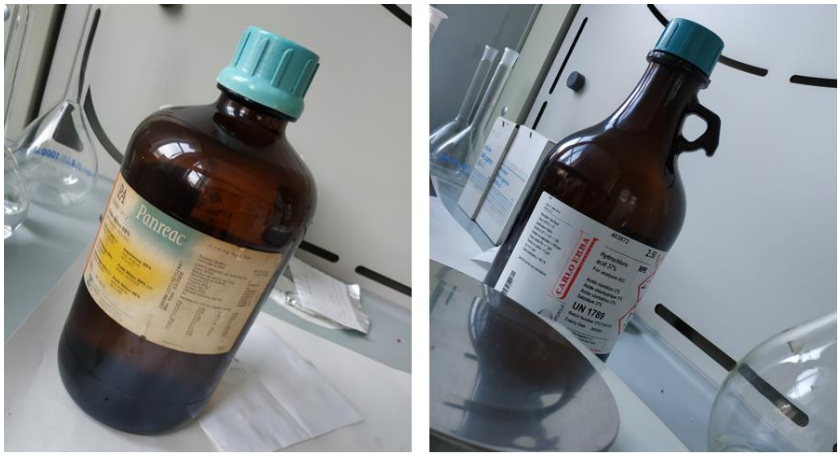

a b

Figure 4.20: *a) 69% Nitric acid solution ; b) 37% Hydrochloric acid solution.*

Chapter 5

Results and discussion

According to the final results, the twenty samples could be classified in three types, on the basis of their corrosion behaviour during the tests:

a) Permanently passivated (PP), the ones which kept passivated for all the testing long. Classified as not corroded.

b) Not permanently passivated (NPP) , the ones which showed short periods of depassivation. Classified as in the initiation corrosion phase.

c) Activated (A) , the ones which showed long period of depassivation, for which it's sure the corrosion process initiation. Classified as in the propagation corrosion phase.

Regardless of the type, each sample has been characterized through graphs plotting the variation of corrosion potential E_{corr} and corrosion rate I_r in respect to the time of applied voltage t, in order to statistically predict the durability. According to the standard norm, the steel has been classified as activated if the measurements reveal its corrosion potential higher than -300 mV and its corrosion rate higher than 0.2 $\mu A/cm^2$ for a period of time of at least ten successive days.

For the not permanently passivated and activated samples it has been possible to detect the depassivation time t_{dep}.

The activated specimens were the only ones for which the chloride threshold for the corrosion initiation and the chloride concentrations profile C_x at different penetration distance at t_{dep} have been evaluated . Moreover, their corrosion surface have been observed and subject to further analysis.

5.1 Overall Results

After a total period of 58 days of testing, among twenty similar samples with the same testing conditions , the overall results are shown below (*Table 5.1*).

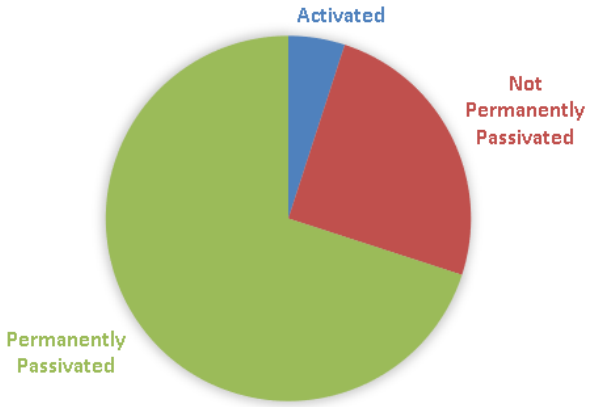

Type	Sample number	Corrosion phase
Permanently passivated	2, 3, 4, 5, 6, 7, 8, 9, 10, 11, 14, 16, 19, 20	Null
Not permanently passivated	1, 12, 13, 17, 18	Initiation
Activated	15	Propagation

Table 5.1: *Overall test results.*

In the following paragraphs:

a) For all the samples (PP, NPP and A) the variation of corrosion potential E_{corr} and corrosion rate I_{corr} for each sample has been shown, over the total period of testing. Furthermore, it has been reported in the table below:

   – The initial data, where B is a constant related to the Tafel slopes, l is the free-window length, D and L are the bar diameter and length respectively, e is the distance chloride solution-steel rebar, I_0 is the initial current measured.

   – the time accumulated of applied voltage (t_{acc})

– the diffusion coefficient in unsteady state (D_{ns}) ,calculated by the eq:

$$D_{ns} = \frac{e^2}{2 \cdot t \cdot 40 \cdot \frac{\Delta V}{L}} \tag{27}$$

– the average value of the measured I_{corr} ($I_{corr,med}$)

b) For the NPP and A samples the time of depassivation t_{dep} has been reported.

c) For the A sample even the $I_{corr,dep,perm}$, the chloride concentration at the steel-concrete interface and the chloride concentration profile at the depassivation time have been assessed. Furthermore, the DSS corrosion surface has been analysed by optical microscopy.

5.2 Corrosion potential E_{corr} and corrosion rate I_{corr}

Permanently Passivated samples

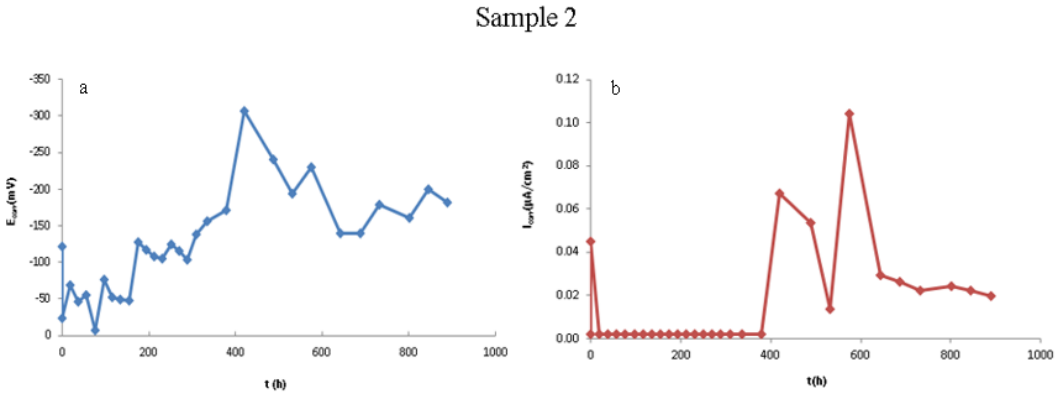

Figure 5.1: *Sample 2: a) E_{corr} vs applied voltage time; b) I_{corr} vs applied voltage time.*

Initial data			Results		
Voltage	10	V			
B	0.026	V	t_{acc}	889	h
l	2	cm			
D	1.2	cm	D_{ns}	$7.22 \cdot 10^{-8}$	cm^2/s
e	4.3	cm			
L	10	cm	$I_{corr,med}$	0.0154	$\mu A/cm^2$
I_0	11.5	mA			

Table 5.2: *Sample 2 initial testing data and results.*

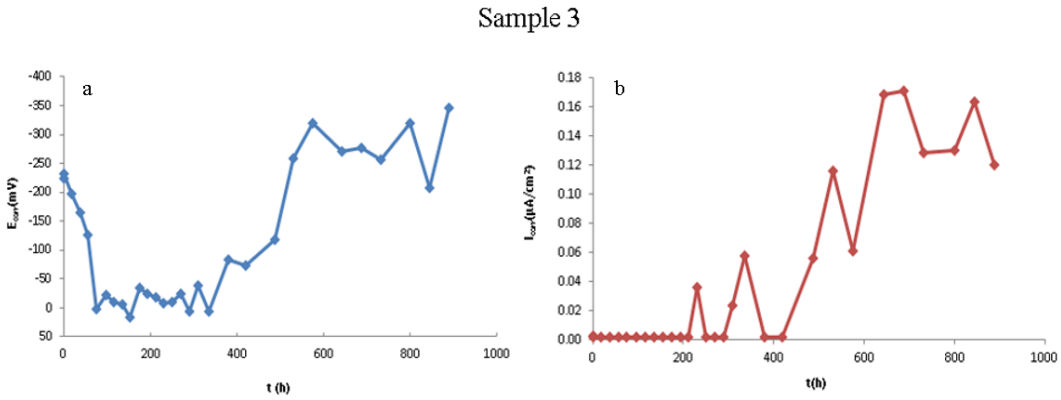

Figure 5.2: *Sample 3: a) E_{corr} vs applied voltage time; b) I_{corr} vs applied voltage time.*

Initial data			**Results**		
Voltage	10	V			
B	0.026	V	t_{acc}	889	h
l	2	cm			
D	1.2	cm	D_{ns}	$8.63 \cdot 10^{-8}$	cm^2/s
e	4.7	cm			
L	10	cm	$I_{corr,med}$	0.0422	$\mu A/cm^2$
I_0	11	mA			

Table 5.3: *Sample 3 initial testing data and results.*

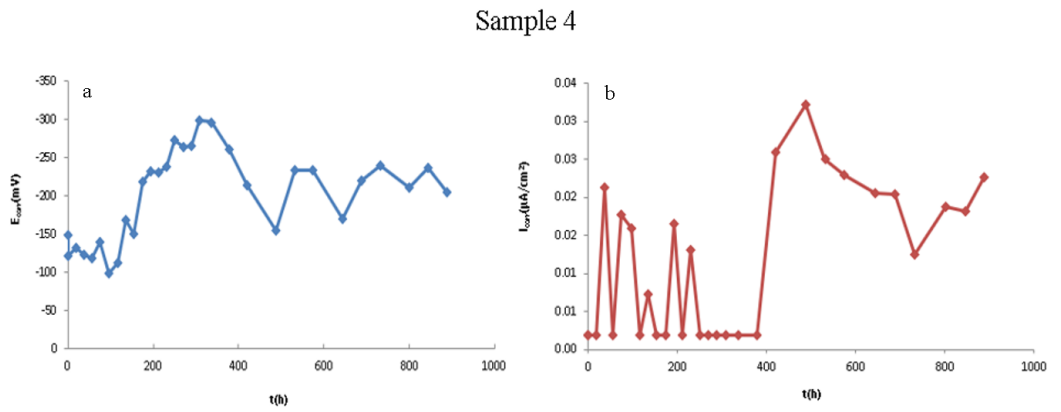

Figure 5.3: *Sample 4: a) E_{corr} vs applied voltage time; b) I_{corr} vs applied voltage time..*

Initial data			**Results**		
Voltage	10	V			
B	0.026	V	t_{acc}	889	h
l	2	cm			
D	1.2	cm	D_{ns}	$8.26 \cdot 10^{-8}$	cm^2/s
e	4.6	cm			
L	10	cm	$I_{corr,med}$	0.0112	$\mu A/cm^2$
I_0	12.6	mA			

Table 5.4: *Sample 4 initial testing data and results.*

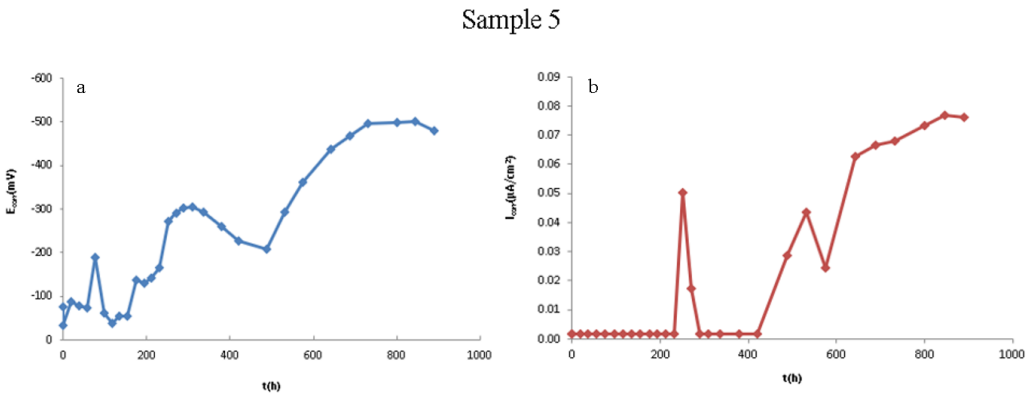

Figure 5.4: *Sample 5: a) E_{corr} vs applied voltage time; b) I_{corr} vs applied voltage time.*

Initial data			**Results**		
Voltage	10	V			
B	0.026	V	t_{acc}	889	h
l	2	cm			
D	1.2	cm	D_{ns}	$8.63 \cdot 10^{-8}$	cm^2/s
e	4.7	cm			
L	10	cm	$I_{corr,med}$	0.0208	$\mu A/cm^2$
I_0	12.1	mA			

Table 5.5: *Sample 5 initial testing data and results.*

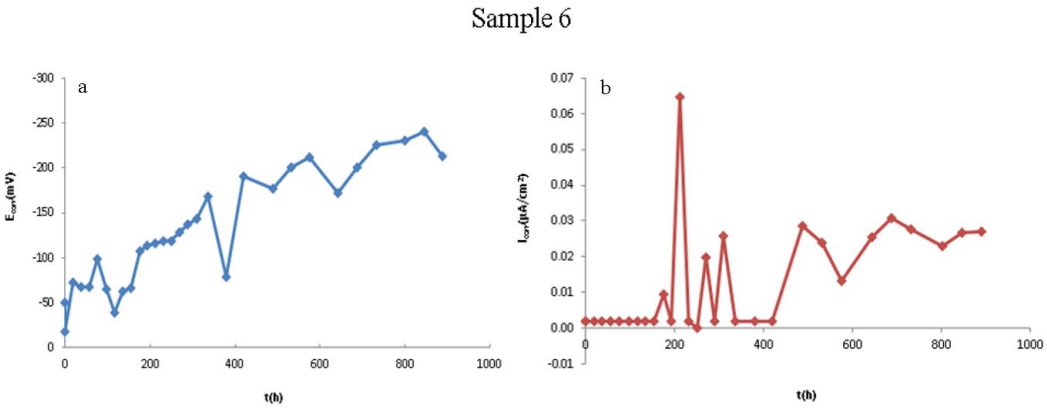

Figure 5.5: *Sample 6: a) E_{corr} vs applied voltage time; b) I_{corr} vs applied voltage time.*

Initial data			**Results**		
Voltage	10	V			
B	0.026	V	t_{acc}	889	h
l	2	cm			
D	1.2	cm	D_{ns}	$9.38 \cdot 10^{-8}$	cm^2/s
e	4.9	cm			
L	10	cm	$I_{corr,med}$	0.0125	$\mu A/cm^2$
I_0	12.6	mA			

Table 5.6: *Sample 6 initial testing data and results.*

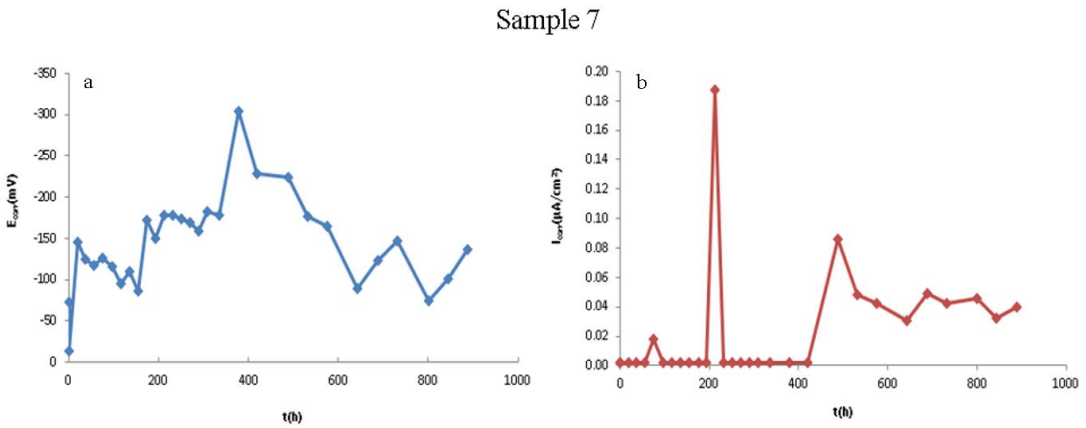

Figure 5.6: *Sample 7: a) E_{corr} vs applied voltage time; b) I_{corr} vs applied voltage time.*

Initial data			**Results**		
Voltage	10	V			
B	0.026	V	t_{acc}	889	h
l	2	cm			
D	1.2	cm	D_{ns}	$9.38 \cdot 10^{-8}$	cm^2/s
e	4.9	cm			
L	10	cm	$I_{corr,med}$	0.0219	$\mu A/cm^2$
I_0	12.6	mA			

Table 5.7: *Sample 7 initial testing data and results.*

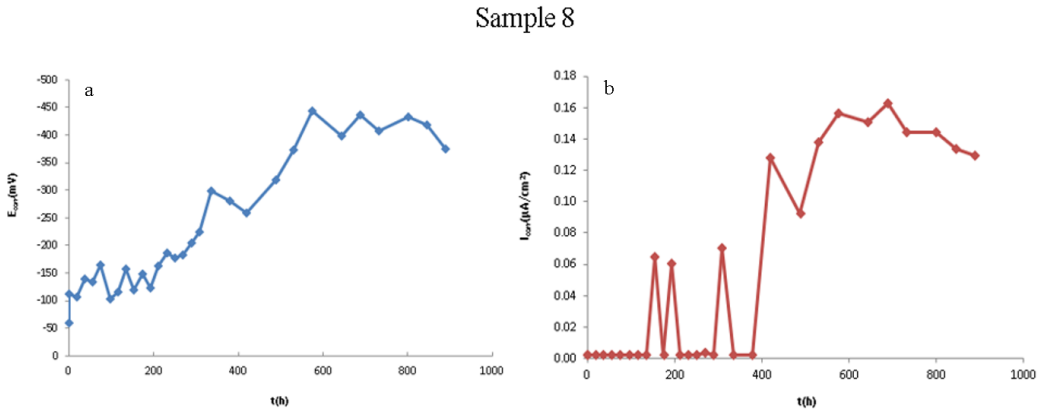

Figure 5.7: *Sample 8: a) E_{corr} vs applied voltage time; b) I_{corr} vs applied voltage time.*

Initial data			**Results**		
Voltage	10	V			
B	0.026	V	t_{acc}	889	h
l	2	cm			
D	1.2	cm	D_{ns}	$5.94 \cdot 10^{-8}$	cm^2/s
e	3.9	cm			
L	10	cm	$I_{corr,med}$	0.0536	$\mu A/cm^2$
I_0	12.9	mA			

Table 5.8: *Sample 8 initial testing data and results.*

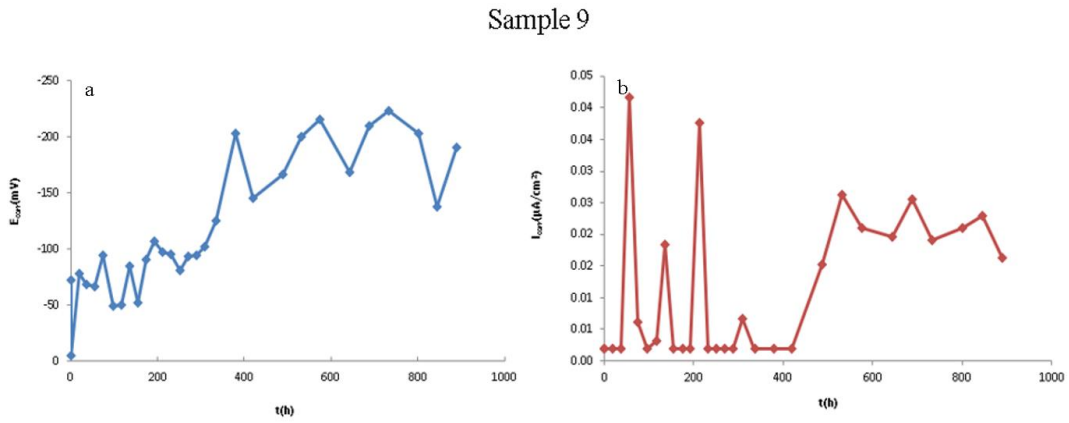

Figure 5.8: *Sample 9: a) E_{corr} vs applied voltage time; b) I_{corr} vs applied voltage time.*

Initial data			**Results**		
Voltage	10	V			
B	0.026	V	t_{acc}	889	h
l	2	cm			
D	1.2	cm	D_{ns}	$8.26 \cdot 10^{-8}$	cm^2/s
e	4.6	cm			
L	10	cm	$I_{corr,med}$	0.0109	$\mu A/cm^2$
I_0	11.1	mA			

Table 5.9: *Sample 9 initial testing data and results.*

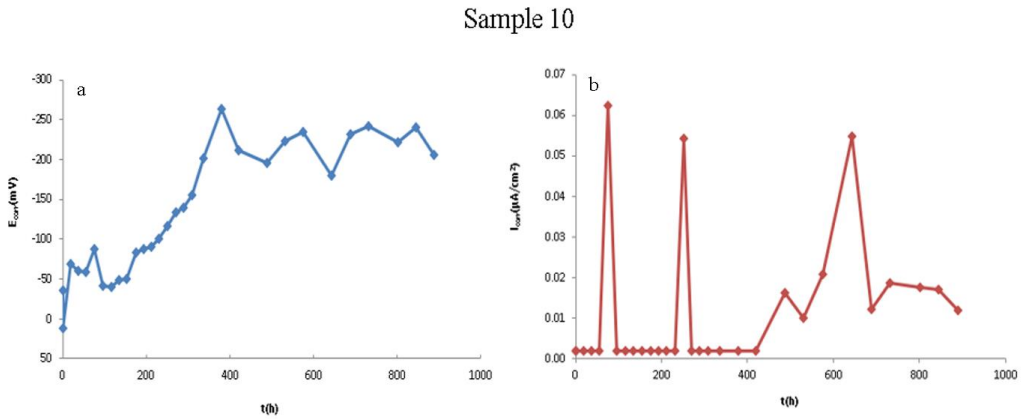

Figure 5.9: *Sample 10: a) E_{corr} vs applied voltage time; b) I_{corr} vs applied voltage time.*

Initial data			**Results**		
Voltage	10	V			
B	0.026	V	t_{acc}	889	h
l	2	cm			
D	1.2	cm	D_{ns}	$6.25 \cdot 10^{-8}$	cm^2/s
e	4	cm			
L	10	cm	$I_{corr,med}$	0.0111	$\mu A/cm^2$
I_0	11.2	mA			

Table 5.10: *Sample 10 initial testing data and results.*

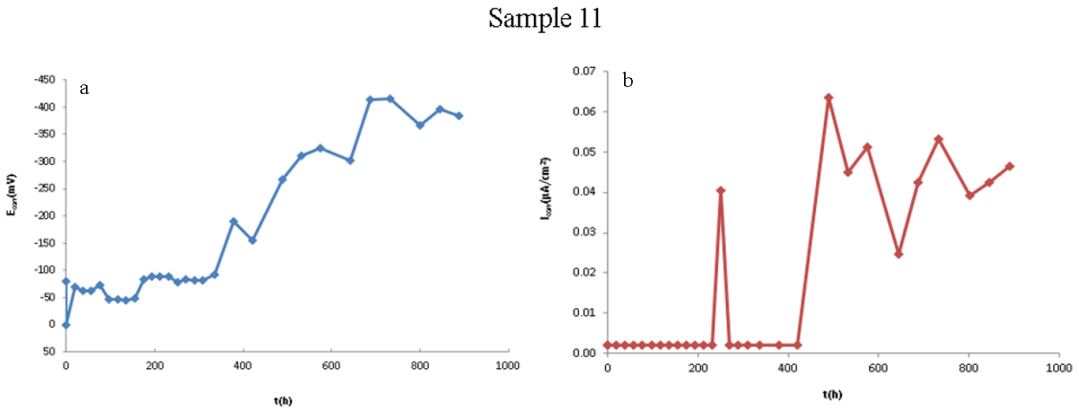

Figure 5.10: *Sample 11: a) E_{corr} vs applied voltage time; b) I_{corr} vs applied voltage time.*

Initial data			**Results**		
Voltage	10	V			
B	0.026	V	t_{acc}	889	h
l	2	cm			
D	1.2	cm	D_{ns}	$9.38 \cdot 10^{-8}$	cm^2/s
e	4.9	cm			
L	10	cm	$I_{corr,med}$	0.0162	$\mu A/cm^2$
I_0	11.2	mA			

Table 5.11: *Sample 11 initial testing data and results.*

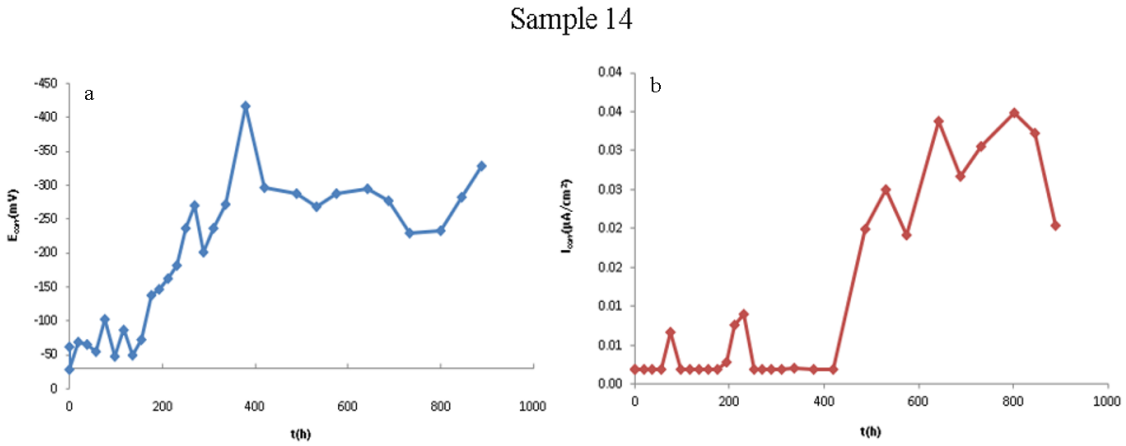

Figure 5.11: *Sample 14: a) E_{corr} vs applied voltage time; b) I_{corr} vs applied voltage time.*

Initial data			**Results**		
Voltage	10	V			
B	0.026	V	t_{acc}	889	h
l	2	cm			
D	1.2	cm	D_{ns}	$7.91 \cdot 10^{-8}$	cm^2/s
e	4.5	cm			
L	10	cm	$I_{corr,med}$	0.0100	$\mu A/cm^2$
I_0	11.5	mA			

Table 5.12: *Sample 14 initial testing data and results.*

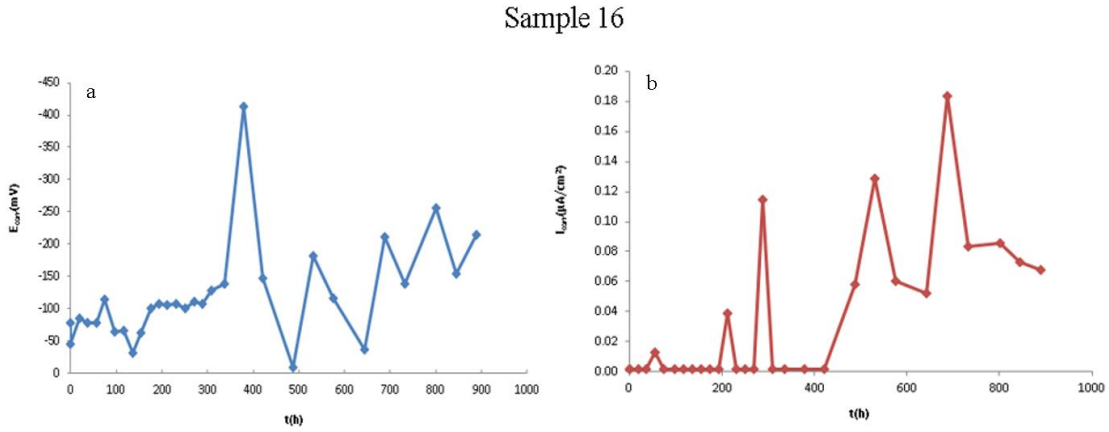

Figure 5.12: *Sample 16: a) E_{corr} vs applied voltage time; b) I_{corr} vs applied voltage time.*

Initial data			**Results**		
Voltage	10	V			
B	0.026	V	t_{acc}	889	h
l	2	cm			
D	1.2	cm	D_{ns}	$7.91 \cdot 10^{-8}$	cm^2/s
e	4.5	cm			
L	10	cm	$I_{corr,med}$	0.0331	$\mu A/cm^2$
I_0	12.9	mA			

Table 5.13: *Sample 16 initial testing data and results.*

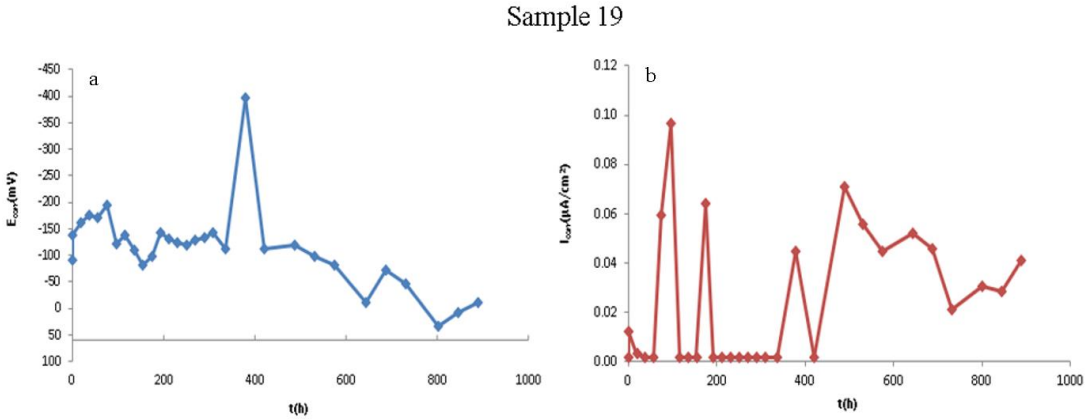

Figure 5.13: *Sample 19: a) E_{corr} vs applied voltage time; b) I_{corr} vs applied voltage time.*

Initial data			**Results**		
Voltage	10	V			
B	0.026	V	t_{acc}	889	h
l	2	cm			
D	1.2	cm	D_{ns}	$7.56 \cdot 10^{-8}$	cm^2/s
e	4.4	cm			
L	10	cm	$I_{corr,med}$	0.0233	$\mu A/cm^2$
I_0	14.5	mA			

Table 5.14: *Sample 19 initial testing data and results.*

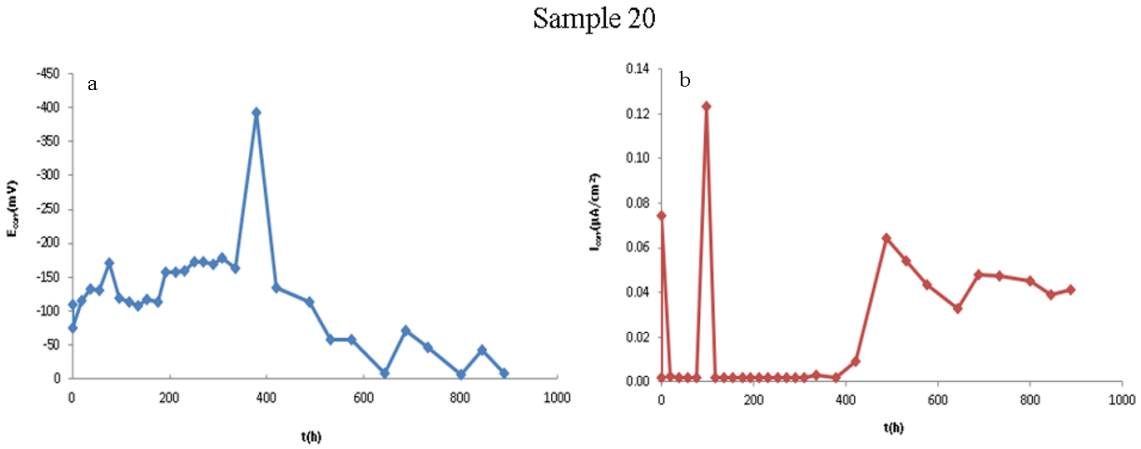

Figure 5.14: *Sample 20: a) E_{corr} vs applied voltage time; b) I_{corr} vs applied voltage time.*

Initial data			**Results**		
Voltage	10	V	t_{acc}	889	H
B	0.026	V			
l	2	cm	D_{ns}	$6.57 \cdot 10^{-8}$	cm^2/s
D	1.2	cm			
E	4.1	cm	$I_{corr,med}$	0.0219	$\mu A/cm^2$
L	10	cm			
I_0	12.2	mA			

Table 5.15: *Sample 20 initial testing data and results.*

At the end, the permanently passivated (PP) samples were the greater part of the total tested samples. As shown in the previous graphs, even in the conditions in which corrosion potential *E_{corr}* increased to values higher than -300mV , in the same time, corrosion rate *I_{corr}* kept lower than 0.2 $\mu A/cm^2$, not triggering the corrosion process. This can be explained by the fact that the protective passivating layer created onto the steel free-window surface had not been affected by the passing of current and chloride ions had not reached the specific threshold value for the initiation of corrosion in the total period of testing. PP samples have been subject to the voltage application for the total period of testing, with a number of total hours of 889, showing a diffusion coefficient D_{ns} ranging from $5.94 \cdot 10^{-8}$ to $9.38 \cdot 10^{-8}$.

Not Permanently Passivated samples

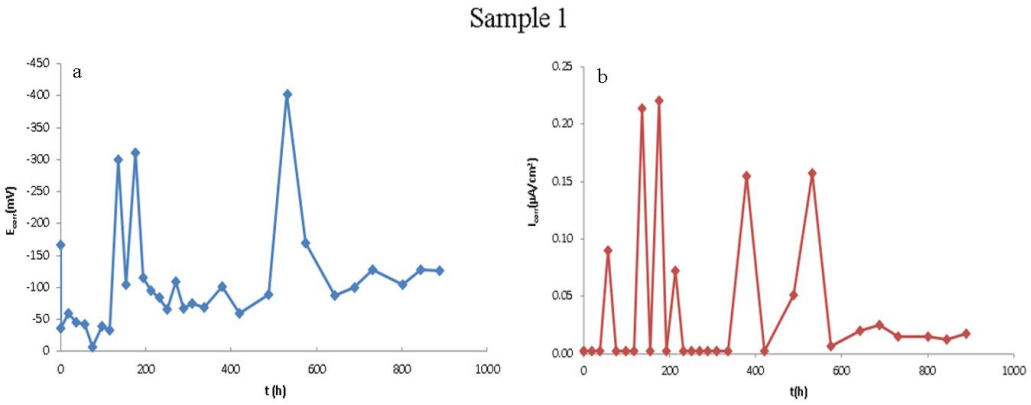

Figure 5.15: *Sample 1: a) E_{corr} vs applied voltage time; b) I_{corr} vs applied voltage time.*

Initial data			**Results**		
Voltage	10	V	t_{acc}	889	h
B	0.026	V	t_{dep}	135	h
l	2	cm			
D	1.2	cm	D_{ns}	$8.26 \cdot 10^{-8}$	cm^2/s
e	4.6	cm			
L	10	cm	$I_{corr,med}$	0.0900	$\mu A/cm^2$
I_0	12.5	mA			

Table 5.16: *Sample 1 initial testing data and results.*

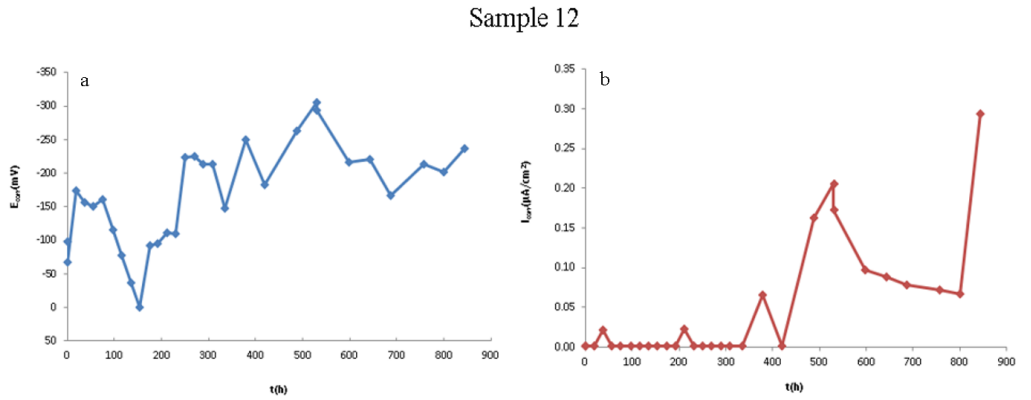

Figure 5.16: *Sample 12: a) E_{corr} vs applied voltage time; b) I_{corr} vs applied voltage time.*

Initial data			**Results**		
Voltage	10	V	t_{acc}	845	h
B	0.026	V	t_{dep}	531	h
l	2	cm			
D	1.2	cm	D_{ns}	$8.69 \cdot 10^{-8}$	cm^2/s
e	4.6	cm			
L	10	cm	$I_{corr,med}$	0.0459	$\mu A/cm^2$
I_0	12.2	mA			

Table 5.17: *Sample 12 initial testing data and results.*

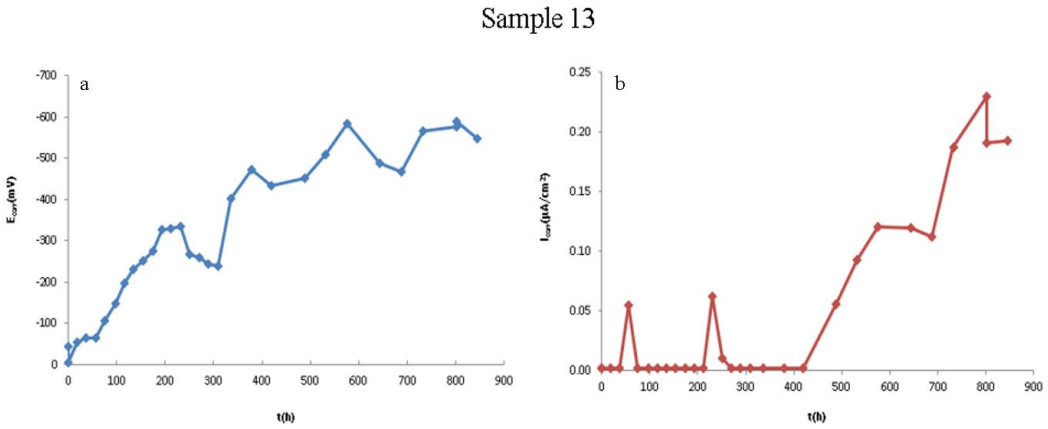

Figure 5.17: *Sample 13: a) E_{corr} vs applied voltage time; b) I_{corr} vs applied voltage time.*

Initial data			**Results**		
Voltage	10	V	t_{acc}	845	h
B	0.026	V	t_{dep}	801	h
l	2	cm			
D	1.2	cm	D_{ns}	$8.32 \cdot 10^{-8}$	cm^2/s
e	4.5	cm			
L	10	cm	$I_{corr,med}$	0.0487	$\mu A/cm^2$
I_0	11.8	mA			

Table 5.18: *Sample 13 initial testing data and results.*

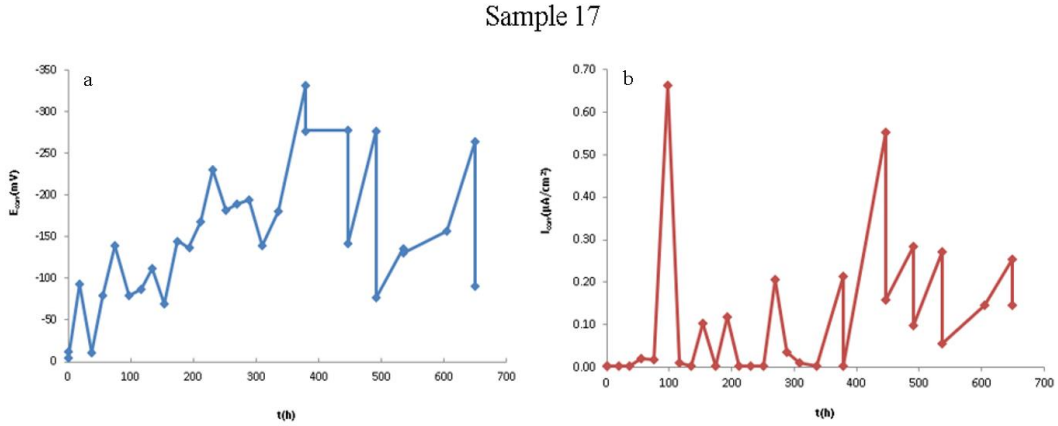

Figure 5.18: *Sample 17: a) E_{corr} vs applied voltage time; b) I_{corr} vs applied voltage time.*

Initial data			**Results**		
Voltage	10	V	t_{acc}	649	h
B	0.026	V	t_{dep}	97	h
l	2	cm			
D	1.2	cm	D_{ns}	$1.13 \cdot 10^{-7}$	cm^2/s
e	4.6	cm			
L	10	cm	$I_{corr,med}$	0.113	$\mu A/cm^2$
I_0	13.1	mA			

Table 5.19: *Sample 17 initial testing data and results.*

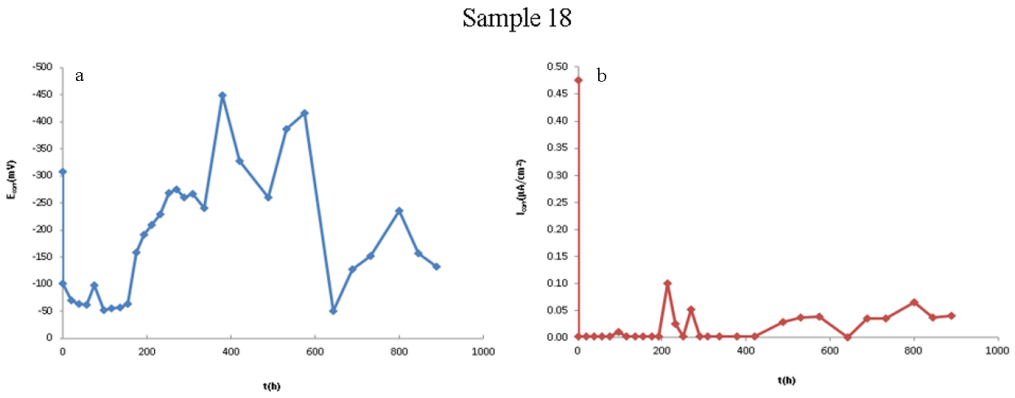

Figure 5.19: *Sample 18: a) E_{corr} vs applied voltage time; b) I_{corr} vs applied voltage time.*

Initial data			**Results**		
Voltage	10	V	t_{acc}	889	h
B	0.026	V	t_{dep}	0	h
l	2	cm			
D	1.2	cm	D_{ns}	$7.56 \cdot 10^{-8}$	cm^2/s
e	4.4	cm			
L	10	cm	$I_{corr,med}$	0.0338	$\mu A/cm^2$
I_0	13.6	mA			

Table 5.20: *Sample 18 initial testing data and results.*

The not permanently passivated (NPP) samples could be further divided into three groups:

a) The ones showing short period of depassivation in the first period of testing, followed by a long period of stabilized passivation. The samples belonging to this group are the ones for which the risk of corrosion was minimum, as their depassivation was very short and probably due to other factors (e.g. problems in the measurement devices) while then resulted to show very low values of E_{corr} and I_{corr} for the rest of the testing period. This group included sample 1 and 18. In particular sample 18 showed depassivation before testing, suggesting an error in the preparation of the testing itself. These specimens could have been classified as permanently passivated.

b) The ones showing short period of depassivation in the final period of testing, preceded by a long period of stabilized passivation; this group included sample 12 and 13. The specimens belonging to this group were not so far from corrosion activation, as they depassivation period was the result of a gradual and coherent increase in the E_{corr} and I_{corr}, which could get higher values in a more extended period of testing.

c) The ones showing a relative long alternated period of passivation-depassivation in the final period of the testing; this group included sample 17. This sample was the NPP with the higher risk of corrosion, as it is on the point to be permanently depassivated. The values of E_{corr} and I_{corr} varied enormously within two consecutive measurements, getting higher and lower than the critical values. This suggested that the protective layer onto the steel could be not uniform and the current could pass or not through the steel with different intensity, depending on the day.

Generally, NPP samples were quite various.

As regards the time of applied voltage t_{acc} was obviously lower than the total testing time of PP samples and distinct between sample and sample, as it depended on how many times they have resulted depassivated, so as for the sample 17 the t_{acc} was the lower one among the NPP samples. The diffusion coefficient D_{ns} ranges within $7.56 \cdot 10^{-8}$ and $1.13 \cdot 10^{-7}$.

Activated samples

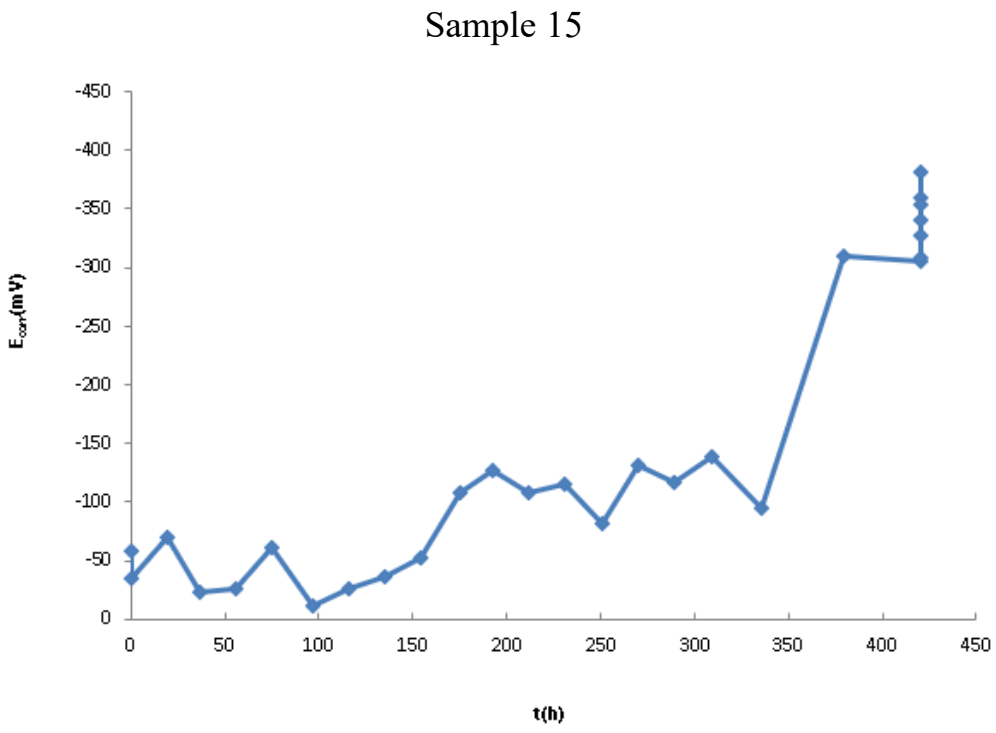

Figure 5.20: *Sample 15: E_{corr} vs applied voltage time.*

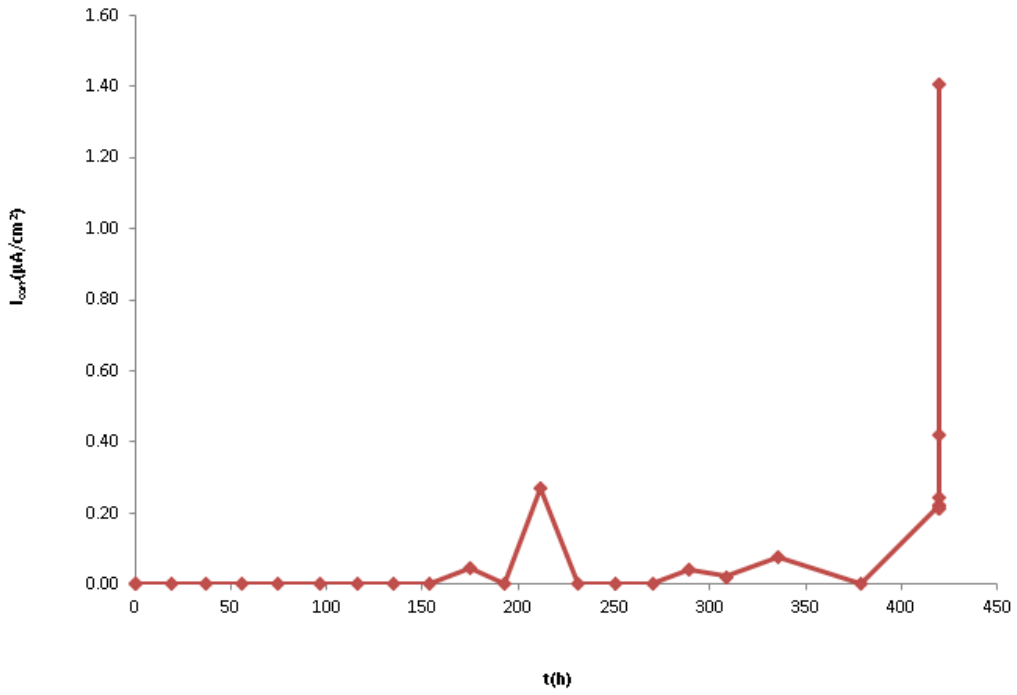

Figure 5.21: *Sample 15: I_{corr} vs applied voltage time.*

Initial data			**Results**		
Voltage	10	V	t_{acc}	420	h
B	0.026	V	t_{dep}	420	h
l	2	cm			
D	1.2	cm	D_{ns}	$1.53 \cdot 10^{-7}$	cm^2/s
e	4.3	cm			
L	10	cm	$I_{corr,med}$	0.132	$\mu A/cm^2$
I_0	12	mA			

Table 5.21: *Sample 15 initial testing data and results.*

Sample 15 was the only activated one among the twenty samples. This meant that the conditions for corrosion occurred inside the specimen, so that the corrosion potential and corrosion rate kept higher than the critical predefined values for a period of time at least of 10 days.

Only for this case , the total time of applied voltage t_{acc} corresponded to the time of depassivation t_{dep}, which was the most useful data in order to predict the structure service life. The time of depassivation for sample 15 was lower than the half of the time of applied voltage for the PP samples.

5.2.1 $E_{corr,med}$, $I_{corr,med}$ and Standard Deviations

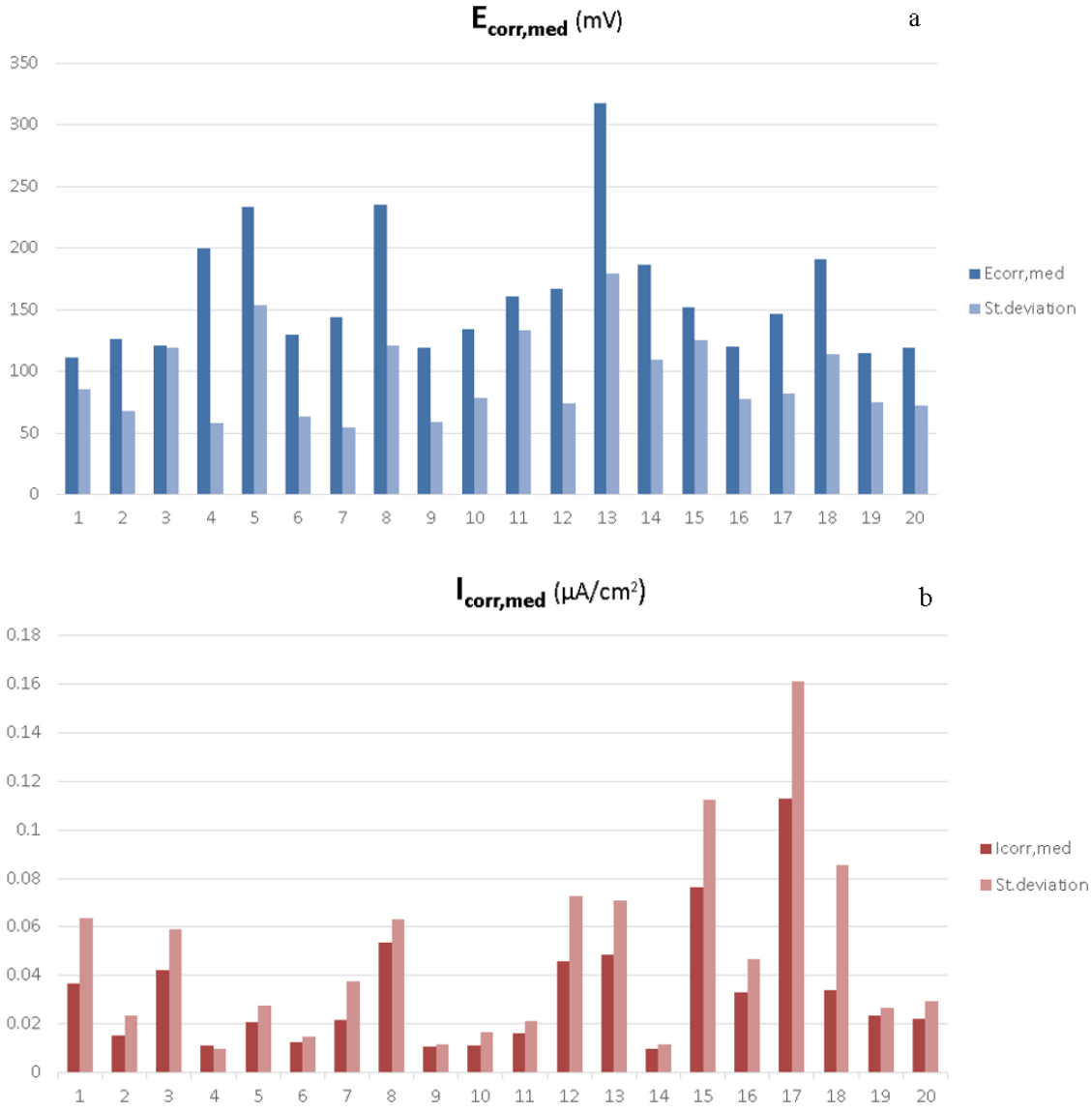

Figure 5.22: *a) $E_{corr,med}$ and standard deviation for each sample;*
b) $I_{corr,med}$ and standard deviation for each sample.

a) The mean corrosion potential $E_{corr,med}$ measured during the testing period was for all the samples lower than the critical value (set at 300 mV), except for the sample 13. This sample has been characterized by a very high value of the corrosion potential during the second part of the testing period. On the other hand, this very high value was not accompanied by a value of corrosion rate higher than 0.2 µA/cm^2, which would have led to permanent depassivation. As concern the standard deviations, they were almost

proportional to the value of corrosion potential, so as higher standard deviations almost corresponded to higher corrosion potential and vice versa.

b) The mean corrosion rate $I_{corr,med}$ varied with higher magnitude compared to the corrosion potential, among the different specimens. It kept under the critical value (set at 0.2 μA/cm^2) for each sample. The higher value was that of sample 17, the only one with showed a large period of alternated depassivation and passivation, followed by that of sample 15, the only activated one. The standard deviations in this case were more interesting than the ones of corrosion potential, as they were higher than the corresponding $I_{corr,med}$ values themselves, in particular for the NPP sample and the A one. This suggested that for these cases, the tested sample behaviour has not been so stable.

5.3 t_{dep} and $I_{corr,dep,perm}$ (only for the corroded sample)

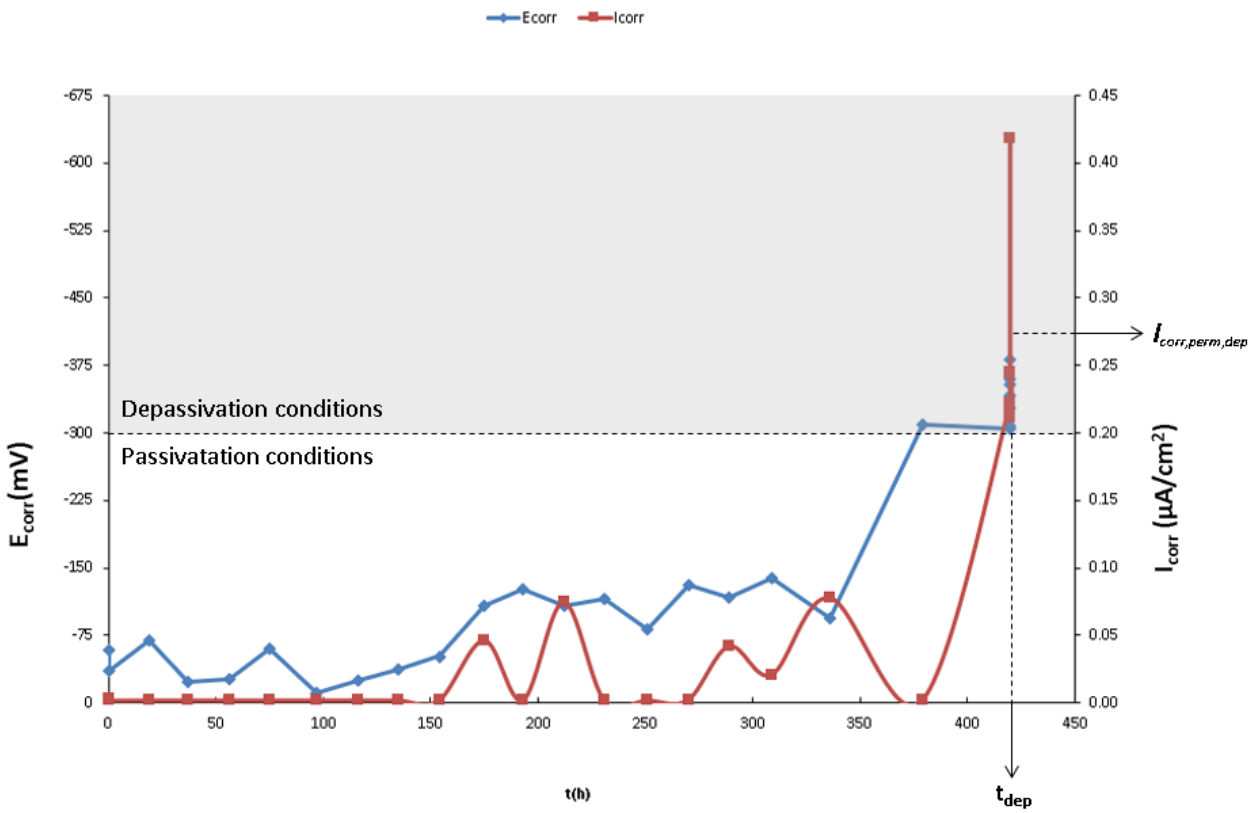

Figure 5.23: *t_{dep} and $I_{corr,dep,perm}$ for sample 15.*

In the table below, E_{corr} and I_{corr} measured together with the corresponding dates of measurement after the starting of depassivation have been listed, for the sample 15. Moreover, the number of depassivation days has been recorded. Then the mean corrosion rate during the permanent depassivation period, known as $I_{corr,perm,dep}$ has been calculated.

Measurement date	Corrosion potential, E_{corr} (mV)	Corrosion rate, I_{corr} (µA/cm^2)	Depassivation time, t_{dep}(h)	Number of depassivation days (d)
05/07/2019	-305	0.223	420	0
08/07/2019	-327	0.245	420	3
10/07/2019	-382	0.244	420	5
12/07/2019	-360	0.418	420	7
15/07/2019	-308	0.220	420	10
17/07/2019	-354	0.211	420	12
19/07/2019	-341	0.215	420	14

Table 5.22: *Sample 15: Corrosion measurements during the depassivation period.*

$I_{corr,perm,dep} = 0.254$ µA/cm^2

The time of depassivation t_{dep} was the time at which the electrochemical measurements were both, for the first time during the testing period, over the critical standard values. So for sample 15 this happened after only 420 hours, moving from the passivation conditions to the depassivation ones. After the depassivation, the applied voltage has been disactivated while successive measurements have been taken at different days (7 corrosion potential and corrosion rate measurements on the same time-line), in order to determine if the sample was permanently depassivated or not. Since it showed to be passivated for a total period of 14 days (> 10 days according to the standard norm) , it has been declared depassivated.

5.4 Chlorides content measurement (only for the corroded sample)

5.4.1 Steel-concrete interface chlorides content

Element	Concentration (PPM)	+/-	Concentration (%)
Ca	>10%		>10%
S	9771	655	≈ 0.98
Fe	9621	82	≈ 0.96
Cl	7749	220	≈ 0.77
K	5415	124	≈ 0.54
Ti	673	18	≈ 0.067
Mn	174	6	≈ 0.017
Cr	137	5	≈ 0.014
V	43	3	≈ 0.043

Table 4.23: *Sample 15: Steel-concrete interface material composition at* t_{dep}.

At t_{dep}= 420 h:

- $[Cl^-]$ = 0.77 % of concrete weight

The content of chlorides in the interface steel-concrete was relative high, whereas the chlorides content was almost null at the beginning of the test. This meant that in the conditions of testing, for sample 15, chlorides ions penetrated into the concrete in great amount, until they reached the steel surface.

5.4.2 Chlorides concentration depth profile

According to the eq. (8) in which D_{ns} has been considered instead of D_{eff}, it has been predicted the concentration of chloride ions at different penetration depth for different possible period of testing (*Figure 5.24*), where the chlorides surface concentration C_s=10%, obtained by the evaluation of the concrete porosity, in order to make a forecast of the sample corrosion behaviour during the time.

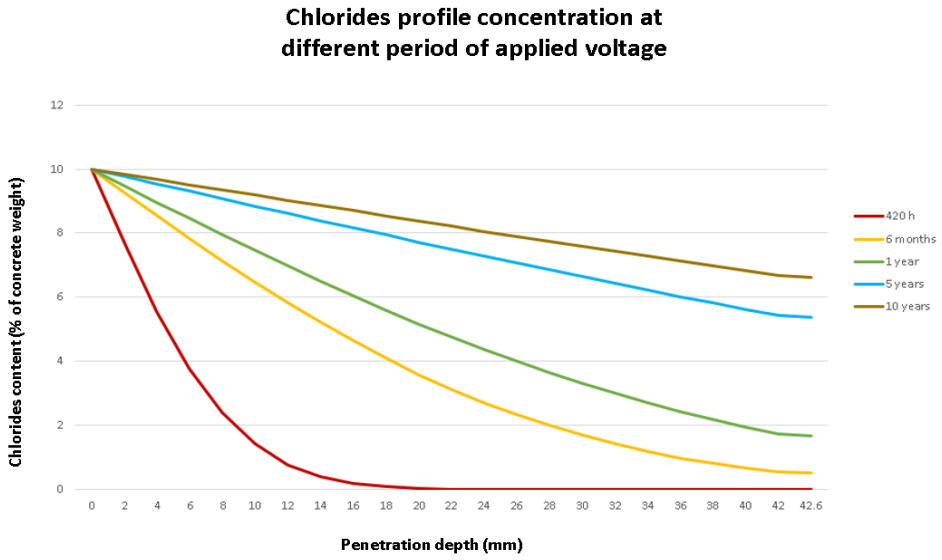

Figure 5.24: *Sample 15: Chloride ions concentration profiles at different depth of penetration for different period of testing.*

The most relevant depth shown in the graph (x-axis) was 42.6 mm, which was the distance between the concrete surface in direct contact with the chlorides solution and the steel surface for sample 15. This was only a theoretical approach and not always it was the mirror of what it really happened. *Figure 5.25* is a prof of this statement.

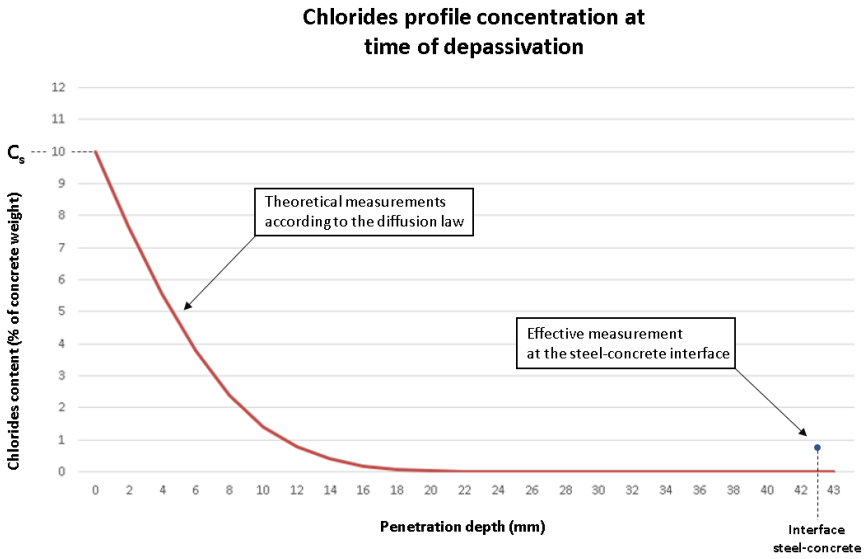

Figure5.25: *Sample 15: Comparison between the chlorides concentration theoretical value and the measured one at the steel-concrete interface at* t_{dep}.

From the comparison between the value of chlorides content at the steel-concrete interface (x=42.6 mm) at t=420 h in the theoretical and in the effective measurement:

- For theoretical diffusion law: $[Cl^-] \approx 0$ % of concrete weight
- For effective measurement : $[Cl^-] = 0.77$ % of concrete weight

Although the theoretical model was not always effective, the difference with the effective measurement seemed to be too high. Given the testing conditions, the critical chlorides concentration at the interface steel-concrete has been reached in a not-reasonable time.

5.5 Corrosion surface analysis (only for the corroded sample)

Figure 5.26: *Sample 15: Corroded Free-window.*

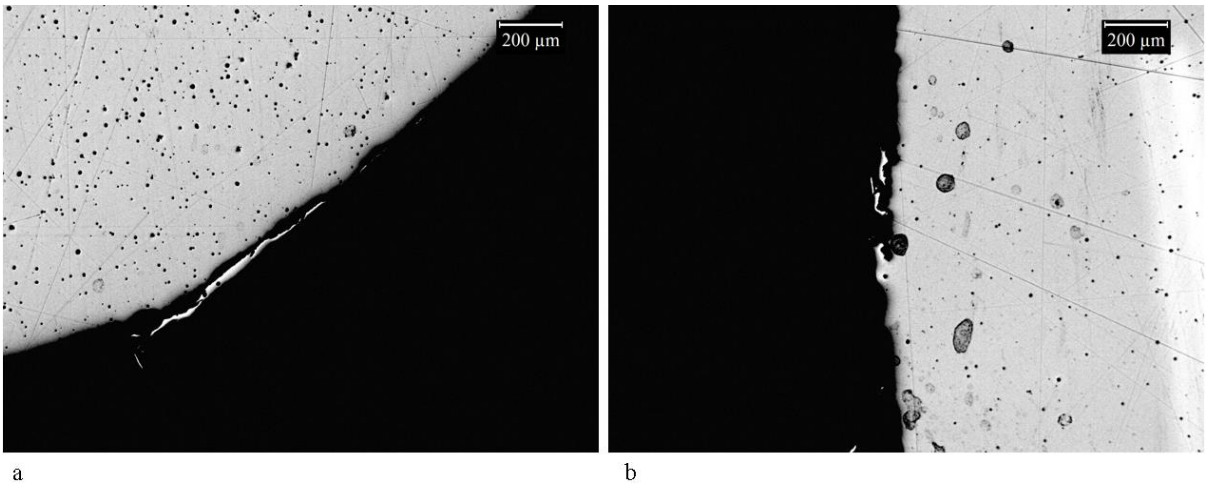

Figure 5.27: *Sample 15: corrosion surface observation at optical microscope (200 µm).*

From *Figure 5.27* it can be noticed the presence of separate areas in the rebar surface, where a corrosion process occurred. Specifically, exfoliation seemed to be the primary cause. It is a form of intergranular corrosion, acting over selective sub-surfaces paths. In the 2304 DSS corroded area, portions of steel detached along planes parallel to the surface could be observed. From the magnitude of the anomalies , the corrosion process could be evaluated as at the earlier stages. Other types of instruments (e.g. *FESEM*) with higher resolution and magnification are needed for a more detailed analysis about the corrosion products.

5.6 Overall discussion

Given the results, whereas the twenty specimens have been prepared and fabricated with the same materials and tested under the same conditions, it is objective the great resistance to chloride-induced corrosion by AISI 2304 Duplex Stainless Steel reinforced concrete structure. Among the total number of specimens, only one showed the evidence of corrosion, but the time of applied voltage needed for that was relatively too short and suggested the presence of relevant defects in the concrete structure. The presence of cracks or anomalies in the specimen concrete could have promoted the chloride ions passage, increasing the penetration rate. Despite this, the rest of the specimens showed extremely high resistance to the passage of current and kept values of E_{corr} and I_{corr} much lower than the critical values, defined by the followed standard norm. The final overall result is the statement that the 2304 DSS rebar in concrete do not suffer chloride-induced corrosion under the testing condition described in this work, for a total period of 58 days of testing in humid conditions and subject to the chloride ions accelerated attack generated by a 10 V applied voltage for an accumulated time of 889 hours.

Chapter 6

Conclusion and future developments

In this conclusive chapter a brief report of the entire thesis work needs to be carried out, in order to make clear the key aspects of the project.

During the five months spent at the *Institute of construction science Eduardo Torroja* in Madrid, the durability of AISI 2304 Duplex Stainless Steel (DSS) reinforced concrete structures for applications in high chloride containing environment has been investigated, as the primary objective of the work was to promote the spreading of above-mentioned DSS in the construction field.

The work has been carried out following the Spanish standard norm UNE 83992 "concrete durability", starting from the fabrication of the twenty equal specimens to their final corrosion surface analysis.

After the initial fabrication of the RC samples, including the DSS rebars preparation with epoxy resins coating and their incorporation in the prepared concrete, they have been left for a 28 days long period in water, in order to achieve high values of relative humidity (>95%). Then, all the RC samples have been completed by the addition of the chloride solution in strict contact with the concrete and the introduction of a copper foil in the solution itself, to make possible the passing of the current inside the sample. Before the effective test, a pre-test has been performed to demonstrate the great resistance to polarization by the DSS.

The effective test consisted of an accelerated attack by chloride ions on the RC systems , favourited by the activation of the electric field between the cathode (copper foil) and a stainless steel mesh anode put just under the samples. The current has been generated, thanks to the application of a ΔV (10V) in the circuit by a DC power supply. The current in the samples have been regularly activated and disactivated for 58 days, keeping the same conditions for all the samples in terms of temperature, relative humidity and chloride concentration in the aggressive solution. During the testing period, periodical measurements of E_{corr} and I_{corr} have been taken by the use of a modular high current potentiostat-galvanostat, named *Metrohm*

Autolab, and the related software *NOVA 1.11*. According to the norm, all the samples keeping a value of E_{corr} and I_{corr} higher than -300 mV and 0.2 μA/cm^2 for at least 10 days, could be declared corroded.

As results, during the testing period among the twenty specimens, six samples showed periods of de-passivation but only one (n. 15) has been permanently de-passivated, as it kept high values of E_{corr} and I_{corr} for a period of 14 consecutive days. The sample n. 15 has been the only subject to the whole corrosion analysis. The time of applied voltage needed for de-passivation, or depassivation time t_{dep} , the mean corrosion rate during the depassivation period, or permanent depassivation corrosion rate $I_{corr,perm,dep}$ have been assessed. Furthermore, the critical chlorides concentration at the steel-concrete interface has been evaluated, through the breaking down of the RC specimen, showing an objectively high value (0.77%) in respect of concrete weight. Finally, the corroded steel surface microstructure has been analysed through optical microscopy, in order to gather more information about the possible causes and mechanism of corrosion.

Given the results, overall the 2304 Duplex Stainless Steel has revealed to be an high performance material in extremely aggressive chlorides environment, as in the total testing period the most of the steel rebars kept intact their passivating layer. Future studies need to be developed before proclaiming this steel as one of the best among the corrosion resistant ones. Firstly, a more aggressive chloride testing could be actuated, as the original purpose of this work was to provoke corrosion in each sample, in order to find the mean chloride threshold value, responsible for the quick increase in corrosion rate, among a great number of specimens. Future further investigations should be carried out on the possibility of monitoring 2304 DSS reinforced structures behaviour in real marine environment for a more extended period of time, so that to estimate if their effective performances are consistent with those shown in laboratory. Only then, it could be possible to make a first effective comparison with other austenitic more common steels (AISI 304L and 316L) in terms of resistance to chloride-induced corrosion, in order to encourage its commercialization, never forgetting the economic factors.

References

[1] Böhni H., *Corrosion in reinforcedconcrete structures* , Woodhead Publishing , 264 pp , 2005.

[2] Fleet Owner, *Remembering the silver bridge collapse,* 2017, web: <https://www.fleetowner.com/open-road/remembering-silver-bridge-collapse>

[3] Evening Standard, *Shocking moment bridge collapse in Taiwan sending oil tanker truck plummeting onto fishing boats below*, 2019 , web: <https://www.standard.co.uk/news/world/shocking-moment-bridge-collapses-in-taiwan-sending-oil-tanker-truck-plummeting-onto-boats-a4250571.html>

[4] The Guardian, *What caused the genoa morandi bridge collapse-and the end of an Italian national myth?,* 2019, web: <https://www.theguardian.com/cities/2019/feb/26/what-caused-the-genoa-morandi-bridge-collapse-and-the-end-of-an-italian-national-myth>

[5] Snow D. A., *Plant engineer's reference book,* 2nd edition, Butterworth-Heinemann, 864 pp , 2003.

[6] Nace international, *Pitting corrosion*, web: <https://www.nace.org/resources/general-resources/corrosion-basics/group-1/pitting-corrosion>

[7] R. Winston Revie, *Uhlig's corrosion handbook*, 3rd edition, CANMET Materials Technology Laboratory Ottawa, Ontario, Canada, 1296 pp, 2011.

[8] Smlease design, *What is dissimilar metal/galvanic corrosion and how to prevent it*, web: <https://www.smlease.com/entries/finish-operations/galvanic-corrosion/>

[9] Ahmad Z. , *Principles of Corrosion Engineering and Corrosion Control*, Butterworth-Heinemann, 672 pp, 2006.

[10] Hänninen H.E. , *Comprehensive Structural Integrity*, Vol. 6, 1-29, 2003

[11] Wikipedia, the free encyclopedia,web: <https://en.wikipedia.org/wiki/Reinforced_concrete>

[12] Kwan A.K.H., Wong H.H.C., *Durability of Reinforced Concrete Structures, Theory vs Practice*, The University of Hong Kong, Hong Kong, 1-20, 2005.

[13] Hunkeler F., *Corrosion in reinforced concrete: processes and mechanisms*, Technical Research and Consulting on Cement and Concrete, TFB,1-45, 2005.

[14] PCA America's cement manufacturers , *Corrosion of embedded metals*, web: <https://www.cement.org/learn/concrete-technology/durability/corrosion-of-embedded-materials>

[15] Ronacrete, *Carbonation of reinforced concrete*, web: < https://www.ronacrete.co.uk/carbonation-reinforced-concrete/>

[16] Ryan P. C., O'Connor A., *Comparing the durability of self-compacting concretes and conventionally vibrated concretes in chloride rich environments*, Ireland, 2016.

[17] Tuutti K., *Corrosion of steel in concrete*, in *Division of Building Materials*, Swedish Cement and Concrete Research Institute, 468 pp , 1982.

[18] C. Andrade, C. Alonso, *Electrochemical Techniques for Measuring Metallic Corrosion. Test methods for on-site corrosion rate measurement of steel reinforcement in concrete by means of the polarization resistance method*, RILEM, vol. 37,623-643, 2005.

[19] Penn Stainless Product, Inc., *The History of stainless steel,* August 2012 , web: <http://www.bssa.org.uk/about_stainless_steel.php?id=31>

[20] MadeHow , *Stainless Steel*, web: <http://www.madehow.com/Volume-1/Stainless-Steel.html#ixzz60eXQTI51>

[21] Metalsupermarkets, *Classes of Stainless Steel*, web: <https://www.metalsupermarkets.com/classes-of-stainless-steel/>

[22] Colpaert H., *Metallography of Steels - Interpretation of Structure and the Effects of Processing*, ASM publisher, 718 pp, 2018.

[23] IMOA, *Stainless grades and properties*, web:< https://www.imoa.info/molybdenum-uses/molybdenum-grade-stainless-steels/steel-grades.php>

[24] Penn Stainless Product, Inc., *The history of Duplex Stainless Steel* , August 2012, web: <http://www.pennstainless.com/blog/2012/08/the-history-of-duplex-stainless-steel/>

[25] IMOA, *Stainless Solutions Architecture, building & construction* , November 2015, web: <https://www.imoa.info/stainless-solutions/archive/16/Cutting-Edge-Pedestrian-Bridge-Design.php>

[26] Essential home, *Helix Bridge: the spectacular bridge of Singapore,* web: <https://essentialhome.eu/inspirations/lifestyle/helix-bridge-spectacular-bridge-singapore/>

[27] Archello, *Harbor Drive pedestrian bridge*, web: <https://archello.com/project/harbor-drive-pedestrian-bridge>

[28] Pachón Montaño A., *Durabilidad de las armaduras corrugadas de acero inoxidable en estructuras de hormigón armado en ambientes marinos*, PhD thesis, Universidad Politécnica de Madrid, 2017.

[29] Sandmayer Steel Company, *Alloy 2304,* web: <https://www.sandmeyersteel.com/2304.html>

[30] Baddoo N.R., Kosmač A., *Sustainable Duplex Stainless Steel Bridges* , 2010.

[31] Outokumpu, *Stainless steel alloy surcharges Europe*, December 2019, web: <https://www.outokumpu.com/it-it/surcharges/stainless-steel-alloy-surcharges-europe>

[32] Precivil basic of civil engineering , *The step by step guide to calculate the density of concrete*, web: <https://precivil.com/density-of-concrete/>

[33] Gonzalez J.A., *Control de la corrosión: Estudio y medida por técnicas electroquímicas,* Consejo Superior de Investigaciones Científicas (CSIC), Madrid, 1989

[34] Kakaei K. ,Esrafili M.D. , Ehsani A. , *Interface science and technology*, vol. 27, 456 pp, 2019.

[35] M. Stern, A. L. Geary, *Electrochemical Polarization I. A Theoretical Analysisi of the Shape of Polarization Curves*, Journal of Electrochemical Society, vol. 104, 56-63,1957.

[36] Metrohm Autolab , *Instruments for electrochemical research*, 2013, web: < https://www.metrohm-autolab.com/download/Autolab_Brochure_2013_EN_LR.pdf>

[37] Radhakrishna Pillai G., Jayachandran K., Dhanya B.S., Sooraj Nair A.O., Santhanam M., Ravindra G., *Enhancing the corrosion resistance of reinforced concrete structures – Indian scenario and challenges ahead,* Indian Institute of Technology Madras, India, 2015.

[38] NOVA open circuit potential tutorial, Version 1.11.0, web: <https://www.ecochemie.nl/download/NovaTutorials/OCP_tutorial.pdf>